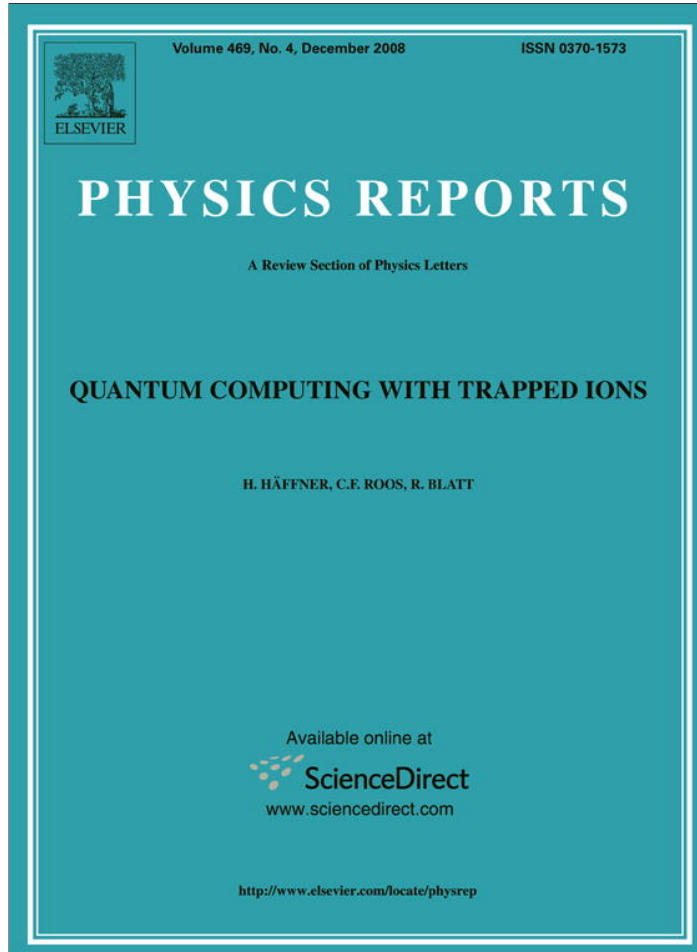


Provided for non-commercial research and education use.
Not for reproduction, distribution or commercial use.



This article appeared in a journal published by Elsevier. The attached copy is furnished to the author for internal non-commercial research and education use, including for instruction at the authors institution and sharing with colleagues.

Other uses, including reproduction and distribution, or selling or licensing copies, or posting to personal, institutional or third party websites are prohibited.

In most cases authors are permitted to post their version of the article (e.g. in Word or Tex form) to their personal website or institutional repository. Authors requiring further information regarding Elsevier's archiving and manuscript policies are encouraged to visit:

<http://www.elsevier.com/copyright>



Contents lists available at ScienceDirect



Physics Reports

journal homepage: www.elsevier.com/locate/physrep

Quantum computing with trapped ions

H. Häffner^{a,b,c,d,*}, C.F. Roos^{a,b}, R. Blatt^{a,b}^a Institut für Quantenoptik und Quanteninformation, Österreichische Akademie der Wissenschaften, Technikerstraße 21a, A-6020 Innsbruck, Austria^b Institut für Experimentalphysik, Universität Innsbruck, Technikerstraße 25, A-6020 Innsbruck, Austria^c Department of Physics, University of California, Berkeley, CA 94720, USA^d Materials Sciences Division, Lawrence Berkeley National Laboratory, Berkeley, CA 94720, USA

ARTICLE INFO

Article history:

Accepted 22 September 2008

Available online 30 September 2008

editor: J. Eichler

PACS:

03.67.-a

03.67.Lx

37.10.Ty

42.50.Dv

Keywords:

Quantum computing and information

Entanglement

Ion traps

ABSTRACT

Quantum computers hold the promise of solving certain computational tasks much more efficiently than classical computers. We review recent experimental advances towards a quantum computer with trapped ions. In particular, various implementations of qubits, quantum gates and some key experiments are discussed. Furthermore, we review some implementations of quantum algorithms such as a deterministic teleportation of quantum information and an error correction scheme.

© 2008 Elsevier B.V. All rights reserved.

Contents

1. Introduction.....	156
2. Ion trap quantum computers	157
2.1. Principles of ion-trap quantum computers.....	158
2.2. The basic Hamiltonian.....	158
2.3. Choice of qubit ions	160
2.4. Initialization and read-out	162
2.5. Single-qubit gates	163
2.5.1. Individual addressing of ion qubits	165
2.6. Two-qubit gates	166
2.6.1. Motion of ion strings	166
2.6.2. Cirac-Zoller gate	168
2.6.3. Mølmer-Sørensen gate	169
2.6.4. Geometric phase gate	170
2.6.5. Other gate types.....	171
2.7. Apparative requirements	172
2.7.1. The NIST setup	172
2.7.2. The Innsbruck setup	174

* Corresponding author at: Institut für Quantenoptik und Quanteninformation, Österreichische Akademie der Wissenschaften, Technikerstraße 21a, A-6020 Innsbruck, Austria.

E-mail address: hartmut.haeffner@uibk.ac.at (H. Häffner).

2.7.3. Composite pulses and optimal control.....	174
3. Decoherence in ion trap quantum computers	175
3.1. Sources of imperfections in ion trap quantum computers	175
3.1.1. Bit-flip errors.....	175
3.1.2. Dephasing.....	175
3.1.3. Imperfect control	177
3.2. Motional coherence	178
3.3. Modeling ion trap quantum computers	181
4. Key experiments	182
4.1. Cirac-Zoller-type gates	182
4.2. Entangled states with trapped ions	182
4.3. Decoherence free subspaces	184
4.4. State tomography	186
4.5. Selective read-out of a quantum register.....	186
4.6. Conditional single-qubit operations.....	188
4.7. Process tomography	188
5. Algorithms with trapped ions	189
5.1. Deutsch-Josza algorithm.....	189
5.2. Teleportation.....	190
5.3. Quantum error correction	192
5.4. Semiclassical quantum Fourier-transform.....	192
5.5. Entanglement purification	193
5.6. Quantum simulations	194
6. Shuttling and sympathetic cooling of ions	195
7. New trap developments	196
8. Future challenges and prospects for ion trap quantum computing	196
Acknowledgments	198
References.....	198

1. Introduction

The aim of this article is to review the recent development of ion trap quantum computing. This field has evolved rapidly in the recent decade. Thus the many facets of experimental ion trap quantum computing and its techniques cannot all be covered. Instead, we want to present here a coherent picture of the most important experimental issues and refer the reader to the original publications for the details. We also describe some of the milestones achieved so far in ion trap quantum computing, such as the teleportation of quantum states and quantum error correction. Still, much of the work especially towards shuttling ions with segmented traps is only touched upon.

A quantum computer uses the principles of quantum mechanics to solve certain mathematical problems faster than normal computers. Such a quantum computer processes quantum information whose most basic unit is called a quantum bit (qubit). Already a small quantum computer, consisting of forty qubits,¹ could solve quantum mechanical problems that are intractable with current computers. In particular, the study of quantum mechanical many-body systems would benefit considerably from such a device (Feynman, 1982; Lloyd, 1996). In 1989, David Deutsch discovered a mathematical problem which can be solved faster with quantum mechanical means than with classical ones (Deutsch, 1989). But it was a few years later when the rapid development of quantum computation set in, marked by Peter Shor's discovery of a quantum algorithm with which large numbers can be factored much faster than with today's classical algorithms (Shor, 1994).

Shortly afterwards, Ignacio Cirac and Peter Zoller found a physical system on which such quantum algorithms could be implemented (Cirac and Zoller, 1995): single trapped ions were supposed to carry the quantum information, which is manipulated and read out with focused laser beams. Already within a year's time, David Wineland's group at National Institute of Standards and Technology demonstrated the heart of such an ion-trap quantum computer (Monroe et al., 1995a), a controlled bit flip on a single ion. Without exaggeration, one can say that those two publications mark the birth of experimental quantum computation. Rapidly, other implementations were also considered. In particular, liquid-state nuclear magnetic resonance was used to demonstrate a quantum algorithm (Gershenfeld and Chuang, 1997; Chuang et al., 1998b; Jones and Mosca, 1998) and later even Shor's algorithm was implemented on a seven qubit register (Vandersypen et al., 2001). On the theoretical side, many new interesting implications were found. For quantum computation, the most relevant implication was the discovery of quantum error correction protocols by Shor (1995) and Steane (1996). These protocols allow for the implementation of arbitrary long quantum algorithms without perfect control.

The basic unit of quantum information (a qubit) can be implemented with a two-level system such as the electron's spin in a magnetic field or using two levels of an atom. A simple quantum computation initializes the qubits, manipulates

¹ To describe the (arbitrary) state of a forty qubit system, 2^{40} complex numbers are necessary. Already this requirement exceeds the capacities of current super computers.

them and finally reads out the final states. Any physical implementation of quantum computation must be able to perform these tasks. Thus the physical system must satisfy the requirements laid out in Section 2.1 to qualify as a universal quantum computer (DiVincenzo, 2001).

- (1) It must be a scalable physical system with well characterized qubits.
- (2) It must be possible to initialize the qubits.
- (3) The qubits must have a coherence time much longer than the operation time.
- (4) There has to be a universal set of quantum gates. In the most simple case one considers single-qubit and entangling two-qubit gates.
- (5) A qubit-specific measurement must be attainable.

Furthermore, to build up a quantum network, one requires:

- (6) The ability to interconvert stationary and flying qubits.
- (7) The ability to faithfully transmit flying qubits between specified locations.

In principle, these requirements can be fulfilled with a number of physical approaches, such as nuclear magnetic resonance (Gershenfeld and Chuang, 1997), cavity quantum electrodynamics (cavity-QED) (Raimond et al., 2001), Josephson junctions (Makhlin et al., 2001), a combination of circuit-QED and Josephson junctions (Wallraff et al., 2004; Majer et al., 2007) and quantum dots (Loss and DiVincenzo, 1998; Petta et al., 2005). Methods using linear optics have also been proposed (Knill et al., 2001b) and actually were used for quantum information processing (Walther et al., 2005; Lanyon et al., 2008), however, here the emphasis is naturally more on the transmission of quantum information rather than processing it.

Using nuclear magnetic resonance, quite a number of impressive demonstration experiments have been performed. Unfortunately, the state of the quantum register (molecules) can only be poorly initialized (except in special cases (Jones, 2000)), making the scaling properties of NMR quantum computation not very promising (Warren, 1997; Jones, 2000; Linden and Popescu, 2001). At the moment Josephson junctions seem to be very appealing, especially when combined with superconducting strip line cavities (Wallraff et al., 2004; Majer et al., 2007). Recently, Steffen et al. (2006) and Plantenberg et al. (2007) demonstrated Bell-states and a controlled-NOT, respectively, with pairs of Josephson junction qubits.

2. Ion trap quantum computers

Of the many approaches that have been proposed for constructing a quantum computer, trapped ions are currently one of the most advanced (Army Research Office, USA, 2005). This is also reflected in the fact that around the year 2000 only half a dozen groups pursued experimental ion-trap quantum computing while in 2008 there are more than 25 groups working in the field.

Already, long before the idea of quantum computation was picked up by experimentalists, four out of the five core criteria required by DiVincenzo for a quantum computer were demonstrated with trapped ions in the laboratory: initialization (Wineland et al., 1980) and read-out of the internal electronic states of trapped ions (Nagourney et al., 1986; Sauter et al., 1986; Bergquist et al., 1986), extremely long coherence times (Bollinger et al., 1991) and laser cooled ion crystals with many ions (Diedrich et al., 1987; Wineland et al., 1987; Raizen et al., 1992a,b) serving as a qubit register. Then Cirac and Zoller (1995) realized that quantum computation can be carried out by coupling the ions via a collective motional degree of freedom. Thus, a route to implement the missing conditional evolution of physically separated qubits (a two-qubit interaction) was introduced. In addition, they proved that the size of the resources necessary to control trapped ions does not increase exponentially with the number of qubits (Cirac and Zoller, 1995).

Soon after the proposal by Cirac and Zoller in 1995, the NIST ion storage group around David Wineland implemented the key idea of the proposal – a conditioned phase shift – with a single Be⁺-ion (Monroe et al., 1995a). Furthermore they demonstrated a few other two-qubit gate candidates (Sackett et al., 2000; DeMarco et al., 2002; Leibfried et al., 2003b), entangled up to four ions (Sackett et al., 2000), demonstrated a so-called decoherence free subspace (Kielpinski et al., 2001) and simulated a nonlinear beam-splitter (Leibfried et al., 2002).

In our group in Innsbruck, the Deutsch–Josza algorithm was demonstrated with a single Ca⁺-ion (Gulde et al., 2003), followed by the first implementation of a set of universal gates on a two-ion string (Schmidt-Kaler et al., 2003c). In addition, the creation of various entangled states and the partial read-out of an entangled quantum register was demonstrated (Roos et al., 2004b).

Further milestones in ion-trap quantum computing were experiments on quantum teleportation by both groups (Barrett et al., 2004; Riebe et al., 2004), an error correction protocol by the NIST-group (Chiaverini et al., 2004), entanglement of six and eight particles (Leibfried et al., 2005; Häffner et al., 2005a) by both groups, respectively and entanglement purification (Reichle et al., 2006b). Recently, ions in separate traps have been also entangled using ion–photon entanglement by the Ann–Arbor group (Blinov et al., 2004; Maunz et al., 2007; Moehring et al., 2007; Matsukevich et al., 2008).

Currently, miniaturization and integration of segmented ion traps is rapidly progressing. Already for some time, the NIST group has been successfully using microfabricated segmented traps to relieve the difficulties of single ion addressing. Inspired by this success, in the meantime virtually all ion trap groups started to develop segmented trap technologies. Furthermore, US funding bodies initiated contacts between the various groups to further ion trap related technologies.

and established contacts to microfabrication laboratories, such as Lucent Technologies and Sandia National Laboratories. In Europe the 'Specific Targeted Research Project' MICROTRAPS with six participating groups has been formed to further microfabricated ion trap technologies.

2.1. Principles of ion-trap quantum computers

A excellent overview and detailed account of the fundamental issues of ion trap quantum computing is given by Wineland et al. (1998) and by Šašura and Bužek (2002). Furthermore, Leibfried et al. (2003a) review the progress towards the manipulation and control of single ions. Very recently, the generation and applications of entangled ions were reviewed by Blatt and Wineland (2008).

We start here by summarizing how ion-trap quantum computers fulfill the DiVincenzo criteria mentioned above (DiVincenzo, 2001):

- (1) *A scalable physical system with well characterized qubits:* long-lived internal levels of the ions serve as the qubits (see Section 2.3). The qubit register is formed by strings of ions in a (linear) trap. While this approach is in principle scalable, it is desirable to distribute the ions among multiple traps (Wineland et al., 1998; Kielpinski et al., 2002). Thus complications, due to the increased mass and more the complicated mode structure of large ion strings can be circumvented. First steps in this direction will be briefly discussed in Section 8.
- (2) *The ability to initialize the state of the qubits:* this is most easily achieved by optical pumping to a well-defined electronic state. Fidelities of 0.99 are typical, in Section 2.4 also methods to achieve much higher fidelities will be discussed.
- (3) *A coherence time much longer than the operational time:* in current quantum computing experiments, typically coherence times of a few milliseconds are achieved, which are about one to two orders of magnitude longer than the time scale for quantum operations (see Section 3 for details). The coherence time is often limited by magnetic field fluctuations. on the other hand, coherence times of more than 10 s have been demonstrated with Raman-transitions between magnetic-field insensitive transitions (Langer et al., 2005). Similar observations were made in $^{43}\text{Ca}^+$ by the Oxford and Innsbruck groups (Lucas et al., 2007; Benhelm et al., 2008a). Furthermore, Bollinger et al. (1991) demonstrated a coherence time of more than 10 min using a microwave drive instead of a Raman-laser setup. However, so far only one experiment demonstrated the combination of high-fidelity quantum gates and magnetic field insensitive transitions (Haljan et al., 2005b).
- (4) *A universal set of quantum gates:*
 - (a) Single qubit gates are implemented by driving Rabi oscillations between the two qubit levels with resonant laser pulses (see Section 2.5). The gates can be represented as rotations of the Bloch sphere where the axis of rotation can be selected by changing the phase of the exciting laser field (single photon transition) or the phase difference of the two Raman beams (see Section 2.5). A single-qubit phase-gate can be produced directly by an off-resonant laser via an AC-Stark shift (see Section 2.5).
 - (b) For two-qubit gates usually the long range interaction due to the Coulomb force is employed. In the original proposal by Cirac and Zoller, the quantum information of one ion is swapped to the common motional degree of freedom of the ion string (Cirac and Zoller, 1995). Then an operation conditioned on the motional state can be carried out on a second ion before the quantum information is swapped back from the motion to the first ion. Section 2.6 details this idea as well as other methods to implement multi-qubit gates. Implementations of some of the two-qubit gate recipes will be discussed in Sections 4.1 and 4.2.
- (5) *A qubit-specific measurement:* one of the qubit levels is excited on a strong transition to a higher lying auxiliary short-lived level while the other qubit level remains untouched. Thus, fluorescence from the decay is detected only if the qubit is projected to the qubit level which is coupled to the auxiliary transition (see Section 2.4).

Additionally DiVincenzo requires:

- (6) *The ability to interconvert stationary and flying qubits:* ions can be stored in a high-finesse cavity. Thus, the ions' internal state can be mapped onto a photonic state (Cirac et al., 1997).
- (7) *The ability to faithfully transmit flying qubits between specified locations:* a photon can be transmitted through a fiber and at the target location coupled via another high-finesse cavity to the target ion.

There exist further possibilities to connect two distant ion trap quantum computers. One of them will be briefly discussed in Section 5.5.

For practical applications, the DiVincenzo criteria have not only to be fulfilled, but also the fidelity and speed of the implementations have to be considered (see Section 8). Furthermore, it is highly desirable to implement all operations as parallel as possible.

2.2. The basic Hamiltonian

We will now briefly discuss the Hamiltonian of two-level systems interacting with a quantized harmonic oscillator via laser light. For more detailed discussions, we refer to Refs. Wineland et al. (1998) and Leibfried et al. (2003a). The basic level scheme of such a system is displayed in Fig. 1. We start out by writing the Hamiltonian for a trapped single ion interacting

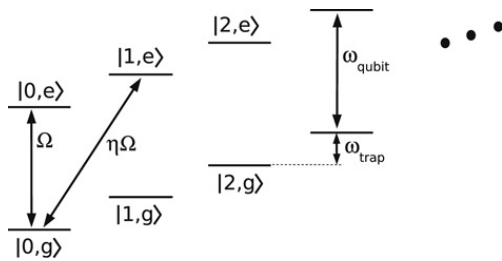


Fig. 1. Energy level scheme of a single trapped ion with a ground ($|g\rangle$) and an excited ($|e\rangle$) level in a harmonic trap (oscillator states are labeled $|0\rangle, |1\rangle, |2\rangle, \dots$). Ω denotes the carrier Rabi frequency. The Rabi frequency on the blue sideband transition $|0, e\rangle \leftrightarrow |1, g\rangle$ transition is reduced by the Lamb-Dicke factor η as compared to the carrier transition (see Eq. (5)). The symbols ω_{qubit} and ω_t denote the qubit and the trap frequency, respectively.

with near resonant laser light, taking into account only two levels of the ion and one vibrational mode (taken to be oriented along the z direction):

$$H = \hbar\Omega\sigma_+e^{-i(\Delta t-\varphi)} \exp(i\eta [ae^{-i\omega_t t} + a^\dagger e^{i\omega_t t}]) + \text{h.c.} \quad (1)$$

Here, σ_\pm is either the atomic raising or the atomic lowering operator, while a^\dagger and a denote the creation and annihilation operator for a motional quantum, respectively. Ω characterizes the strength of the laser field in terms of the so-called Rabi frequency, φ denotes the phase of the field with respect to the atomic polarization and Δ is the laser-atom detuning. ω_t denotes the trap frequency, $\eta = k_z z_0$ is the Lamb-Dicke parameter with k_z being the projection of the laser field's wavevector along the z direction and $z_0 = \sqrt{\hbar/(2m\omega_t)}$ is the spatial extension of the ion's ground state wave function in the harmonic oscillator (m is here the ion's mass). We mention also that the rotating wave approximation has been applied which assumes that both the laser detuning and Rabi frequency are much smaller than optical frequencies. A similar treatment can be carried out for qubits based on Raman-transitions by eliminating the virtual level through which the two qubits are coupled. Please note that in our definition the Rabi frequency measures the frequency with which the population is exchanged in contrast to the definition used by Wineland et al. (1998) and Leibfried et al. (2003a).

Using the Lamb-Dicke approximation ($\eta\sqrt{\langle(a + a^\dagger)^2\rangle} \ll 1$) which is almost always valid for cold tightly bound ion strings, we can rewrite Eq. (2) (Leibfried et al., 2003a; Jonathan et al., 2000):

$$H = \hbar\Omega \{ \sigma_+ e^{-i(\Delta t-\varphi)} + \sigma_- e^{i(\Delta t-\varphi)} + i\eta(\sigma_+ e^{-i(\Delta t-\varphi)} - \sigma_- e^{i(\Delta t-\varphi)}) (ae^{-i\omega_t t} + a^\dagger e^{i\omega_t t}) \}. \quad (2)$$

Three cases of laser detuning Δ are of particular interest (see Fig. 1): $\Delta = 0$ and $\Delta = \pm\omega_t$. This becomes apparent if a second rotating wave approximation is carried out where it is assumed that only one transition is relevant at a time. Discarding time dependent terms, we thus arrive at

(1) the Hamiltonian describing the carrier transition ($\Delta = 0$)

$$H^{\text{car}} = \hbar\Omega(\sigma_+ e^{i\varphi} + \sigma_- e^{-i\varphi}). \quad (3)$$

Here only the electronic states $|g\rangle$ and $|e\rangle$ of the ion are changed.

(2) the Hamiltonian describing the blue sideband transition ($\Delta = \omega_t$)

$$H^+ = i\hbar\Omega\eta(\sigma_+ a^\dagger e^{i\varphi} - \sigma_- a e^{-i\varphi}). \quad (4)$$

Simultaneously to exciting the electronic state of the ion, in this case, a motional quantum (a phonon) is created. Within this two-level system, Rabi flopping with the Rabi frequency

$$\Omega_{n,n+1} = \sqrt{n+1}\eta\Omega \quad (5)$$

occurs, where n describes the number of motional quanta (phonons). For convenience, we define the blue sideband Rabi frequency $\Omega_+ = \Omega_{0,1}$ which describes the flopping frequency between the $|g, 0\rangle$ and the $|e, 1\rangle$ state.

(3) the Hamiltonian describing the red sideband transition ($\Delta = -\omega_t$)

$$H^- = i\hbar\Omega\eta(\sigma_- a^\dagger e^{-i\varphi} + \sigma_+ a e^{i\varphi}). \quad (6)$$

Simultaneously to exciting the electronic state, here a phonon is destroyed and Rabi flopping with the Rabi frequency

$$\Omega_{n,n-1} = \sqrt{n}\eta\Omega \quad (7)$$

takes place.

Naturally, one is interested in driving the sideband transitions as fast as possible to speed up the quantum operations based on the sideband transitions. However, especially for small Lamb-Dicke factors, the second rotating wave approximation performed to obtain Eqs. (3)–(6) is then not satisfied for Rabi frequencies Ω comparable with the trap

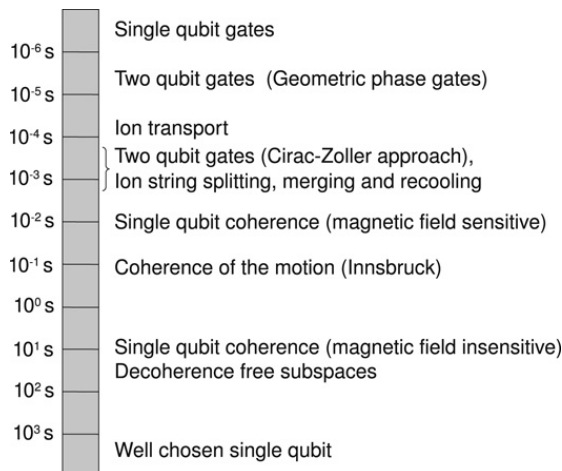


Fig. 2. Currently achieved time scales in ion trap quantum computing. All operations can be implemented faster than the relevant decoherence mechanisms.

frequency ω_t : as can be seen from Eq. (5) for ions in the motional ground state, the carrier transition is stronger by a factor of $1/\eta$ as compared with the sideband transitions. Therefore, driving the weak sideband transitions with strong laser fields, Stark shifts and off-resonant excitations arise (Steane et al., 2000). For example, to achieve a side-band Rabi frequency Ω_+ of a fraction f of the trap frequency ω_t , we need a laser field of strength $\Omega = \Omega_+/\eta = f\omega_t/\eta$. The Stark shift ΔE of the qubit transition due to the presence of the carrier transition is given by

$$\frac{\Delta E}{\hbar} = \frac{\Omega^2}{2\Delta} = \frac{1}{2\omega_t} \frac{f\omega_t\Omega_+}{\eta^2} = \frac{f}{2\eta^2} \Omega_+. \quad (8)$$

The phase evolution $\Delta Et/\hbar$ due to the AC-Stark shift becomes comparable with the desired Rabi flopping with frequency Ω_+ already for $f \sim \eta^2$ and thus typically for $f \sim 0.01$ ($\eta \sim 0.1$). Similarly, off-resonant excitations on the carrier transition might spoil the fidelity in this regime. In particular, Rabi oscillations on the carrier transition occur with amplitude A (Steane et al., 2000)

$$A = \frac{\Omega^2}{\Omega^2 + \omega_t^2} \approx \frac{\Omega^2}{\omega_t^2} = \frac{f^2}{\eta^2}, \quad (9)$$

where we assumed $\Omega \ll \omega_t$, which is justified by the conclusions from Eq. (8). Both the AC-Stark shift and the off-resonant excitations, can be at least partially canceled with methods described in Section 3.1.3. However, it still remains very difficult to drive Rabi flops on sidebands much faster than $\eta \omega_t$. Thus, it is hard to implement a two-qubit gate based on sideband transitions within one trap period.

2.3. Choice of qubit ions

A good qubit candidate must meet certain criteria. In the case of trapped ions it is usually sufficient to concentrate on long coherence times on the qubit transition compared with the manipulation times and on the technical feasibility of the required lasers. The scale to which the coherence time has to be compared with is given by the gate operation times of typically 0.1–500 μ s (c.f. Fig. 2).

Currently, two different schemes are used to store quantum information in trapped ions: In the first scheme, superpositions between the electronic ground state and an excited metastable electronic state provide the two-level system (optical qubit) (see Fig. 3a and 4). The excited $D_{5/2}$ -level in Ca^+ – similarly to Sr^+ and Ba^+ – has a life time of more than one second (Barton et al., 2000; Kreuter et al., 2004, 2005). In a second scheme, even larger coherence times can be achieved with superpositions encoded in the electronic ground-state of the ions (radio-frequency qubits) (see Fig. 3). Here, either the Zeeman or the hyperfine structure can be used. The lifetimes of these states are estimated to be much larger than any currently experimentally relevant timescales.

There are different aspects to be considered for optical and radio-frequency qubits: to fully exploit the potential of the optical qubit provided by the $S_{1/2}$ and $D_{5/2}$ -level in Ca^+ , a laser line width of less than 200 mHz is required. This fractional stability of about 10^{-15} is technically quite demanding, however, it has already been implemented for metrology purposes (Young et al., 1999a,b; Hall et al., 2006). The transition frequencies for radio-frequency qubits are usually below 10 GHz. Thus, it is much easier to get the required stable phase reference.

Radio-frequency qubits can be manipulated either directly by microwaves (Mintert and Wunderlich, 2001) or – as it is usually the case – by a Raman-process (Monroe et al., 1995a). Here, a single atom absorbs a photon from one laser field and

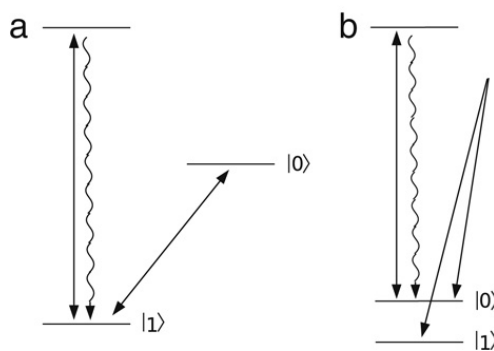


Fig. 3. Generic level schemes of atoms for optical qubits (left) and radio-frequency qubits (right). In addition to the two qubit levels $\{|0\rangle, |1\rangle\}$ usually a third rapidly decaying level is used for laser cooling and state read-out. While the optical qubit is typically manipulated on a quadrupole transition, radio-frequency qubit levels are connected with Raman-transitions.

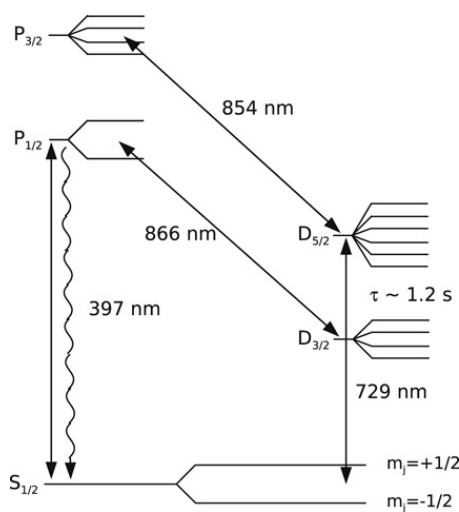


Fig. 4. Level scheme of $^{40}\text{Ca}^+$, with Zeeman substructure and required laser wavelengths for manipulation of the calcium ions.

emits a second one into a second laser field. The frequency difference of the two laser fields provides the necessary energy for the population transfer and thus only this frequency difference is important. The two laser fields are either derived from the same laser or a phase locking between two lasers can be implemented without resorting to optical frequency standards. Using optical fields instead of microwaves has the advantage that a much better spatial concentration of the power can be achieved and much higher Rabi-frequencies can be attained as with microwaves. Furthermore, by driving radio-frequency qubits optically with two anti-parallel beams, two photons can transfer their recoil onto the atom. Thus, the coupling to the ion motion is increased as compared with single photon transitions (larger Lamb–Dicke factors η) and as a consequence the speed of two-qubit gates can be higher. Choosing co-propagating beams, the coupling to the motion can be inhibited efficiently which has the benefit of suppressing the sensitivity to the ion motion.

For optical as well as for rf-qubits, coherence times are often limited by fluctuations of the magnetic fields. The reason is that usually the qubit basis states employed have different magnetic moments such that they experience an additional phase evolution due to the (fluctuating) magnetic field. Strategies to avoid these decoherence sources will be discussed in Section 3.1.2.

We note here that a good qubit must not necessarily combine a large coherence time to manipulation time ratio with high fidelity initialization and read-out capabilities: initialization and read-out can be implemented with an additional auxiliary ion of a different ion species. This idea has already been demonstrated by the NIST group (Schmidt et al., 2005): in this experiment aimed at implementing a frequency standard, the state of an individual Al^+ ion was detected via a Be^+ ion. However, for practical purposes it is desirable to initialize and read out the qubit ion directly.

Finally, a good qubit candidate must have all the relevant transitions in an accessible frequency regime. Generally, laser sources, fibers and detectors for short wavelengths are more expensive, less efficient and often more fault-prone than for longer wavelengths. However, ions tend to have short wavelength transitions. Thus, there are only a very limited number of ions which have strong transitions in the visible frequency range. In the quantum computing context, calcium, strontium and ytterbium ions appear to be attractive due to their relative large wavelength transitions. However, beryllium and magnesium have a relatively small atomic mass which leads to large Lamb–Dicke factors ($\eta \approx 0.3$ in some of the NIST experiments)

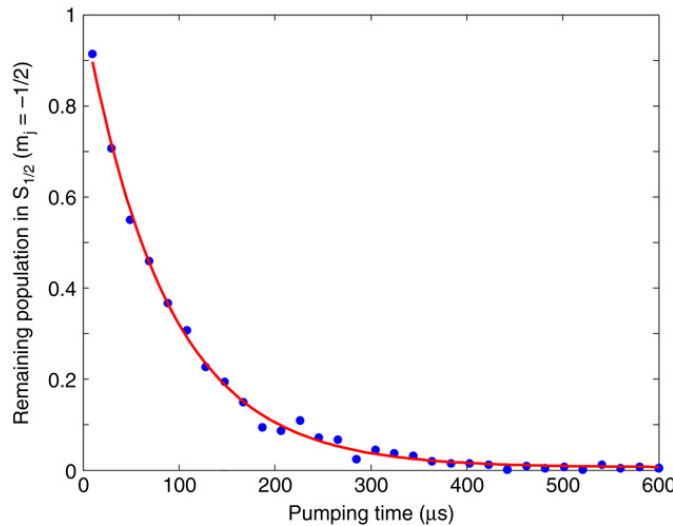


Fig. 5. Optical pumping of the $^{40}\text{Ca}^+$ $S_{1/2}$ ($m_j = +1/2$) level using frequency selection rather than polarization selection.

and eases coupling of the electronic and motional degrees of freedom and thus makes them attractive in spite of difficulties with laser radiation generation, manipulation and fiber optics.

2.4. Initialization and read-out

Prior to the implementation of a quantum algorithm, the qubits must be initialized in a well-defined state. For atoms, in general, this can be most conveniently achieved by optical pumping. This idea was introduced by Kastler (1950) and first implemented by Brossel et al. (1952) and by Hawkins and Dicke (1953). For reviews on optical pumping see Refs. Happer (1972), Weber (1977) and Wineland et al. (1980).

The general idea of optical pumping is that an atom is driven until it decays into a state where the drive does not act any longer. Usually, circularly polarized light is used to pump the atom into one of the extreme Zeeman-levels. Typically, the target state is occupied in less than 1 μs with a probability larger than 0.99. The initialization fidelity is usually limited by the quality of the polarization of the driving laser along the preferred axis of the qubit. In most cases, this axis is given by the direction of the magnetic field.

For fault-tolerant quantum computing, however, it appears that initialization fidelities exceeding 0.9999 are desirable. It is not clear whether such high preparation fidelities can be achieved with the methods described above. Furthermore, there exist situations where it is not possible to achieve a pure circular polarization along the quantization axis. The latter might happen for instance, because there is no optical access along the direction of the magnetic field to send a laser in. In these cases, a frequency rather than a polarization selection can be used for optical pumping if the ions offer a spectrally narrow transition (Roos et al., 2006).

We illustrate this procedure here for the $^{40}\text{Ca}^+$ -ion: with a narrow band laser the ion is excited on the $S_{1/2}$ ($m_j = +1/2$) \longleftrightarrow $D_{5/2}$ ($m_j = -3/2$) transition (see Fig. 4) and simultaneously the D level is coupled to the $P_{3/2}$ level with a broad band laser at 854 nm. In this way the population of the $S_{1/2}$ ($m_j = +1/2$) state is effectively coupled to the rapidly decaying $P_{3/2}$ ($m_j = \{-3/2, -1/2\}$) levels while the $S_{1/2}$ ($m_j = +1/2$) level is not touched. Fig. 5 shows the depletion of the initially fully populated $S_{1/2}$ ($m_j = +1/2$) level with time. Pumping time constants of about 10 μs have been demonstrated in Innsbruck.

In principle, the attainable pumping efficiency is only limited by the strongest Rabi frequency and pumping time. Assuming a typical transition splitting of the various Zeeman transitions of a few MHz, Rabi frequencies Ω_{Rabi} lower than $2\pi \times 10$ kHz are required to keep the off-resonant excitations $P_{\text{off}} \approx \Omega^2/\Delta^2$ (see Eq. (9)) of the unwanted transitions below 10^{-4} . From that, we estimate that within 1 ms an initialization fidelity of 0.9999 can be reached. In experiments in Innsbruck, preparation fidelities exceeding 0.999 have already been observed (Roos et al., 2006).

At the end of a quantum algorithm the quantum register needs to be measured. Radiation coupling to only one of the qubit levels can be used here. This idea was introduced by Dehmelt (1975) and is often termed electron shelving. Experimentally it was first implemented by Nagourney et al. (1986), Sauter et al. (1986), and by Bergquist et al. (1986).

Referring to the level scheme of $^{40}\text{Ca}^+$ in Fig. 4, the ion does not fluoresce under irradiation of light on the $S_{1/2} \rightarrow P_{1/2}$ and $D_{3/2} \rightarrow P_{1/2}$ transitions if its valence electron is in the $D_{5/2}$ -state. If the electron, however, is in either the $S_{1/2}$ -, $P_{1/2}$ - or $D_{3/2}$ -state, the ion will scatter approximately 10^7 – 10^8 photons/s. A lens system collects typically 10^{-3} – 10^{-2} of this fluorescence light such that with a photomultiplier tube (quantum efficiency $\sim 30\%$) about 30 photons/ms can be detected. As typical background count rates of photomultiplier tubes are usually well below 1 count/ms, one expects exceedingly high state detection fidelities when collecting fluorescence for detection times of more than one millisecond. However, this reasoning

holds only if the ion has a negligible probability to decay either from the $P_{1/2}$ to the $D_{5/2}$ or from the $D_{5/2}$ to the $S_{1/2}$ or the $D_{3/2}$ level during the detection time. In practice, these two constraints lead to an optimal detection time where the error due to the Poissonian spread of the number of scattered photons is balanced with the relaxation time scales (Roos, 2000; Acton et al., 2006; Myerson et al., 2008). Typical detection times are about one millisecond with detection fidelities exceeding 0.99. The fidelity can be further increased by analyzing the arrival times of the photons with a maximum likelihood method and thus identifying some events when the $D_{5/2}$ level decayed during the detection (Myerson et al., 2008).

Other qubits can be detected very similarly. If the energy separation of the two qubits, however, is not large enough to allow for selection via the laser frequency, polarization of the laser field can be used. For instance for ${}^9\text{Be}^+$, circular polarization ensures that predominantly only one of the two qubit states scatters photons (Sackett et al., 2000; Langer, 2006).

The detection efficiency can be further increased when the quantum state is mapped onto auxiliary qubits prior to its measurement: for this, one prepares first an additional qubit (the ancilla qubit) in state $|0\rangle$. A controlled-NOT operation maps then the qubit $\alpha|0\rangle + \beta|1\rangle$ onto the combined state $\alpha|00\rangle + \beta|11\rangle$ of the two qubits. Measuring both qubits yields an improved fidelity as compared with measuring a single qubit if the fidelity of the ancilla qubit state preparation and the controlled-NOT operation are high enough. Schatz et al. (2005) demonstrated this procedure, albeit preparing the ancilla ion in $(|0\rangle + |1\rangle)/\sqrt{2}$ and replacing the controlled-NOT with a controlled phase gate (see Section 2.6.4) followed by a single-qubit rotation on the ancilla.

Hume et al. (2007) present another variant to improve the state detection fidelity by measuring the qubit repeatedly. In this experiment, the qubit is encoded in superpositions of the ground state and the excited qubit level of ${}^{27}\text{Al}^+$. This qubit state is first transferred to a ${}^9\text{Be}^+$ ion by a series of laser pulses (Schmidt et al., 2005): a first pulse on the red sideband on an auxiliary transition of the Al^+ ion inserts one motional quantum only if the Al^+ ion is in the ground state. This motional excitation is transferred to the ${}^9\text{Be}^+$ ion with a red sideband pulse on the ${}^9\text{Be}^+$ ion which is then detected via the usual state dependent fluorescence method. Most importantly, the electronic auxiliary state of the Al^+ ion decays back to the ground state on a timescale of about 300 μs and not to the excited qubit state. Thus the information in which state the qubit is projected is still available in the Al^+ ion and this procedure can be repeated. Based on the photon counts from the ${}^9\text{Be}^+$ ion and previous detection results, another detection step is carried out. Repeating this procedure on average 6.5 times, Hume et al. (2007) achieve a detection efficiency of 0.9994. The accuracy of this method is only limited by processes which couple the excited qubit state of the Al^+ ion ($\sim 21\text{ s}$) to one of the electronic levels which does not decay to the ground state.

Very recently, Myerson et al. (2008) took advantage of the arrival times of the photons and combined it with the adaptive scheme just discussed. Thus they reached within an average detection time of 145 μs efficiencies of about 0.9999 of a qubit encoded in the S-D manifold of a single ${}^{40}\text{Ca}^+$.

2.5. Single-qubit gates

It can be shown that all quantum algorithms can be broken down into a sequence of single-qubit operations plus a specific two-qubit operation, e.g. a conditional phase gate, a controlled-NOT gate or a $\sqrt{\text{SWAP}}$ gate (Deutsch, 1989; Nielsen and Chuang, 2000). In ion traps, single-qubit operations are usually easy to implement and thus it is reasonable to use this approach to attain universal quantum computing.

Rabi oscillations between the two qubit levels (see Fig. 6) implement such single-qubit operations. Mathematically, we can describe the effect of resonant radiation inducing such a coupling by a rotation $R^C(\theta, \varphi)$ acting on the state vector $\alpha|0\rangle + \beta|1\rangle$ (c.f. Nielsen and Chuang (2000)):

$$\begin{aligned} R^C(\theta, \varphi) &= \exp(i\theta/2(e^{i\varphi}\sigma_+ + e^{-i\varphi}\sigma_-)) = I \cos \theta/2 + i(\sigma_x \cos \varphi - \sigma_y \sin \varphi) \sin \theta/2 \\ &= \begin{pmatrix} \cos \theta/2 & ie^{i\varphi} \sin \theta/2 \\ ie^{-i\varphi} \sin \theta/2 & \cos \theta/2 \end{pmatrix}, \end{aligned} \quad (10)$$

where $\sigma_+ = \begin{pmatrix} 0 & 1 \\ 0 & 0 \end{pmatrix}$ and $\sigma_- = \begin{pmatrix} 0 & 0 \\ 1 & 0 \end{pmatrix}$ are the respective atomic raising and lowering operators. $\sigma_x = \begin{pmatrix} 0 & 1 \\ 1 & 0 \end{pmatrix}$ and $\sigma_y = \begin{pmatrix} 0 & -i \\ i & 0 \end{pmatrix}$ are the Pauli-spin matrices. The angles θ and φ specify the rotation.

Often single-qubit operations are visualized by use of the so-called Bloch sphere. We identify the north pole of the Bloch sphere with logical $|0\rangle$ (the energetically higher state) and the south pole with $|1\rangle$ (see Fig. 7). In the Bloch picture, the angle φ specifies the axis of rotation in the equatorial plane and θ the rotation angle (pulse area), and thus any linear combination of σ_x and σ_y operations can be implemented with laser pulses.

Rotations around the z axis can be decomposed into rotations around the x and the y axis. Alternatively, all following rotations on that qubit can be shifted by $-\Delta\varphi$ to achieve effectively a rotation about the z axis by $\Delta\varphi$. Finally, a far detuned laser beam can shift the relative energy ΔE of the eigenstates due to an AC-Stark effect by $\Delta E = \Omega^2/2\Delta$ (c.f. Eq. (8)). Thus, after a time $t = \hbar\Delta\varphi/\Delta E$ the desired phase shift is acquired.

The relevant control parameters in the ion trap experiments are the pulse area $\theta = \Omega\tau$ (Rabi frequency Ω , pulse length τ) and the phase of the laser field φ . These control parameters can be conveniently controlled with an acousto-optical

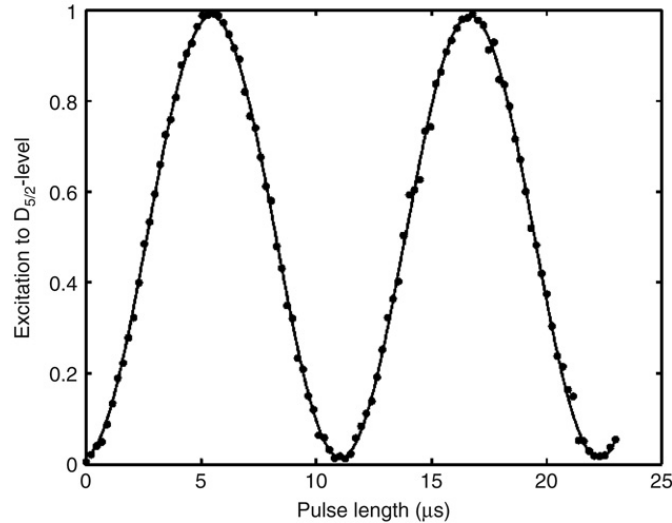


Fig. 6. Rabi oscillations of a single Ca^+ ion. Each dot represents 1000 experiments, each consisting of initialization, application of laser light on the qubit transition and state detection.

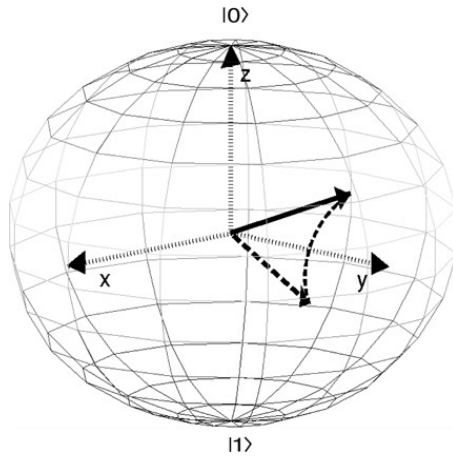


Fig. 7. Rotation around the y axis visualized on the Bloch-sphere.

modulator in double-pass configuration (c.f. [Donley et al. \(2005\)](#)) by changing the amplitude and phase of the RF field driving the acousto-optical modulator.

We will give here a quick interpretation of the phase φ : After optical pumping the experiments start with the ion qubits in an energy eigenstate. Thus the electric field of the resonant excitation laser builds up a dipole (or quadrupole) moment oscillating in phase with the field at the laser frequency. In this way, the first laser pulse (whose length is not a multiple of π) sets the phase reference for all subsequent operations on that ion. Thus, it becomes very intuitive to see e.g. that shifting the phase of a second excitation field by π inverses the evolution.

In ion traps, single-qubit manipulations are routinely carried out with fidelities exceeding 0.99 ([Knill et al., 2008](#)). Single-qubit-gate fidelities are usually limited by laser intensity fluctuations and in the case of single photon transitions by the finite temperature of the ion crystal and in the case of Raman transitions also by spontaneous emission from the intermediate level. In the Lamb-Dicke limit (i.e. the extension of the ground-state wave function is much smaller than the projection of wavelength of the light onto the motion), the effective Rabi frequency Ω_{eff} of the transition is given by ([Wineland et al., 1998](#))

$$\Omega_{\text{eff}} \approx \Omega \prod_i (1 - n_i \eta_i^2), \quad (11)$$

where i labels all motional modes, n_i is their vibrational quantum number and η_i denotes the corresponding Lamb-Dicke factor. Here, in contrast to Eq. (2), the second order in η was taken into account. Ω is the Rabi frequency for an ion (string) completely cooled to the ground state of the trap. For Raman transitions, η_i can be made quite small ($\sim 10^{-7}$) by using co-propagating beams such that the Rabi frequency is given just by Ω (the same reasoning holds for microwaves). Thus, in practice, only single-qubit operations on optical qubits suffer from finite temperature effects.

The speed of single-qubit rotations is often limited by the acousto-optical modulator used to control the light field: during switching the light field, phase and amplitude chirps appear which can spoil gate fidelities considerably. Further

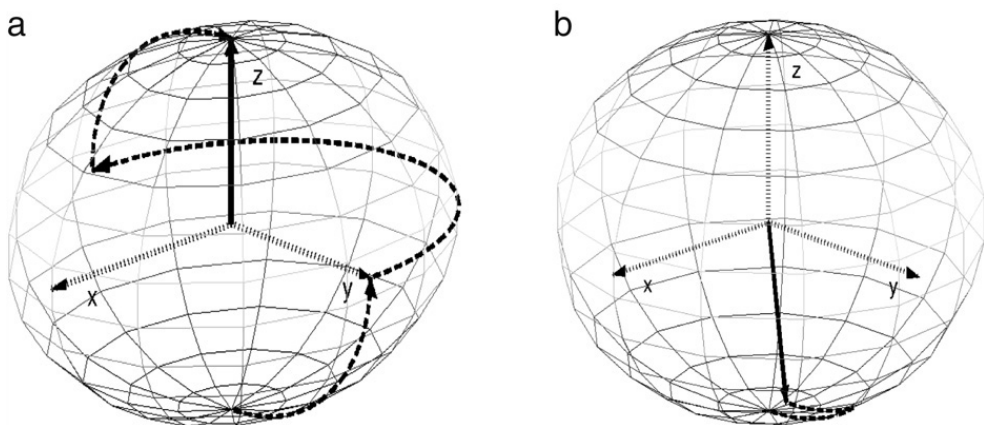


Fig. 8. Evolution of the Bloch vector on the Bloch sphere for a bit flip with the pulse sequence $R^C(\pi/2, \pi)R_z(\pi)R^C(\pi/2, 0)$ (left-hand side, see text for an explanation). The right-hand side displays the state evolution for a Rabi frequency corresponding to 0.3 of the one on the left-hand side (pulse sequence $R^C(0.3\pi/2, \pi)R_z(0.3^2\pi)R^C(0.3\pi/2, 0)$).

speed limitations are set by the amount of available laser power and more fundamentally by transitions close by, e.g. due to other Zeeman levels. Excitations on unwanted transitions due to strong laser fields transfer the population out of the computational subspace and thus spoil the fidelity.

2.5.1. Individual addressing of ion qubits

Individual addressing of qubits is particularly difficult if multi and single-qubit gates have to be carried out in the same trap: reasonable gate times are only possible for high trap frequencies resulting in small ion-ion spacings, which, in turn, require very well-shaped laser beams to address the ions.

The most straightforward way to achieve single ion addressing is to focus the qubit manipulation laser strongly. In the Innsbruck experiments a waist of 2 μm FWHM reliably distinguishes between ions spaced by 5 μm. Including deviations from a Gaussian beam shape, a 1000-fold reduction of the light intensity at the position of the adjacent ions as compared with the addressed ion can be achieved. This corresponds to an unwanted Rabi frequency of 0.03 on the adjacent ions with respect to the addressed ion (addressing error $\epsilon = \frac{\Omega_{\text{neighboring}}}{\Omega_{\text{addressed}}} = 0.03$). A complication arises from the fact that one would like to irradiate the ion string with the laser beam perpendicular to the trap axis to resolve the ion positions. This, in turn, leads to a strongly reduced coupling of the laser field to the ion motion along the axial direction. In Innsbruck, an angle of about 68° between the laser beam and the trap symmetry axis was chosen as a compromise between the two diametral requirements.

To fulfill the stringent requirements for quantum computation, one could use only every second ion thus increasing the qubit–qubit distance. However, with an increasing number of ions, the Lamb–Dicke factor tends to become smaller which in turn results in slower two-qubit operations. Furthermore, the more complicated normal mode spectrum might reduce the obtainable fidelity.

A more favorable method to reduce the effect of addressing imperfections is to use composite pulses also discussed in Section 2.7.3: here a single pulse is split into several smaller pulses. As an example, we consider here the realization of an $R^C(\pi, 0)$ operation with the pulse sequence $R^C(\pi/2, \pi)R_z(\pi)R^C(\pi/2, 0)$ (see Fig. 8). The first pulse ($R(\pi/2, 0)$) moves the Bloch vector of the addressed qubit into the equatorial plane, while the Bloch vectors of the unaddressed qubit i is rotated by the addressing error angle $\epsilon_i \pi/2$. The AC-Stark pulse $R_z(\pi)$ (e.g. implemented with the laser tuned off resonance) rotates the phase of the addressed qubit by π , while the phases of all other qubits are rotated only by $\epsilon_i^2 \pi$. The last $R(\pi/2, \pi)$ pulse finalizes then the rotation on the addressed qubit, while on the other qubits the effect of the first pulse is undone to a large extent for sufficiently small ϵ_i^2 . Fig. 8b illustrates this behavior on the Bloch sphere for a rather large addressing error of 0.3. We note that if the addressing imperfection of the operations is well-known, much better results can be achieved. For instance Haljan et al. (2005b) choose the length of a spatially inhomogeneous R_z pulse such that two qubits acquire a phase difference of π (Lee, 2006). In this way, one can afford addressing errors ϵ close to unity. Similar techniques were also used by Kielinski et al. (2001).

This composite pulse technique uses the fact that single-qubit operations commute on different ions. This is not the case for sideband transitions as multiple ions interact simultaneously with the a vibrational mode. However, it can be shown that by splitting sideband pulses into a sufficiently large number of pulses (~ 5) errors in the population of the vibrational mode are undone before they get large (Hänsel, 2003). Thus, addressing errors can also be suppressed in this case with composite pulses. A related technique is addressing in frequency space (Staanum and Drewsen, 2002; Schrader et al., 2004; Haljan et al., 2005b): here an inhomogeneous laser or a magnetic field gradient induces different transition frequencies for each qubit. Thus the laser predominantly interacts with the qubit whose transition frequency matches the laser frequency. The disadvantage, however, is that in this case one must keep track of the phases of all qubits individually. In addition, it is necessary to control the strength of the gradient field sufficiently well to avoid dephasing of the qubits. This can be a serious

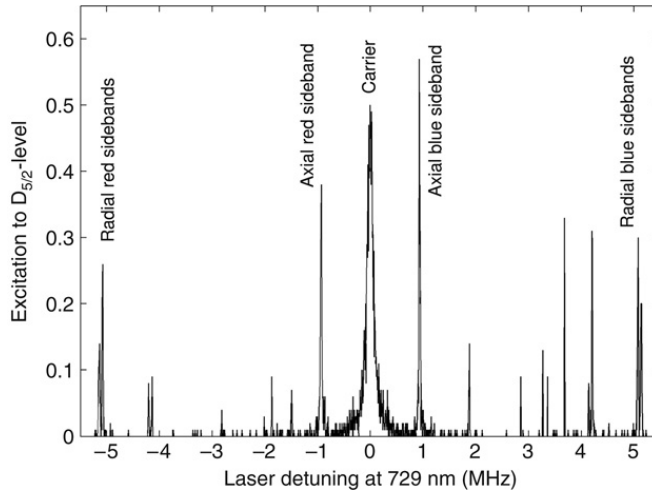


Fig. 9. Spectrum of a single trapped $^{40}\text{Ca}^+$ ion cooled close to the Doppler limit (see text). On resonance ($\Delta = 0$) the strong carrier transition appears as well as for positive (negative) detunings Δ blue (red) sidebands are visible. The motional frequencies of the single ion can be deduced from the spectrum to amount to $\omega_z \approx 2\pi \times 1$ MHz (axial frequency) and $\omega_{r_{x,y}} \approx 2\pi \times 5$ MHz (radial frequencies). In addition, higher order modes are visible at $\Delta = m\omega_z \pm m\omega_r$.

problem when the qubit register is large and some of the qubits experience a very fast phase evolution due to the gradient field.

There are various other possibilities to achieve effective addressing (see e.g. Wineland et al. (1998)): One particularly useful trick consists in changing the distance of the ions between the quantum operations by altering the trap stiffness (see e.g. Refs. Rowe et al. (2001) and Reichle et al. (2006b)). In this way the relative phase of the operations on the individual ions can be changed allowing one to address even individual groups of ions for non-local operations. In addition, it was demonstrated that a two-ion string can be placed in such a way in the trap that the ions have a different micromotion amplitudes. This in turn leads to different transition strengths and thus to single particle addressing capabilities (Monroe et al., 1999; King, 1999).

2.6. Two-qubit gates

One route to achieve a universal set of gates (Deutsch, 1989), is to complement single-qubit operations with two-qubit gate operations. These operations are one of the most important ingredients of a quantum computer as they provide the possibility to entangle two qubits. In combination with single-qubit operations they allow for implementation of any unitary operation (Barenco et al., 1995).

In many implementations of quantum algorithms with trapped ions, the fidelity of the whole algorithm was limited by the fidelity with which the two-qubit operations were implemented. Thus, currently the implementation of high-fidelity entangling gates is of crucial importance. In the following, we will discuss the Cirac-Zoller gate (Section 2.6.2), the Mølmer-Sørensen gate (Section 2.6.3) and the so-called geometric phase gate (Section 2.6.4), before we briefly summarize various additional proposals for two-qubit gates (Section 2.6.5).

2.6.1. Motion of ion strings

The interaction between the ionic qubits can be mediated by motional degrees of freedom that serve as a quantum bus for distributing quantum information between the ions. Therefore, we will discuss first the manipulation of the motion of single ions and ion strings (see also Ref. Leibfried et al. (2003a)). The basic level scheme representing a single ion coupled to a single motional mode is depicted in Fig. 1. A laser field resonant with the carrier transition of frequency ω_{qubit} drives transitions with Rabi frequency Ω_{eff} where the motional state is not changed (see Eq. (11)). If the laser field, however, is detuned by the trap frequency towards higher energies, the so-called blue sideband is excited (see Eq. (5)) and the operation

$$R^+(\theta, \varphi) = \exp \left[i \frac{\theta}{2} (e^{i\varphi} \sigma^+ a^\dagger + e^{-i\varphi} \sigma^- a) \right] \quad (12)$$

is carried out. Here σ^\pm are the atomic flip operators which act on the electronic quantum state of an ion by inducing transitions from the $|g\rangle$ to $|e\rangle$ state and vice versa (notation: $\sigma^+ = |e\rangle\langle g|$). The operators a and a^\dagger denote the annihilation and creation of a phonon at the trap frequency ω , i.e. they act on the motional quantum state. As in Eq. (10), the parameter θ depends on the strength and the duration of the applied pulse, and φ denotes the relative phase between the optical field and the atomic polarization. Importantly, the electronic and motional degree of freedom change simultaneously. Similarly for the opposite detuning the red sideband can be excited. Fig. 9 shows a spectrum of a single trapped $^{40}\text{Ca}^+$ ion near the qubit transition. At a detuning of ± 1 MHz, the red and the blue axial sidebands appear, respectively. In addition, radial sidebands

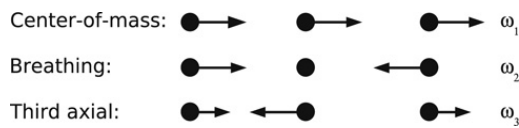


Fig. 10. Normal modes of a three-ion crystal along the axial direction with motional frequencies ω_i .

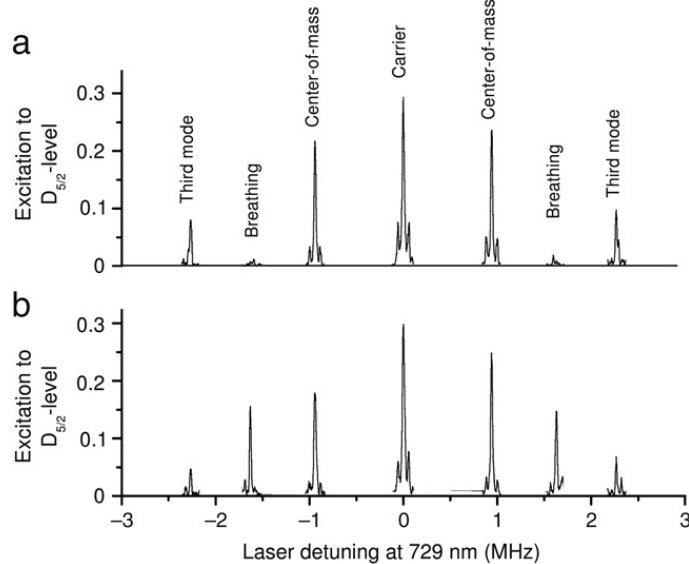


Fig. 11. Excitation spectra of a three-ion string. In Fig. 11(a), the exciting laser is addressed to the center ion, while in Fig. 11(b) the laser is addressed to the left ion. Visible are excitations of the motional modes as well as of the carrier transition. If the center ion is addressed Fig. 11(a), the breathing mode cannot be excited efficiently. The residual excitation of the breathing mode is most likely due to laser light interacting with the outer ions (see Section 2.5.1 on imperfect addressing).

(detuning $\sim \pm 5$ MHz) and higher order sidebands are visible. For the applied laser power and excitation time, the carrier transition is strongly saturated while the sidebands are only weakly saturated. This indicates that the sideband transitions are weaker than the carrier transition as is expected from Eqs. (5) and (7). For the experiment shown in Fig. 9, the single $^{40}\text{Ca}^+$ -ion was cooled to a temperature of $(\bar{n}_x, \bar{n}_y, \bar{n}_z) \approx (3, 3, 16)$ via Doppler cooling, while the Lamb-Dicke factors were $(\eta_x, \eta_y, \eta_z) \approx (0.01, 0.01, 0.08)$ (in this particular experiment the angle of the laser beam was given by (49.2, 49.2, 22.5)).

For quantum logic experiments, however, the case of multiple ions is more interesting. Since the Coulomb interaction couples the ions strongly together, it is useful to find the normal modes of the ion string (Steane, 1997; James, 1998; Šašura and Bužek, 2002). Taking a three ion string as an example and concentrating on the axial direction, we find three normal modes: center-of-mass, breathing (or stretch) and an additional axial mode. Fig. 10 illustrates the motion of each ion associated with each mode. Denoting the center-of-mass modes frequency ω_1 , the breathing mode has a frequency of $\omega_2 = \sqrt{3}\omega_1$ and the third axial mode has a frequency of $\omega_3 = \sqrt{29/5}\omega_1$. Fig. 10 indicates the relative motions of the ions. The strength with which each mode couples to the motion is characterized by the eigenvectors $(1, 1, 1)/\sqrt{3}$ for the center-of-mass, $(1, 0, -1)/\sqrt{2}$ for the breathing and $(1, -2, 1)/\sqrt{6}$ for the third axial mode (James, 1998). This means that the center ion does not couple to the breathing mode and that the left and right ions couple with opposite phase factors to it. Fig. 11 illustrates that the breathing mode cannot be efficiently excited when the center ion is addressed (see Section 2.5.1 for addressing of individual ions). For further details of the normal modes of ion strings (including larger ion strings), we refer to James (1998).

While measuring the spectra of ion strings needs only reasonably cold temperatures (e.g. ions cooled to the Lamb-Dicke limit), coherent operations on the sideband need usually ground state cooling of this particular mode. The reason can be seen already in Eq. (5) which predicts that the sideband Rabi frequency strongly depends on the vibrational quantum number of the corresponding motional mode and thus excitation on the sideband is incoherent for a finite temperature of this motional mode. On the other hand, this strong sensitivity of the sideband excitations to the motion will be the key to couple ion qubits. To allow for coherent sideband operations, the motion of the mode in question is cooled to the ground state, although one could also imagine using any well-defined motional quantum number. Finally, we extend Eq. (5) to take all motional modes into account (c.f. Eq. (11) and Wineland et al. (1998)):

$$\Omega_{\text{eff}}^+ = \Omega (\sqrt{n_{\text{bus}} \eta_{\text{bus}}}) \prod_m (1 - n_m \eta_m^2). \quad (13)$$

Here Ω_{eff}^+ is the effective Rabi frequency on the blue sideband, Ω the ideal carrier Rabi frequency and n_{bus} denotes the quantum number of the bus mode (i.e. the mode which will be used to couple the qubits), while η_{bus} labels its corresponding

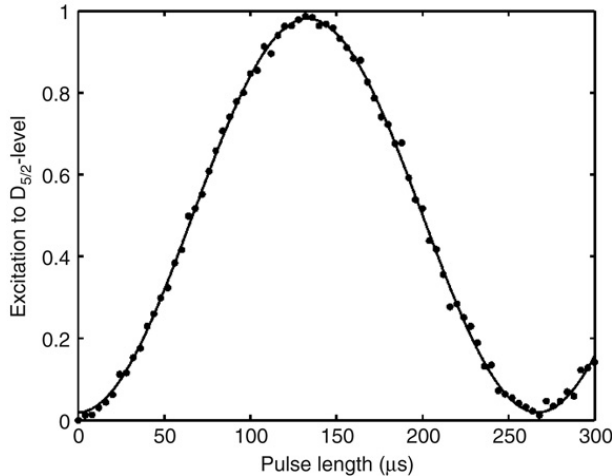


Fig. 12. Rabi oscillation on the blue sideband of the center-of-mass mode. The data were taken on a string of two $^{40}\text{Ca}^+$ ions whose center-of-mass mode was cooled to the ground state. Only one of the ions was addressed. The population oscillates between the $|S, 0\rangle$ and the $|D, 1\rangle$ state of the addressed ion.

Lamb-Dicke factor. The index m runs here over all modes except the bus mode. Since the influence of these modes on the sideband Rabi frequency Ω_{eff}^+ is strongly reduced, they are often termed spectator modes.

As discussed in Refs. Neuhauser et al. (1978), Wineland and Itano (1979) and Marzoli et al. (1994), ground state cooling in ion traps can be achieved by driving the red sideband (c.f. Fig. 1). Each absorption of a photon on the red sideband followed by a spontaneous emission on the carrier transition takes out one motional quantum of energy (Stenholm, 1986; Eschner et al., 2003). It usually takes too long to wait for spontaneous decay of the upper level. Therefore, in most experiments, the lifetime of the upper state is shortened by quenching the state with a laser connecting it to a fast decaying state.

Experimentally, sideband cooling to the motional ground state was demonstrated first by the NIST-group with a single mercury ion (Diedrich et al., 1989) and then later with various other ion species ((Monroe et al., 1995b; Roos et al., 1999; Peik et al., 1999); for a review see Leibfried et al. (2003a)). For ion strings sideband cooling works similarly as for single ions. The multiple normal modes can be cooled sequentially (Monroe et al., 1995b; Roos et al., 1999). However, for ion crystals, the Lamb-Dicke factors η_i tend to be smaller due to the increased mass as compared with single ions (for a definition of η see Section 2.2) and thus the cooling process is slowed down.

Once the motion of a particular mode of the ion string is cooled to the ground state, irradiation on the respective blue sideband leads to Rabi oscillations (assuming the electronic degree of freedom of the ion is also in the ground state). Fig. 12 shows such a Rabi oscillation on the blue sideband of the center-of-mass mode of a string of two $^{40}\text{Ca}^+$ ions.

Another promising route to cool ions below the Doppler limit is based on electromagnetically induced transparency (EIT) (Roos et al., 2000; Morigi et al., 2000). Here, two interfering laser fields are used to shape the atomic absorption spectrum in such a way that sharp features appear in it which can be used to suppress heating effects on the carrier and blue sideband transitions while still maintaining absorption on the red sideband transitions. In general, EIT is a very versatile tool as the free parameters of the two laser intensities and detunings from the atomic resonance allow one to adjust the atomic absorption spectrum to the actual needs (equilibrium temperature and cooling speed). Furthermore, Roos et al. (2000) achieved simultaneous cooling of up to three modes close to the ground state with a single setting.

2.6.2. Cirac-Zoller gate

Conceptually, the Cirac-Zoller phase gate is the simplest of the two-qubit gates presented here and is therefore discussed first (Cirac and Zoller, 1995). It requires single ion addressing and ground-state cooling of the bus mode. On the other hand, for the Mølmer-Sørensen type gates (Sørensen and Mølmer, 1999; Milburn et al., 2000; Leibfried et al., 2003b) both ions are illuminated simultaneously and the ion string have to be cooled only into the Lamb-Dicke limit. The geometric phase gate (Leibfried et al., 2003b) is closely related to the Mølmer-Sørensen gate. However, it will be presented separately as its implementation looks different.

Cirac and Zoller proposed the following procedure to perform a two-qubit gate between two ions in an ion string (Cirac and Zoller, 1995): First, the quantum information of the first qubit is transferred to the motional degree of freedom of a mode (the bus mode) of the ion crystal. Importantly, the resulting motional state affects not only the addressed ion itself but the ion string as a whole. Therefore, on a second ion, operations conditioned on the motional state of the ion string can be carried out. Finally, the quantum information of the motion is mapped back onto the first ion of the string.

The individual steps of the Cirac-Zoller phase gate are as follows: a laser pulse directed to the first ion with length $\theta = \pi$ and frequency $\omega_{\text{qubit}} - \omega_{\text{trap}}$ (red sideband) moves all population present in the $|0, e\rangle$ -state to $|1, g\rangle$ -state (see left panel in Fig. 13). However, if the first ion is in the $|0, g\rangle$ -state, no state transfer happens. Thus, we have effectively mapped the quantum information from the electronic degree of freedom to the motion. Note that the coupling strength on the sideband depends strongly on the vibrational excitation. Therefore, this procedure works only if one knows the vibrational state such

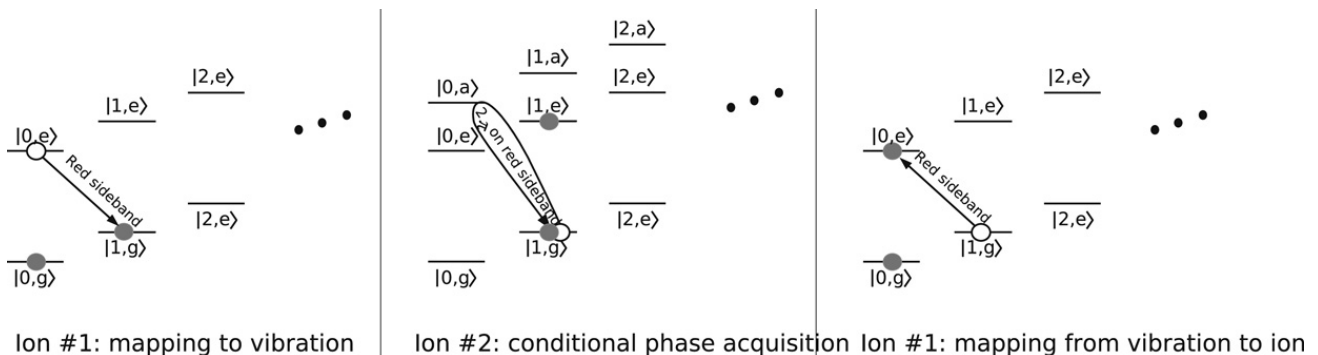


Fig. 13. Graphical representation of the three steps to perform a phase gate between two ions with an electronic ground state $|g\rangle$, an excited state $|e\rangle$ and an auxiliary state $|a\rangle$.

that one can properly adjust the laser intensity to achieve a π pulse. With the quantum information of the first ion in the motion, we can exploit the common motion of the two ions and perform a conditional operation on the second ion. We follow here the original proposal (Cirac and Zoller, 1995) and use a 2π rotation between $|1, g\rangle$ and a third auxiliary state $|0, a\rangle$ on the red sideband (see center panel in Fig. 13). Importantly, only the $|1, g\rangle$ state is coupled to another level; for the states $|0, e\rangle$, $|1, e\rangle$ and $|0, g\rangle$, however, the coupling vanishes as there are no levels present with the appropriate energy. Effectively, we have therefore performed the following operation:

$$\begin{array}{rcl} 2\pi \\ |0, e\rangle & \longrightarrow & |0, e\rangle \\ |1, e\rangle & \longrightarrow & |1, e\rangle \\ |0, g\rangle & \longrightarrow & |0, g\rangle \\ |1, g\rangle & \longrightarrow & -|1, g\rangle \end{array} \quad (14)$$

This implements a phase shift of the second ion conditioned on the motional state. Finally, another π pulse on the red sideband addressed to the first ion maps the quantum information present in the motion back onto the first ion and in total a phase gate between the two ions is performed. To turn this phase gate into a controlled-NOT operation, one can apply an $R^c(\pi/2, \varphi_i)$ pulse ($i = 1, 2$) to the target ion on the carrier transition (see Eq. (10)) before and after the phase gate. Choosing a particular phase relation $\varphi_2 - \varphi_1$ either an ordinary controlled-NOT gate or a zero controlled-NOT operation is obtained.

The heart of this procedure, i.e. the dynamics presented in Eq. (14), was demonstrated by the NIST group with a single beryllium ion (Monroe et al., 1995a). The Innsbruck group implemented the complete protocol with individual addressing of two calcium ions (Schmidt-Kaler et al., 2003c,b). Section 4.1 describes both experiments.

Jonathan et al. (2000) present a generalization of this gate where they propose to drive the system so strongly that due to AC-Stark shifts the eigenstates of different vibrational quantum numbers (the dressed states) get the same energy. Thus a motional dynamics can be achieved just with carrier pulses of appropriate phase. Essentially, this proposal trades faster gate speeds against more sensitivity to laser intensity noise as the energy of the dressed states depends strongly on the laser power.

2.6.3. Mølmer–Sørensen gate

Another possibility to implement a two-qubit gate is to use laser radiation tuned close to the motional sidebands (Sørensen and Mølmer, 1999; Mølmer and Sørensen, 1999; Sørensen and Mølmer, 2000; Solano et al., 1999). The basic principle is as follows: both ions are irradiated with a bichromatic laser field with frequencies $\omega_0 \pm (\omega_{\text{qubit}} + \delta)$, tuned close to the red and the blue sideband of a collective mode, respectively (see Fig. 14). The two frequencies sum up to twice the qubit frequency ω_{qubit} , each laser field itself, however, is not resonant to any level. Thus both ions can change their state only collectively and choosing an interaction time appropriately, the dynamics

$$\begin{aligned} |ee\rangle &\rightarrow (|ee\rangle + i|gg\rangle)/\sqrt{2} \\ |eg\rangle &\rightarrow (|eg\rangle + i|ge\rangle)/\sqrt{2} \\ |ge\rangle &\rightarrow (|ge\rangle + i|eg\rangle)/\sqrt{2} \\ |gg\rangle &\rightarrow (|gg\rangle + i|ee\rangle)/\sqrt{2} \end{aligned} \quad (15)$$

is achieved. To see that this gate leads to a universal set of gates, we introduce the new basis $|\pm\rangle_i = (|e\rangle_i \pm |g\rangle_i)/\sqrt{2}$. $|\pm\rangle_i$ are eigenstates of the unitary operation described by Eq. (15) and transform as $|++\rangle \rightarrow |++\rangle$, $|+-\rangle \rightarrow i|+-\rangle$, $|-+\rangle \rightarrow i|-+\rangle$, $|--\rangle \rightarrow |--\rangle$ by the action of the gate, where we omitted a global phase factor of $e^{-i\pi/4}$ on the

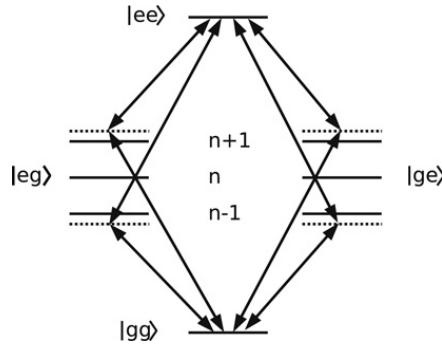


Fig. 14. Energy-level diagram of two trapped ions illustrating the principle of the Sørensen and Mølmer gate. The bus mode is populated with n phonons. Two laser beams tuned close to the blue and red sideband, respectively, drive the system via the dashed virtual levels between the $|n, gg\rangle$ and $|n, ee\rangle$ state. A similar process takes place if the ion string is either in the $|n, eg\rangle$ or in the $|n, ge\rangle$ state.

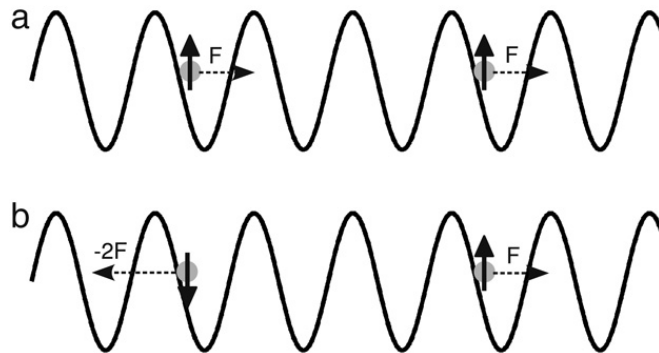


Fig. 15. Force on two ions in a standing wave of two laser fields. (a): both ions spin up. Both ions experience the same force (b) one ion spin down, the other spin up. Both ions experience opposing forces. Tuning the frequency difference of the two laser fields close to the breathing mode frequency, in (a) the motion of the ion string cannot be excited efficiently, while in (b) the breathing mode is excited.

right hand sides. This transformation is a conditional phase gate up to single-qubit phase-shifts and is known to be universal together with single-qubit operations.

The Mølmer–Sørensen gate has the particular feature that it does not require individual addressing of the ions and that it does not fail completely if the ion string were not cooled to the ground state. As will be described in Section 4.2, the NIST group entangled up to four ${}^9\text{Be}^+$ ions with this gate type (Sackett et al., 2000). Furthermore, Haljan et al. (2005b) created all four Bell states and implemented Grover's search algorithm with ${}^{111}\text{Cd}^+$ ions using this gate operation (see also Refs. Lee et al. (2005), Brickman et al. (2005) and Brickman (2007)).

Very recently, the application of a Mølmer–Sørensen gate to optical qubits excited on dipole-forbidden transitions has been analyzed (Roos, 2008). It was shown that fast, high-fidelity gate operations are achievable by smoothly switching on and off the bichromatic laser fields inducing the gate action. The experimental implementation of this technique has resulted in the creation of Bell states with a fidelity of 99.3(1)% (Benhelm et al., 2008b).

2.6.4. Geometric phase gate

The so-called geometric phase gate uses also two laser fields irradiating multiple ions at the same time. An interesting feature of this gate is that ideally during the gate operation the electronic state of the ions is not touched. Only a force dependent on the electronic states is applied such that for the various electronic states different phases are acquired (Milburn et al., 2000). In the scheme implemented by the NIST group (Leibfried et al., 2003b) two non-co-propagating laser fields create a standing wave (see Fig. 15). The difference of the two laser frequencies is tuned closely to one of the axial frequencies which leads to a walking wave. Thus, each ion experiences a periodic AC-Stark shift and a force depending on the slope of the spatial variation of the AC-Stark shift. Most importantly, the size and even the direction of the force can depend on the electronic state of the ion. Choosing the distance between the ions such that each ion experiences the same phase of the walking wave for a given time (see Fig. 15), ions are pushed in the same direction if they have the same electronic state. In this way, the breathing mode cannot be excited. However, if the ions are in different electronic states the forces on the ions are not the same and the breathing mode can be excited. Detuning of the drive from the motional mode is chosen such that the phase between the motion and the drive changes its sign after half the gate time. In this way, the ion string is driven back to the original motional state after the full gate time. This ensures that the motion is disentangled from the electronic state after the gate operation. The intermediate energy increase as compared to situations where the motion is not excited leads to the desired phase factor and the ions have picked up a phase factor that depends non-linearly on the internal states of both ions.

Leibfried et al. (2003b) implemented this gate with a fidelity of 0.97, limited mainly by the spontaneous decay from the P manifold of the Be^+ ions during the gate operation. This exceptional fidelity was reached because the gate avoids a number of imperfections in the first place. We mention here the absence of off-resonant excitations on the carrier transition. Furthermore, the gate execution time of about 10 μs is two to three orders of magnitude faster than the corresponding coherence time of the qubits and thus decoherence effects are small. To obtain a differential force on the ions, the NIST group used two laser beams detuned blue from the $S_{1/2} \rightarrow P_{1/2}$ transition by $2\pi \times 82$ GHz (fine structure splitting of the P state is 200 GHz). For the ratio of the forces on the $|\downarrow\rangle = |F=2, m_f=-2\rangle$ and the $|\uparrow\rangle = |F=1, m_f=-1\rangle$ state this yields: $F_\downarrow = -2F_\uparrow$. Additional Stark shifts can be efficiently suppressed by choosing almost perpendicular and linear polarizations for the laser beams (Wineland et al., 2003). Finally, Leibfried et al. (2007) discuss a version of this gate where the laser intensities impinging on the ions are controlled by transporting the ion crystal through the laser fields. Controlling the interaction of the ions by transport also offers the possibility of using spatially modulated magnetic fields to create the state dependent oscillating force (Leibfried et al., 2007).

These three gate types have different strengths and weaknesses. Both, the geometric phase gate and the Mølmer–Sørensen gate do not need single ion addressing. While this is often advantageous, it has the inconvenience that it is not straightforward to carry out these gates between specific ions in a string. Using segmented traps for moving and splitting ion strings (see Section 6) resolves this issue. Another route to introduce ion specific gates is to hide certain ions with single ion operations (see Section 4.5) such that these ions are not affected by the multi-qubit gate operation. The Cirac–Zoller gate on the other hand demands single ion addressing but allows for a straightforward implementation of quantum algorithms.

Another aspect is speed. The geometric phase gate can be executed quite fast as the laser can be tuned such that off-resonant transitions are quite unlikely. The Cirac–Zoller and Mølmer–Sørensen gates on the other hand require a laser tuned to or tuned close to a sideband transition. This automatically implies that the laser is detuned only by (approximately) the trap frequency from the strong carrier transition. Thus, it seems that the gate speed has to be much slower than a trap frequency (see Section 2.2). However, for special temporal and spectral arrangements of the laser field, it is possible to suppress the spectral contribution on the carrier transition so that gate times close to the trap period seem feasible.

Finally, it is important whether the gate works efficiently with magnetic field insensitive transitions. Qubits encoded in superpositions of levels connected via a magnetic field insensitive transition provide very long coherence times of many seconds (Section 3.1.2). In its originally proposed form, the geometric phase gate is very inefficient on magnetic field insensitive transitions because hyperfine states with a similar magnetic moment appear to experience similar AC-shifts (Langer, 2006). However, this could be circumvented by using a pair of laser beams tuned close (as compared to the qubit difference frequency) to a spectrally narrow transition to induce the state-dependent force (Aolita et al., 2007). In this way, one induces a spectral rather than a polarization dependent force. Another option is to recode the qubits for the conditional phase gate from a magnetic insensitive coding to a different coding (Langer, 2006). The Mølmer–Sørensen gate, on the other hand, has been already applied on magnetic field insensitive transitions (Haljan et al., 2005b). The Cirac–Zoller gate (either with composite pulses described in Section 2.7.3 or a third magnetic field insensitive transition as available for instance with the D manifold in $^{43}\text{Ca}^+$) can be also directly applied in these situations.

2.6.5. Other gate types

Another possibility to employ AC-Stark shifts for a two-qubit gate was demonstrated by Brune et al. (1994) with Rydberg atoms passing through a microwave cavity. We summarize here, the ion trap version implemented by Schmidt-Kaler et al. (2004). In these experiments, a laser was tuned close to the axial motional sideband of a single ion. The Rabi frequency of the blue motional sideband Ω_+ depends on the phonon occupation number n_z such that the resulting AC-Stark shift of the electronic levels due to the sideband resonance depends on the motional state:

$$\Delta E = \hbar \frac{\Omega_+^2}{2\Delta} = \hbar \frac{\eta_i^2 \Omega^2}{2\Delta} (n_z + 1), \quad (16)$$

where we used Eq. (5). Rotating the frame by $\exp(-\frac{\eta_i^2 \Omega^2}{2\Delta} t)$ removes the phase evolution of the two electronic levels in motional ground state $n_z = 0$. The relative phase of the two electronic states in the first excited state $n_z = 1$, however, evolves as $\varphi = \frac{\eta_i^2 \Omega^2}{2\Delta} t$. Thus, choosing the interaction time $t = \frac{2\pi\Delta}{\eta_i^2 \Omega^2}$, the phase gate operation $\text{diag}(1, 1, -i, i)$ is implemented, where we used the basis $\{|e, 0\rangle, |g, 0\rangle, |e, 1\rangle, |g, 1\rangle\}$.

This gate can also be generalized to multiple ions (Schmidt-Kaler et al., 2004). Here, all ions simultaneously interact with the laser beam. The situation is very reminiscent of the Mølmer–Sørensen gate: taking as an example a two-ion crystal, only transitions between the eigenstates with the same number of excited ions can be induced, e.g. between the $|ge\rangle$ and the $|eg\rangle$ (see Fig. 16). All other basis states acquire only a phase factor which can be corrected for with single-qubit operations. Using this method, starting from the $|eg\rangle$ state, the Bell state $(|ge\rangle + |eg\rangle)/\sqrt{2}$ was generated with a fidelity close to 0.9 by applying a pulse corresponding to a $\pi/2$ dynamics with trapped $^{40}\text{Ca}^+$ ions (H. Häffner et al., Innsbruck, unpublished).

Another gate type uses the dependence of the carrier Rabi frequency from the motional state (see Eq. (11)). Proposed by Monroe et al. (1997), it was implemented later by the same group on a single $^9\text{Be}^+$ ion (DeMarco et al., 2002). Essentially, a laser pulse on the carrier transition is applied, with the Lamb–Dicke parameter chosen such that for one motional state an even number of Rabi oscillations occurs, while for the other motional state an odd number of Rabi cycles occurs. This

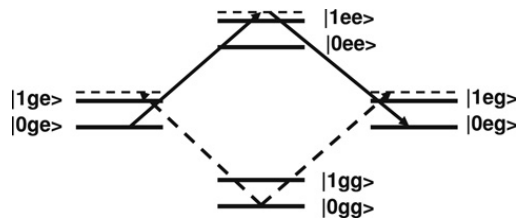


Fig. 16. Simplified level scheme of two trapped $^{40}\text{Ca}^+$ ions including the motional state of the bus mode (from Schmidt-Kaler et al. (2004)). The virtual levels are represented by dashed lines. A monochromatic laser beam can only induce transitions between the $|ge\rangle$ and the $|eg\rangle$ state (solid arrows). In addition, the $|gg\rangle$ state acquires an additional phase factor due to an AC Stark effect (dashed arrows).

way, the phase of an electronic state is only flipped in the latter case, while it remains unaffected in the former case. This implementation of a controlled-NOT operation requires, however, a reasonably large and tunable Lamb–Dicke factor of the bus mode η_b (the gate time is quadratic in $1/\eta_b$), while either all other motional modes are cooled to the ground state or their Lamb–Dicke factors are much smaller than η_b .

Finally, there have been quite a number of other promising gate proposals which are not implemented as of yet. Some of them rely – as some of the already presented gates – on state dependent AC-Stark shifts, albeit in the static regime (Cirac and Zoller, 2000; Steane, 2004; Staunum et al., 2004). The general idea here, is that an inhomogeneous laser beam changes the distance between the ions depending on their electronic state. Simulations show that the fidelities can be quite high and that the experimental requirements are not very demanding. For instance, only moderately low temperatures are required. Alternatively, the state dependent potential can be created with strong magnetic field gradients (Mintert and Wunderlich, 2001). Creation of sufficiently strong field gradients might be eased by implementing these gates in microfabricated ion traps where smaller ion-surface distances and microstructured current carriers would facilitate the generation of the required static or dynamic field gradients (Leibfried et al., 2007; Chiaverini and Lybarger, 2008; Ospelkaus et al., 2008).

Another gate class, which recently received much attention, uses short but strong laser pulses to strongly kick the ion string (García-Ripoll et al., 2003). Most interestingly, the corresponding gate operation times can be shorter than even one trap period. Choosing proper phases and amplitudes of the pulses, the ions are kicked in such a way that they acquire a state dependent phase due to their motion. Another gate variant uses a continuous irradiation with fast phase modulations (García-Ripoll et al., 2005). Based on these ideas, Duan and Kimble (2004) propose quantum computation in an array of trapped ions where the fast gates are used to induce a next neighbor interaction.

2.7. Apparative requirements

Experimental quantum computation requires exceedingly long coherence times as well as an exquisite control over the qubits. The former is achieved by decoupling the qubits from the environment, while the latter requires a well-defined and switchable interaction with the environment. In ion trap quantum computing, the qubits are held in free space with electromagnetic forces which hardly couple to the ion's internal degree of freedom. The control is achieved with strong laser fields such that during their interaction they still can be treated classically and entanglement between the laser field and ions is negligible. Thus the seemingly contradictory requirements – decoupling from the environment and controlled interactions – can be fulfilled.

For ion-trap quantum computing usually so-called linear Paul traps are used where the ions can form a linear ion chain (Raizen et al., 1992b; Drees and Paul, 1964). In these devices, a radio-frequency potential is applied to two electrodes which are parallel with the axis of the trap (see Fig. 17). These electrodes create an oscillating two-dimensional quadrupole potential that is translation invariant along the trap axis. If the frequency of the RF field is sufficiently large, the ions experience an effective restoring force to the center axis. Additionally, static electric fields confine the ions along the trap axis. The trap resides in an ultra-high vacuum vessel to reduce collisions with residual molecules and atoms as much as possible. For typical experiments, it is sufficient to describe the time dependent confining forces of the ion trap as if they resulted from a static three-dimensional harmonic potential. If the confinement perpendicular to the trap axis (radial direction) is much larger than the confinement along the trap axis, cold ions form a linear chain. Typical trap frequencies for the radial frequencies are between 4 and 10 MHz, while axial frequencies range mostly between 0.5 and 5 MHz.

For the control of electronic and motional states of the ions, lasers with high frequency and intensity stability are used. Acousto-optical modulators allow one to control both the frequency and the intensity. Typically, the lasers are either referenced to an ultra-stable cavity or to a molecular transition. Ions tend to have higher energy splittings as compared with atoms. Therefore, lasers emitting in the ultraviolet are often required. In the next paragraphs, we briefly describe the experimental setups used in the NIST and the Innsbruck experiments.

2.7.1. The NIST setup

Details of the NIST setup can be found in the Ph.D. thesis of Langer (2006), Kielpinski (2001) and King (1999). The NIST group uses $^9\text{Be}^+$ ions whose level scheme is depicted in Fig. 18. Qubits are encoded in the hyperfine manifold of the

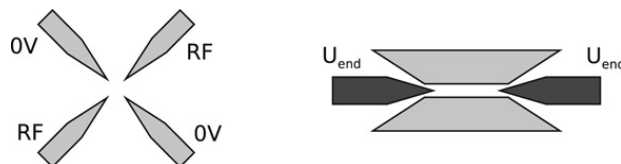


Fig. 17. Front (left) and side (right) view of the Innsbruck trap (from Schmidt-Kaler et al. (2003b)). It consists of four blades (light gray) and two end caps (dark gray). A radio-frequency drive is applied to two opposing blades while the other blades are held at ground. This provides confinement perpendicular to the trap axis. The two end caps held at a positive DC-potential U_{end} prevent the ions to escape along the axis.

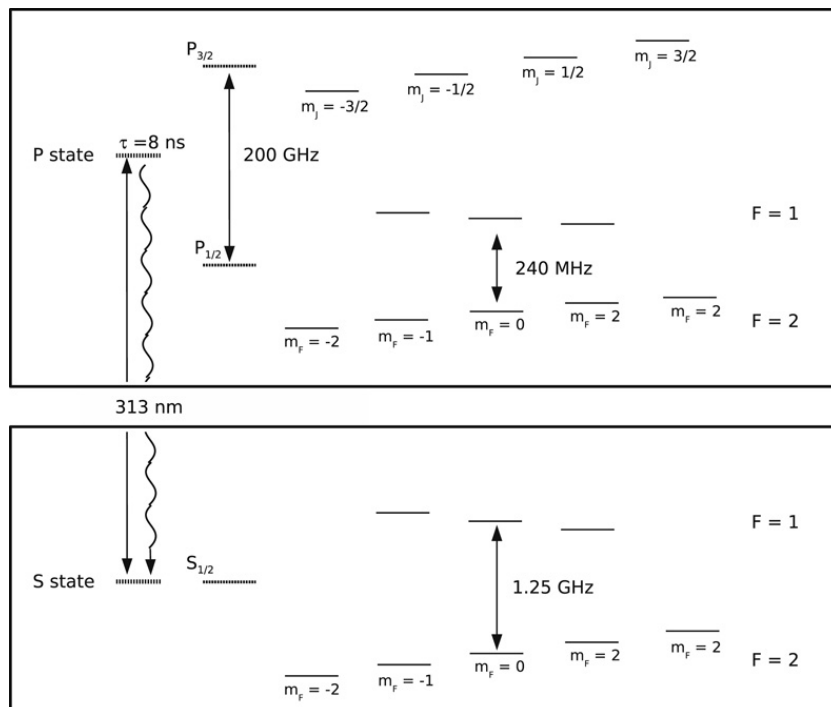


Fig. 18. Energy level scheme of a ${}^9\text{Be}^+$ ion (nuclear spin: 3/2). The hyperfine splitting of the $P_{3/2}$ state is smaller than 1 MHz and not shown.

$S_{1/2}$ electronic ground state split by 1.25 GHz. For most of the experiments discussed here, the qubit was encoded in the $|F = 2, m_F = -2\rangle \leftrightarrow |F = 1, m_F = -1\rangle$ -transition as the levels are easily prepared and distinguished from each other. Doppler cooling at 313 nm (laser power $\sim \mu\text{W}$ at a waist of $\sim 25 \mu\text{m}$) and optical pumping with σ^- polarized light on the $|S_{1/2}, F = 2, m_F = -2\rangle \leftrightarrow |P_{3/2}, F = 3, m_F = -3\rangle$ transition along the quantization axis given by a weak magnetic field (typically $B \sim 1 \text{ m T}$) initializes the ions in the $|F = 2, m_F = -2\rangle$ state. Finally, pulsed resolved sideband cooling on the $|F = 2, m_F = -2\rangle \leftrightarrow |F = 2, m_F = -1\rangle$ transition is used to prepare the ions' motion with a probability of about 0.99 in the ground state (Wineland et al., 1998), before the quantum information is manipulated.

The qubit states are coupled with a Raman transition via the P manifold. The NIST group generates the necessary Raman beams from the same laser source such that the relative phase of the beams is well-defined. Therefore the dominant decoherence source is dephasing due to magnetic field fluctuations (e.g. due to the mains supply at 60 Hz) causing a qubit lifetime on the order of a few milliseconds. However, recently the NIST group used a magnetic field insensitive transition and measured coherence times on the order of a few seconds (see Section 3.1.2).

Read-out is performed again on the cycling transition $|S_{1/2}, F = 2, m_F = -2\rangle \leftrightarrow |P_{3/2}, F = 3, m_F = -3\rangle$ with σ^- polarized light. This light does not couple efficiently to the $|S_{1/2}, F = 1, m_F = -1\rangle$ state as it is detuned from any possible transition by a little bit more than 1 GHz. In order to avoid pumping into the bright state by the still present off-resonant excitations, the $|S_{1/2}, F = 1, m_F = -1\rangle$ population is transferred with two π pulses to the $|S_{1/2}, F = 1, m_F = +1\rangle$ level. In this state, absorption of a single off-resonant photon cannot lead to a population of the $|S_{1/2}, F = 2, m_F = -2\rangle$. Thus the ion remains dark. The theoretical analysis by Langer (2006) shows that with this method, detection errors can be kept smaller than 10^{-4} . At the moment, due to stray light background and imperfections in the π transfer pulses, typically detection efficiencies of about 99% are attained in the NIST setups (Langer, 2006).

The small atomic mass of beryllium allows for high trap frequencies and comparatively large Lamb-Dicke factors. Both factors alleviate a strong coupling to the motional degree of freedom and thus facilitate fast multi-qubit operations. In order to initialize, manipulate and detect the quantum states, light sources in the ultraviolet at 313 nm are required.

The NIST group uses various microstructured traps. Many of these traps have multiple trapping zones, which ease the scaling of ion trap quantum computers to larger ion numbers (Kielinski et al., 2002). In addition, segmented traps allow for single-qubit addressing without tightly focused laser beams (see Section 5.2) and a separate loading zone avoiding patch effects (see Section 3.2).

2.7.2. The Innsbruck setup

The experimental setup used by Innsbruck group is described in Refs. Schmidt-Kaler et al. (2003b) and Gulde (2003). As qubits, superpositions of the $S_{1/2}$ ground state and the metastable $D_{5/2}$ state of $^{40}\text{Ca}^+$ are used (see Fig. 4). The $D_{5/2}$ state has a lifetime $\tau \simeq 1.16$ s.

A magnetic field of 300 μT lifts the degeneracies of the Zeeman manifolds. For the experiments, the entire quantum register is prepared by Doppler cooling, followed by sideband cooling to the motional ground state. Normally, only the center-of-mass mode ($\omega_{\text{CM}} \approx 1.2$ MHz) is cooled to the ground state. The ions' electronic qubit states are initialized in the $S_{1/2}$ ($m_j = -1/2$) state by optical pumping with σ^- light. Then each ion-qubit is individually manipulated by a series of laser pulses on the $S \equiv S_{1/2}$ ($m_j = -1/2$) to $D \equiv D_{5/2}$ ($m_j = -1/2$) quadrupole transition near 729 nm. In order to guarantee phase coherent manipulation, the laser frequency is stabilized to about 50 Hz on a time scale of 1 min by locking it to an ultra-stable reference cavity with a similar design as presented by Notcutt et al. (2005). This time scale corresponds to the typical duration of a full set of quantum computing experiments. On time scales of a few seconds even a 3 Hz linewidth has been observed. The slow drift of the reference cavity – typically about 1 Hz/s – is monitored every few minutes by interrogating the qubit transition and compensated with a feedback loop. Thus many thousands of experiments under comparable conditions are feasible.

Spectroscopy on a transition more sensitive to magnetic field fluctuations ($S_{1/2}$ ($m_j = -1/2$) $\rightarrow D_{5/2}$ ($m_j = -5/2$)) is used to monitor slow magnetic field drifts continuously. In addition, a passive magnetic shield reduces the magnetic field fluctuations on timescales longer than 1 s by about a factor of 30 and by more than 2 orders of magnitude for frequencies higher than 10 Hz. The total field amplitude noise is on the order of a few nT. Thus, typically coherence times of about 5 ms on the $S_{1/2}$ ($m_j = -1/2$) $\rightarrow D_{5/2}$ ($m_j = -5/2$) transition and 15 ms on the $S_{1/2}$ ($m_j = -1/2$) $\rightarrow D_{5/2}$ ($m_j = -1/2$) transition are achieved. The laser driving these transitions is tightly focused onto individual ions in the string with a waist size of 2 μm (inter-ion distance $\sim 5 \mu\text{m}$).

While the NIST group uses predominantly global addressing and state read-out, the Innsbruck-group uses tightly focused laser beams to address individual ions (see Section 2.5.1). Thus, in principle, any quantum algorithm can be implemented straightforwardly, only limited by the decoherence time. The trade-off of this method, however, is that the axial trap frequency cannot be increased too much, since then the ions move closer to each other, thwarting single ion addressing. A consequence of a lowered trap frequency is a reduced speed of the entangling operations on the sidebands.

2.7.3. Composite pulses and optimal control

Quantum algorithms are usually implemented by a sequence of a few fundamental gates. Many of those gates can be carried out with single laser pulses. However, using a set of pulses sometimes offers an advantage over using single pulses (as demonstrated already in Section 2.5.1). In NMR, the composite pulse technique is well known and allows for the compensation of many systematic effects like intensity mismatch and detuning errors (Freeman, 1997; Levitt and Freeman, 1979; Levitt, 1986). The spin echo sequence discovered by Hahn (1950) is such a sequence with which a constant detuning between the excitation and the transition can be removed to a large extent.

In addition to the many sequences discovered and used in NMR, there are a few sequences which are important in the context of ion traps. We present here two of those which were used in the implementation of the Deutsch–Josza algorithm (Gulde et al., 2003) (see Section 5.1) and were described first by Childs and Chuang (2000). The first sequence uses four sideband pulses (Childs and Chuang, 2000; Gulde et al., 2003; Schmidt-Kaler et al., 2003b) to implement a phase gate in the computational subspace $\{|D, 0\rangle, |S, 0\rangle, |D, 1\rangle, |S, 1\rangle\}$. The advantage over the method laid out in Section 2.6.2 is that no third level is required to implement the gate. To achieve the desired gate with just two levels, cleverly chosen pulse lengths and phases avoid leakage into higher phonon number states. Using the definitions from Eq. (12), the pulse sequence (to be read from right to left) is: $R^+(\pi/2, \pi/2)R^+(\pi/\sqrt{2}, 0)R^+(\pi/2, \pi/2)R^+(\pi/\sqrt{2}, 0)$. Having Fig. 1 in mind, we analyze the effect of this pulse sequence on the four physical eigenstates $\{|D, 0\rangle, |S, 0\rangle, |D, 1\rangle, |S, 1\rangle\}$. The $|D, 0\rangle$ state is not affected at all and therefore $|D, 0\rangle \rightarrow |D, 0\rangle$. Fig. 19 illustrates the evolution of the respective Bloch vector in the $|S, 0\rangle \leftrightarrow |D, 1\rangle$ and $|S, 1\rangle \leftrightarrow |D, 2\rangle$ manifold, respectively. Because the couplings and thus the effective pulse lengths differ by a factor of $\sqrt{2}$ between the two manifolds, the Bloch vector follows different paths. Still, it reaches always its original position when the pulse sequence is finished. Using Eqs. (12) and (12), one can show that for the three remaining cases, each time a phase factor of -1 is picked up and thus the diagonal matrix $\text{diag}(1, -1, -1, -1)$ is implemented.

Similarly, three blue sideband pulses can be employed to implement a SWAP operation between an electronic and a motional degree of freedom of trapped ions (Gulde et al., 2003): $R^+(\pi/\sqrt{2}, 0)R^+(2\pi/\sqrt{2}, \varphi_{\text{swap}})R^+(\pi/\sqrt{2}, 0)$, where $\varphi_{\text{swap}} = \arccos(\cot^2(\pi/\sqrt{2}))$. This pulse sequence was used by Gulde et al. (2003) to implement the Deutsch–Josza algorithm (Deutsch, 1989). Already, these two pulse sequence examples demonstrate that composite pulses are a quite versatile tool.

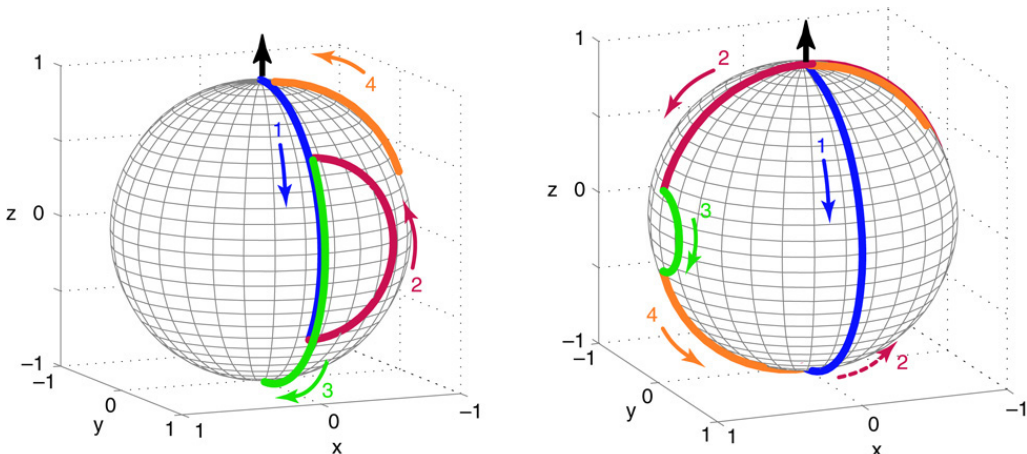


Fig. 19. Evolution of the Bloch vector during the composite phase gate in the $|S, 0\rangle \leftrightarrow |D, 1\rangle$ (left) and $|S, 1\rangle \leftrightarrow |D, 2\rangle$ manifold (right) (from Schmidt-Kaler et al. (2003b)).

Especially, gradient ascent pulse engineering (GRAPE) developed in the context of NMR carries the idea of composite pulses to its extreme (Khaneja et al., 2005). Here, a pulse sequence thought to implement a particular unitary operation is split into many pulses. Then, a special algorithm is used to vary amplitudes and phases of the pulses to perfect the desired unitary that is optimal with respect to certain quality criteria (e.g. execution time) with a special algorithm (Khaneja et al., 2005). In addition, various boundary conditions (e.g. experimental constraints such as finite pulse rise times) can be included in form of cost functions. Thus, significant performance improvements in terms of speed and reduced susceptibility to experimental imperfections can be achieved. Most interestingly, the sensitivity to control parameters can be minimized with GRAPE, too. However, note that in spite of the fact that the execution time can be reduced considerably, composite pulses lead usually to a larger total pulse area. Thus decoherence effects which scale with the pulse area might become relevant. One such source of decoherence is spontaneous emission during Raman transitions (see Section 3.1.3).

The first steps in applying such optimal control techniques to trapped ions have already been taken. Timoney et al. (2008) devised pulse sequences to robustly perform $\pi/2$ and π rotations between two hyperfine qubits of a single $^{171}\text{Yb}^+$. Creating the states $|0\rangle + e^{i\varphi}|1\rangle$ and $|1\rangle$ from $|0\rangle$, this work also experimentally demonstrates the robustness of these pulse sequences as compared with simple $\pi/2$ or π pulses, respectively, with respect to intensity and detuning errors.

Furthermore, Nebendahl et al. (2008) modify a GRAPE algorithm to construct a controlled-NOT operation from a global Mølmer-Sørensen interaction and single qubit operations. The algorithm allows for the optimization of whole algorithms. Taking as an example a quantum error correction scheme for bit flips based three qubits and two ancilla qubits, the original length of more than 100 pulses was reduced to 34 pulses.

3. Decoherence in ion trap quantum computers

This section describes the most relevant decoherence mechanisms for ion trap quantum computers. For further discussions, we refer to Ref. Wineland et al. (1998).

3.1. Sources of imperfections in ion trap quantum computers

3.1.1. Bit-flip errors

Bit-flip errors occur when a process transfers populations between the physical eigenstates of the qubit. Usually, the physical eigenstates are the energy eigenstates of the system and bit-flips are connected to radiation or absorption of photons. Thus, bit-flip errors are usually caused by spontaneous emission. The frequency differences of hyperfine and Zeeman qubits are quite small and therefore the time constants for spontaneous emission are usually longer than a year and thus are of no relevance if the ions are not irradiated with electromagnetic radiation. For optical qubits, usually superpositions of the ground state and the metastable state D -level in earth-alkali elements are used. Typical life times of the D -levels are about 1 s (Barton et al., 2000; Kreuter et al., 2005; Letchumanan et al., 2005), which is long as compared with the gate time of less than 1 ms. Therefore, most current experiments are not yet limited by bit-flip errors during their free evolution. Bit-flip errors on the motional degree of freedom are discussed in Section 3.2.

3.1.2. Dephasing

The phase evolution of a superposition often depends on a classically well-defined parameter such as the magnetic field. Ignoring the time evolution of the classical parameter leads to dephasing of the superposition. For instance, a superposition consisting of two levels with differing magnetic moments experiences energy shifts due to a (fluctuating) magnetic field.

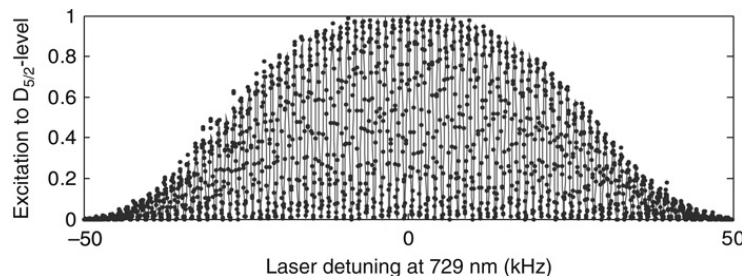


Fig. 20. Ramsey fringes with a free precession time of $T = 100 \mu\text{s}$ (Chwalla et al., Innsbruck, unpublished). The data points indicate the excitation probability to the metastable D level in a single $^{40}\text{Ca}^+$ ion.

Thus, the phase of the superposition depends on the particular magnetic field history and dephasing occurs. Similarly, dephasing also takes place for the ion motion if the trap frequency is not constant, e.g. due to voltage fluctuations on the trap electrodes (see Section 3.2).

A typical experimental sequence to test the phase coherence consists of two $\pi/2$ pulses separated by a waiting time T (a Ramsey experiment). During the waiting time, any difference between the atomic transition frequency and the laser frequency will lead to an evolution of their relative phase. The second $\pi/2$ pulse will then rotate the atomic state according to the phase difference either towards the excited or the ground state. This effect can be seen in Fig. 20 when the population of the ion oscillates with the detuning of the laser frequency from the atomic transition (Ramsey fringes). The contrast ($\frac{\max - \min}{\max + \min}$) in the center of this curve is in the following termed Ramsey contrast.

Experimentally, fluctuations of the atomic resonance frequency, e.g. typically due to fluctuations of the magnetic field and of the laser frequency, lead to dephasing. Sometimes it is useful to distinguish between fast fluctuations (the relative frequency changes during the waiting time), slow fluctuations (the relative frequency is constant in each experiment, but not the same in the next experiment(s)) and an intermediate regime. It can be shown that with an increasing waiting time, fast fluctuations lead to an exponential decay of the Ramsey contrast, while slow fluctuations lead to a Gaussian decay of the Ramsey contrast (Sengstock et al., 1994). Furthermore, slow fluctuations can be compensated for by spin-echo techniques (Hahn, 1950).

Currently, the coherence time of most qubits is limited by magnetic field fluctuations to a few milliseconds. Usually Fourier components at multiples of the mains frequency contribute most to the magnetic field changes. Synchronizing the experiment with the phase of the mains supply effectively counters time variations of the magnetic field.

A more generic way to reduce magnetic field fluctuations is shielding of ambient magnetic fields with μ -metal and/or active cancelation with a feedback loop. Currently, the Innsbruck group uses an aluminum/ μ metal shield which suppresses the magnetic field fluctuations by more than two orders of magnitude. However, in most cases a finite magnetic field is needed to lift the degeneracy of the electronic levels. Therefore, a very stable magnetic field has to be created inside the magnetically shielded region without saturating the μ -metal. The standard procedure is to use a pair of Helmholtz coils through which a current is passed. As it is very difficult to stabilize currents to better than 10^{-6} , in the future it might be worth while going through the trouble to use superconducting solenoids. Here magnetic field stabilities of better than 10^{-11} at 6 T have been attained. These experiments were made possible by choosing a particular geometry of the superconducting coils to shield the external magnetic fields (Dyck et al., 1999), especially of high importance for small fields. It remains to be seen to what extent these exceptional field stabilities can be obtained at the relatively small fields of 1 m T as required for quantum computation.

A more elegant solution to reduce dephasing due to magnetic field fluctuations is to use qubit levels having the same magnetic moment. For this, especially, ions with a hyperfine structure have interesting levels. Obvious choices for the qubit transitions are of the form $m_F = 0 \rightarrow m_F = 0$, which experience only a quadratic Zeeman-effect at small magnetic fields. However, at the magnetic fields required to lift the Zeeman degeneracies, a considerable linear Zeeman-effect is present. Therefore, it seems advantageous to work with stronger magnetic fields where transitions with a purely quadratic Zeeman-effect can be found.

While magnetic field insensitive transitions were extensively explored in microwave precision experiments (Bollinger et al., 1991; Thompson, 1990), in the context of quantum computing it has been implemented only very recently by the NIST group on $^9\text{Be}^+$ (Langer et al., 2005), by the Oxford (Lucas et al., 2007) and the Innsbruck groups on $^{43}\text{Ca}^+$ (Benhelm et al., 2007, 2008a) and by the Ann Arbor group on $^{111}\text{Cd}^+$ (Haljan et al., 2005b). To achieve a reasonable spatial selectivity, the qubits are manipulated with an optical Raman drive (c.f. Section 2.3). However, care has to be taken to maintain the phase coherence between both laser fields on time scales of several seconds. Using co-propagating laser beams simplifies this obstacle considerably as both beams propagate along the same path such that effects of mirror vibrations as well as of air currents cancel. However, a co-propagating geometry does not allow for easy coupling to the motional degree of freedom. On the other hand, if only phase gates are used as two-qubit gates, the phase stability only has to be maintained during each phase gate operation.

Langer et al. (2005) demonstrated coherence times $\tau > 10$ s using a magnetic-field-independent hyperfine transition in $^9\text{Be}^+$ at a magnetic field of $B_0 \simeq 0.01194$ T. In these experiments, Ramsey spectroscopy was carried out on the

$|F = 2, m_F = 0\rangle \longleftrightarrow |F = 1, m_F = -1\rangle$ qubit transition to measure the phase coherence. The optimal magnetic field was determined by measuring this transition frequency (~ 1 GHz) as a function of the magnetic field. The minimum of the resulting parabola (second order derivative $B_2 \simeq 0.305 \text{ Hz}/\mu \text{ T}^2$, $B_0 \simeq 0.01194 \text{ T}$) corresponds to the desired magnetic field with the least magnetic field dependency. The coherence time of this qubit is limited by slow drifts of the ambient magnetic field within the typical measurement times of a few hours especially for scans with long Ramsey waiting times. These experiments demonstrate a qubit memory error rate on the order of $t_0/\tau \approx 10^{-5}$ where the time scale t_0 is set by the detection time of $t_0 = 200 \mu\text{s}$, which is the longest operational time of the NIST ion-trap quantum computer.

The Oxford group carried out coherence measurements on $^{43}\text{Ca}^+$ with a microwave drive (Lucas et al., 2007). They used the $|F = 3, m_F = 0\rangle \leftrightarrow |F = 4, m_F = 0\rangle$ transition in the hyperfine ground state manifold of $^{43}\text{Ca}^+$ at small magnetic fields ($B \approx 0.178 \text{ mT}$) and observed a dephasing time of $1.2(2) \text{ s}$. Additionally, they investigated the coherence properties in a spin echo configuration and could not detect any decay of the Ramsey contrast on time scales of up to 1 s . From this, they deduce a spin-echo dephasing time of larger than 45 s . Similar results were obtained by the Innsbruck group in microwave-induced Ramsey experiments on the $|F = 3, m_F = 0\rangle \leftrightarrow |F = 4, m_F = 0\rangle$ clock transition of $^{43}\text{Ca}^+$. For Ramsey interrogation periods $\tau = 1 \text{ s}$, the Ramsey contrast was still 88% while for $\tau = 50 \mu\text{s}$, a contrast of 97% was found. The experiment was carried out at a field of 0.05 mT (Benhelm et al., 2008a; Benhelm, 2008).

3.1.3. Imperfect control

Other serious sources of decoherence are imperfect realizations of the intended gate operations, usually caused by fluctuating or insufficiently calibrated control parameters. Typical candidates for these parameters are intensity and frequency fluctuations of the laser and beam pointing instabilities. In addition, pulses on a particular ion can have unwanted side effects on the ion itself (AC-Stark shifts, off-resonant excitations) or on neighboring ions (addressing errors). Many of these errors can be greatly reduced with composite pulse and optimal control techniques (c.f. Section 2.7.3). We list here some of these imperfections:

- *Pulse length errors* arise from intensity fluctuations of the laser beam, beam pointing instabilities or just miscalibration. All of these reasons are almost equally relevant in current experiments. Common to all of them is also that the fluctuations take place at frequencies below a kHz, such that they can be considered constant during the execution of a pulse sequence. Relative amplitude fluctuations of 10^{-2} are typical.
- Insufficient cooling can also lead to effective intensity fluctuations. During each run, the phonon numbers n_m have different values (which corresponds to a finite temperature of the ion crystal) and thus for a non-vanishing Lamb-Dicke factor the Rabi frequencies are different (see Eqs. (11) and (13)). Interestingly, for an increasing number of ions the Innsbruck group observes that this effect is reduced. In fact, in their current experiments it is only relevant for single ions. As detailed by Wineland et al. (1998), there are two reasons for this:
 - (1) With an increasing ion number the Lamb-Dicke factor for each mode tends to get smaller.
 - (2) The contributions of the increasing number of modes averages, such that the variance of the effective Rabi frequency narrows.
- *Detuning errors* take place when the qubit transition frequency is miscalibrated or the drive frequency fluctuates slowly as compared to the duration of the coherent manipulation. Furthermore, magnetic field fluctuations have the same effect and usually are also slow as compared with the coherent manipulation time. The effect of a detuning error is a constant phase evolution during the experiment. A simple and effective method to remove such a constant phase evolution is the so-called spin-echo method (Hahn, 1950). The idea is that after half the evolution time the roles of the upper and the lower qubit level are exchanged. Thus the phase rewinds during the second half and – if the detuning is constant – arrives at zero after the complete evolution time. Often, this method can be implemented quite straightforwardly. An example in the ion trap context can be found in Leibfried et al. (2003b). However, usually during algorithms the qubits state is changed. In this case either more spin-echo sequences might have to be used (e.g. for each free evolution one as in Barrett et al. (2004)) or an effective spin echo sequence can be found. For instance, Riebe et al. (2004) optimized the time position of the population inverting pulses both in simulations and in the actual experiment.
- *Addressing error* While addressing a single ion with a focussed laser beam, residual light might affect other ions in the trap and thus perform an undesired unitary evolution. See Section 2.5.1 for more details.
- *Off-resonant excitations* also limit the obtainable fidelity. Off-resonant excitation is usually a problem if one drives a weak transition in the presence of a nearby strong transition (c.f. Eq. (9)). Exactly this situation occurs in ion traps, when driving the sideband transition (Steane et al., 2000). The transition matrix element of the sideband transition is weaker by a factor η than the one of the carrier transition as can be inferred from Eqs. (13) and (11). Thus, strong laser fields are required to obtain a reasonable gate speed which can then yield high gate fidelities in the presence of dephasing mechanisms.

However, the strong laser field, characterized by the Rabi frequency Ω , leads to off-resonant excitations on the carrier transition (see Eq. (9)). The Innsbruck experiments suffered particularly from this effect (Schmidt-Kaler et al., 2003c). Quantum mechanically, the off-resonant excitation can be understood as Rabi oscillations induced by a non-adiabatic switching of the energy eigenbasis while the laser power is changed. Thus, a system initially being in an energy eigenstate finds itself no longer in an eigenstate of the Hamiltonian and consequently oscillations between the newly populated energy eigenstates occur.

Off-resonant excitations can be greatly reduced with pulse shapes which have no spectral Fourier components at the carrier-transition. In the simplest case, the laser pulse powers are switched smoothly such that during the smooth turn on and off the system follows adiabatically.

- *Unwanted AC-Stark shifts* have a similar origin as off-resonant excitations (see Eq. (8)), however, affect the phase of the qubit rather than the population. Here the carrier transition nearby leads to an AC-Stark shift of the qubit levels and thus the qubit phase evolves (Häffner et al., 2003b). In principle, this phase evolution can be measured and then taken into account in the algorithm to be implemented. In the Innsbruck setup, the problem, however, with this approach is that the acquired phase shift during a controlled-NOT operation is typically on the order of 20π . In order to obtain a reasonable phase stability of 0.1π , one needs an intensity reproducibility of better than 0.005. To achieve this intensity stability of a particular polarization at the ion position with a narrow beam waist is quite demanding. To relieve this stringent condition, a second light field can be used which induces an AC-Stark shift of the same magnitude but of opposite sign (Häffner et al., 2003b; Kaplan et al., 2002). This field can be most conveniently derived by driving the acousto-optical modulator (AOM) used to control the qubit-control field with a second RF signal. Thus the two laser fields, for qubit manipulation and for AC-Stark shift compensation, are generated simultaneously by the same AOM. Both light fields pass then along the same path to the ions such that they pick up virtually the same intensity, polarization and beam pointing fluctuations, removing the AC-Stark shifts to a large extent.

In the Innsbruck experiments, a considerable AC-Stark shift also appears due to dipole-allowed transitions (Häffner et al., 2003b). For the blue sideband, the presence of the dipole-allowed transitions partially cancels the shift induced by the presence of the carrier transitions, whereas for the red sideband they add. Thus, in the Innsbruck experiments for coupling the ions to the motion, the blue sideband is preferred over the red one. Another possibility to reduce AC-Stark shifts is to use the polarization degree of freedom. The NIST group tunes the polarization of the Raman-laser beam pair to minimize the shift (Wineland et al., 2003).

- For Raman-driven qubits, spontaneous decay from the levels used to couple the two qubit levels has to be considered. Ozeri et al. (2005) show that using very large detunings this decoherence effect can be reduced sufficiently, however, at the expense of requiring large laser powers. For a detailed discussion of these issues, we refer here to Ozeri et al. (2007).

Most of these decoherence sources can be minimized by changing external parameters. For example, the laser intensity can be reduced such that AC-Stark shifts become negligible at the expense of slow gates. Slow gates in turn increase the susceptibility to dephasing due to fluctuating magnetic fields and laser frequencies. Similarly high trap frequencies allow for faster gates (Steane et al., 2000), but make good addressing of the individual qubits more difficult. In the experiments therefore a compromise has often to be made to keep all decoherence mechanisms reasonably small.

The previous paragraphs listed the most common important imperfections. However this list is of course incomplete: for instance, a finite residual temperature of the ion string leads to single and two-qubit gate errors. Especially, the Cirac–Zoller gate is very susceptible to imperfect cooling. This error source is very special, since the combined fidelity of two concatenated gates is not the product of the individual gate fidelities as discussed in Section 4.7. Therefore, a full simulation of the whole algorithm is required to make reliable predictions on its performance.

3.2. Motional coherence

In the Cirac–Zoller proposal, quantum information is temporarily stored in the motional degree of freedom. Some other gate types, such as the Mølmer–Sørensen gate require the ion string to be only well within the Lamb–Dicke regime (Section 2.6.3). Both gate types are affected by population changes (motional heating) and dephasing (e.g. trap frequency fluctuations) during the gate operation. Dephasing is often caused by slow drifts of the trap voltage on the order of a few Hertz, whereas motional heating can be caused by electromagnetic background radiation at the trap frequencies. This background stems predominantly from voltage fluctuations in material close to the trap. The most fundamental source of these voltage fluctuations should be the thermal motion of the electrons inside the conductors. This mechanism has been thoroughly investigated, both theoretically and experimentally, by Wineland and Dehmelt (1975) with electrons in Penning traps. The Johnson noise heating power P is given by:

$$P_{\text{noise}} = kT \Delta\nu, \quad (17)$$

where kT is the thermal energy and $\Delta\nu$ is the frequency bandwidth in which the ion accepts the power. The time τ in which one motional quantum of energy $E_q = \hbar\nu$ is generated is given by

$$\tau^{-1} = \frac{P_{\text{noise}}}{E_q} = \frac{kT \Delta\nu}{\hbar\nu} = \frac{kT}{\hbar Q}, \quad (18)$$

where we introduced the quality factor Q of the ion motion. This quality factor can be derived from the dissipated power $P_{\text{dis}} = I^2 \text{Re}Z$ of the current induced by a single ion with an energy E_{ion} at the real part of the impedance $\text{Re}Z$. For this, we assume a lumped circuit model (see Fig. 21) where the ion induces a current $I = q\dot{x}/D$ with q being the charge and \dot{x} the

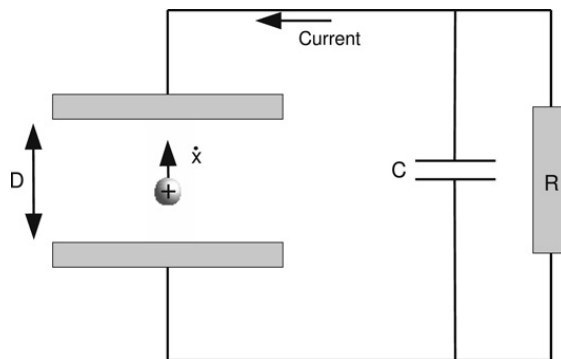


Fig. 21. Lumped circuit model of a single ion at velocity \dot{x} interacting with the trap electrodes. The connection between the trap electrodes is mainly characterized by the resistivity R and capacitance C between the electrodes.

velocity of the ion (Shockley, 1938). The characteristic dimension D is on the order of the ion-electrode distance. Using this, we obtain for the quality factor:

$$Q = \frac{E_{\text{ion}}}{P_{\text{dis}}/\nu} = \frac{m\dot{x}^2\nu}{I^2\text{Re}Z} = \frac{mvD^2}{q^2\text{Re}Z}. \quad (19)$$

Inserting Eq. (19) into Eq. (18), we arrive for the time in which one motional quantum is acquired at

$$\tau^{-1} = \frac{kT}{h\nu} \frac{q^2\text{Re}Z}{mD^2}. \quad (20)$$

For typical values of $D = 100 \mu\text{m}$, $\text{Re}Z = 1 \Omega$ at room temperature, the expected heating time from Johnson noise is $\tau \sim 200 \text{ s}/\text{quantum}$ and thus very small.

In order to measure a heating rate, one can cool the ion (string) to the ground state, wait for some time to allow for some heating and then probe the strength of the motional sideband. Assuming thermal distribution, the mean phonon number is deduced by employing Eq. (13). Depending on the thermal excitation, the Rabi oscillations on the blue sideband speed up and eventually degrade (c.f. Section 2.6.1). Repeating this procedure for various waiting times yields the heating rate. Seidelin et al. (2006), Epstein et al. (2007) and Wesenberg et al. (2007) developed and applied another method which is based on the strength of the ion fluorescence. The basic idea is that the ion motion leads to Doppler broadening of the absorption spectrum. The change in fluorescence is recorded as a function of a waiting time when cooling is switched off. The latter method is less sensitive than the first one, however, it does not require manipulation of the sidebands.

The NIST group observed heating rates of a few phonons per ms (Leibfried et al., 2003a; Turchette et al., 2000) in various traps. This is orders of magnitude more than what is expected from fundamental electrical noise in the trap electrodes (Eq. (20)). Patch charges on the trap electrodes have been suspected to cause these excessive heating rates (Wineland et al., 1998; Turchette et al., 2000). The former publication also discusses various other sources of heating in detail. Patch charges can be generated when an electron beam is used to ionize the atoms during trap loading. Indeed, many experiments suggest that using photo ionization techniques to produce the ions (Kjærgaard et al., 2000) can help to reduce the heating rate. A reason for the seemingly reduced heating rate could be the reduced vapor pressure of the atoms during photo ionization as compared with the less efficient electron beam ionization. Thus a much reduced atom flux can be used which reduces deposition of atoms on the trap electrodes. Furthermore, ionization with a laser produces only a minimum of charged particles whereas the electron beam can charge any insulating layer on the trap electrodes. While photoionization seems to lead to reduced heating rates, no experiment with laser cooled ions was reported as of yet where the fundamental thermal noise given in Eq. (20) dominated the heating rate. Only in some Penning trap experiments using a resonance circuit to enhance the real part of the resistivity in Eq. (20), thermal noise plays the dominant role (Wineland and Dehmelt, 1975; Häffner et al., 2003a).

The Ann Arbor group observed much reduced heating rates by cooling the trap electrodes (see Ref. Deslauriers et al. (2006) and Fig. 22). In the course of cooling the trap electrodes from 300 K to 150 K, the heating rate dropped by more than one order of magnitude. This strong dependence on the temperature hints at a thermally activated process causing the unexplained heating in ion traps. In addition, the authors measured heating rates as a function of the trap size d . From Eq. (20), a $1/d^2$ scaling is expected while one expects a $1/d^4$ dependence in the case of heating due to moving patch charges (Turchette et al., 2000; Epstein et al., 2007). The Ann Arbor group extracted from the data in Fig. 22 an exponent of 3.5 (Deslauriers et al., 2006) only slightly different from the postulated exponent of 4 (Turchette et al., 2000).

The MIT-group has investigated various planar traps made of silver electrodes on a quartz substrate close to 4 K as well as one trap at room temperature (Labaziewicz et al., 2008a). They measured a heating rate as low as 2 quanta/s for trap sizes on the order of $100 \mu\text{m}$ while a similar trap at room temperature had a devastating heating rate seven orders of magnitude larger. Even the extremely small heating rates for the 4 K experiments cannot be explained by Johnson noise, only. They

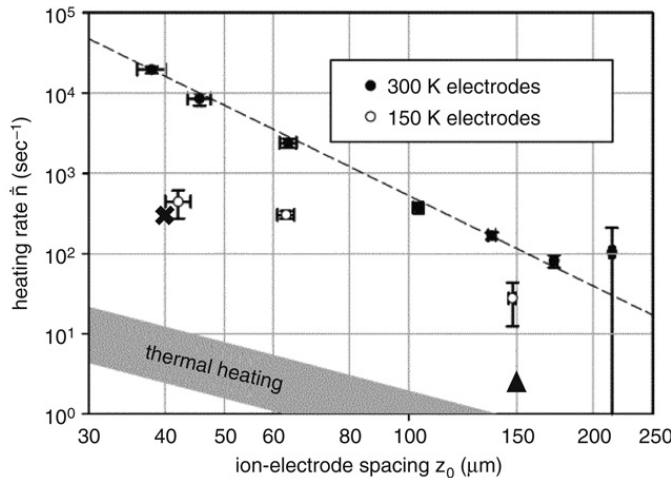


Fig. 22. Single ion heating rate as function of ion-electrode distance (a measure of the trap size) (from Deslauriers et al. (2006)). The trap consists of two needles to which the radio frequency is applied to. Furthermore, two heating rates from planar surface traps are added: the cross shows the heating rate of a $^{25}\text{Mg}^+$ ion in a room temperature trap (electrode material: gold) (Epstein et al., 2007), while the triangle shows the heating rate of a single Sr^+ ion where the silver trap electrodes were held at 6 K (Labaziewicz et al., 2008a).

also measured heating rates for three different trap sizes and found them to be consistent both with a $1/d^2$ and a $1/d^4$ scaling. In addition, a strong dependence of the heating rate on the annealing temperature used in the fabrication process was found. Furthermore, the MIT group investigate the heating rate of the ions as a function of the electrode temperature T (Labaziewicz et al., 2008b). Above $T = 40$ K, they found that the heating rate is proportional T^β with $2 < \beta < 4$ depending on the trap. Overall, these findings suggest that with improved fabrication methods, smaller heating rates can be achieved. Furthermore, the NIST group observed heating rates of 300 quanta/s for a $^{25}\text{Mg}^+$ ion 40 μm above the gold surface of a planar trap (Epstein et al., 2007). This heating rate is significantly smaller than what one would expect from the MIT measurements and supports the conclusion that choice of materials and fabrication methods are very important to achieve small heating rates.

To speed up quantum gates and to ease cooling, there is a strong tendency towards constructing small ion traps. On one hand, small traps with characteristic dimensions of a few tens of microns allow for large trap frequencies on the order of 10 MHz, on the other hand they seem to lead to unacceptable heating rates. Therefore, heating in ion traps is not only an interesting topic on its own but needs a lot of attention from a technological point of view. Cooling the traps to 4 K seems to offer a solution to the heating problem.

Many two-qubit gate implementations, however, store quantum information in the motional degree of freedom. Therefore, dephasing of the motional states must be also taken into account. To measure the motional coherence, a superposition of two motional states can be created whose phase coherence is tested after some waiting time. In the Innsbruck experiments, the pulse sequence (read from right to left) $R^+(\pi, 0)R^C(\pi/2, 0)$ creates the state $(|D, 0\rangle + |D, 1\rangle)/\sqrt{2}$. The inverse pulse sequence $R^C(\pi/2, \varphi)R^+(\pi, 0)$ closes the interferometric procedure after some waiting time T . From the contrast of the interference fringes obtained by varying φ with waiting time T , the coherence time can be directly deduced. One might be tempted to use just a pair of two $R^+(\pi/2)$ pulses to implement the Ramsey experiment. In this case, however, motional as well as electronic dephasing mechanisms lead to decoherence of the intermediate state $(|S, 0\rangle + |D, 1\rangle)/\sqrt{2}$. The former pulse sequence, however, is insensitive to phase decoherence of the electronic qubit, and waiting times T of many tens of milliseconds are possible. Thus, with the former pulse sequence, the trap frequency can be easily determined with an accuracy of a few Hertz.

Using this method, the Innsbruck group observed a motional coherence time on the order of 100 ms (Schmidt-Kaler et al., 2003a) on the center-mass-mode, being consistent with expected voltage fluctuations on the order of 10^{-5} . Furthermore, the Oxford group observed on a single $^{40}\text{Ca}^+$ ion a motional coherence time of 182 (36) ms, limited most likely by motional heating of about 3 quanta/s (Lucas et al., 2007). However, the Innsbruck group found that for the axial breathing mode (and other higher axial modes) coherence times of about 5 ms are more typical (Roos, 2008). Thus, it must be concluded, that on the breathing mode, a dephasing mechanism is present which can be neglected for the center-of-mass mode. Roos (2008) show, both theoretically and experimentally, that for a two-ion crystal the breathing mode frequency depends on the motional state of some of the radial modes. The basic mechanism responsible is that an anti-correlated motion (the rocking mode) along a radial direction changes the mean distance between the ions (see Fig. 23). Thus, the repelling force between the ions is reduced leading to a reduction of the axial breathing mode frequency with increasing excitation of the rocking mode. Therefore, if the rocking modes are not in a well-defined state, the breathing mode frequency is different for each experimental realization which in turn is interpreted as dephasing of the breathing mode.

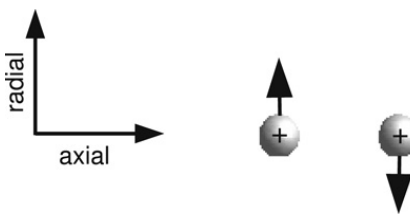


Fig. 23. An anti-correlated radial motion (excited rocking mode) of a two-ion crystal changes the mean distance between the two ions.

3.3. Modeling ion trap quantum computers

The influence of each imperfection on the performance of the quantum computer can be reliably estimated with numerical simulations. In this way the necessary steps to improve the performance can be analyzed and planned in detail. For ion trap quantum computers this procedure is relatively straightforward as the Hamiltonians are well-known (see Eq. (2)) (Wineland et al., 1998; Leibfried et al., 2003b; Jonathan et al., 2000). Here we describe the simulations as appropriate for the Innsbruck set-up. With small modifications, these simulations should also be applicable to other ion trap set-ups.

Eq. (2) is a good starting point to model ion trap quantum computers. The Hamiltonian is first generalized to multiple ions:

$$H = \hbar \sum_{n,m} \Omega_n \left\{ \sigma_+^{(n)} e^{-i\Delta t} + \sigma_-^{(n)} e^{i\Delta t} + i\eta_{nm} (\sigma_+^{(n)} e^{-i\Delta t} - \sigma_-^{(n)} e^{i\Delta t}) (a_m e^{-i\omega t} + a_m^\dagger e^{i\omega t}) \right\}. \quad (21)$$

Here, the indices n and m denote the various ions and motional modes taken into account, respectively, and η_{nm} accounts for the different coupling strengths of the ions to the motional modes (James, 1998).

For the simulations, the initial state vector is first transformed into the rotating frame of the laser field such that Eq. (21) becomes time independent and the Hamiltonian can be directly integrated. A quantum algorithm usually consists of laser pulses with different frequencies. Therefore, this procedure has to be carried out for each pulse, separately. For the bi-chromatic laser fields employed for the AC-Stark shift compensation (c.f. Section 3.1.3) and Mølmer–Sørensen-gates (Section 2.6) this method fails. In these cases the differential equation can be numerically integrated. In the following we describe how almost all experimental imperfections were incorporated into the simulations:

AC-Stark effects due to the carrier transition are described by Eq. (21) and appear with increasing Ω_n (see Section 2.2).

Therefore, these shifts are automatically included in the simulation. AC-Stark shifts due to other (dipole) transitions are not taken into account by Eq. (21). However, in the experiments a second light field is used anyways to minimize the total effect of all AC-Stark shifts. Therefore the light shifts must be artificially removed from the Hamiltonian to match the experiments.

Off-resonant excitations (c.f. Eq. (9)) are described by Eq. (21) and are therefore automatically included.

Laser frequency noise and magnetic field noise are divided into fluctuations slower and faster as compared with typical coherent manipulation times (on the order of 1 ms in current experiments). In the experiments slow fluctuations usually dominate and the laser detuning remains to a large extent constant during coherent state manipulation. The observed increase in the coherence time – when spin echo sequences are used – supports this conjecture. These slow fluctuations can be modeled by running the simulations for several detunings from the qubit transition and by averaging the measured populations. On the other hand, fast fluctuations can be taken into account by transforming Eq. (21) into a master equation. In this case, the dimension of the state space describing the system is squared as compared to the Schrödinger approach and thus this method already starts to get tedious for simulations of a five-ion algorithm. In fact, even today's supercomputers cannot hold the complete density matrix of an arbitrary twenty qubit system in their memory.

Laser intensity fluctuations are assumed to be constant during the coherent state manipulation and therefore can be modeled by simulating the algorithms a few times for various laser intensities.

Addressing errors are described by setting the Rabi frequencies Ω_n in Eq. (21) to the corresponding values. However, it should be noted that there is an additional degree of freedom connected with addressing errors: the phase of the laser at an ion position when directed on this particular ion and when mainly directed on another ion is in general not the same. This is due to the different paths the light field takes in these two cases. Usually, in the simulations all phases are taken to be the same as they seem to give an upper bound for most algorithms.

Imperfect ground state cooling can be taken into account by running the simulation with the different initial states and averaging the results appropriately.

These simulations allow one to reduce the sensitivity of quantum algorithms to the respective imperfections. In the Innsbruck experiments, especially the influence of laser frequency and addressing errors issues was reduced considerably by optimizing the implementations taking the simulations as a guide.

Finally, we document some of the imperfections not taken into account in the simulations for the Innsbruck experiments. In Eq. (21) each ion was approximated as a two level system. For ${}^{40}\text{Ca}^+$ the $S_{1/2}$ -ground state is split into two Zeeman levels

and the upper qubit level $D_{5/2}$ into six levels. The level separation is about 5 MHz and therefore not much larger than the involved trap frequencies. Therefore, off-resonant excitations of the additional transitions are possible. Furthermore, AC-Stark effects arise due to the presence of the other Zeeman levels as well as due to dipole transitions (Häffner et al., 2003b). Finally, the AC-Stark effect was canceled with a second off-resonant laser field. Treating this second light field leads to a time dependent Hamiltonian and was therefore usually not taken into account in the simulations.

4. Key experiments

4.1. Cirac-Zoller-type gates

The NIST group demonstrated the central part of the Cirac-Zoller gate on a single ${}^9\text{Be}^+$ ion by implementing the operations displayed in Eq. (14) (Monroe et al., 1995a). The phase gate was turned into a controlled-NOT operation by inserting two Ramsey $\pi/2$ pulses, one before and one after the phase gate, to verify the quantum nature of the phase gate. The first two motional excitations $n = \{0, 1\}$ (see Fig. 1, $\omega_{\text{trap}} = 2\pi \times 11$ MHz) served as the control bit, while the target bit was represented by superpositions of the $|F = 2, m_f = -2\rangle$ and $|F = 1, m_f = -1\rangle$ states. For the auxiliary state, the $|F = 2, m_f = 0\rangle$ state was used.

The complete Cirac-Zoller gate was finally implemented by Schmidt-Kaler et al. (2003c): two ${}^{40}\text{Ca}^+$ ions were addressed individually using a laser beam with a waist of about 2 μm . First, the quantum state of ion #1 was mapped onto the breathing mode with a blue sideband pulse $R^+(\pi)$. Then, a controlled-NOT gate with the motion as the control bit and the electronic state of ion #2 as the target bit was carried out, before the motional state was mapped back onto ion #1. However, to implement the conditional phase shift, the Innsbruck group did not use an auxiliary level but the composite pulse sequence $R^+(\pi/2, \pi/2)R^+(\pi/\sqrt{2}, 0)R^+(\pi/2, \pi/2)R^+(\pi/\sqrt{2}, \pi)$ discussed in Section 2.7.3. In the first experiments (Schmidt-Kaler et al., 2003c), the controlled-NOT mapped the four logical eigenstates and one superposition state to their desired respective output states with an average fidelity of 0.73(2) (coherence time $\tau \sim 800$ μs , addressing error $\epsilon \sim 0.05$). After several improvements of the experimental set-up ($\tau \sim 2$ ms, $\epsilon \sim 0.03$, more flexible computer control, etc.), fidelities as large as 0.910(6) were observed (Riebe et al., 2006) where, here, the fidelity is defined as an average of the overlap of the produced output states with the ideal output. Additionally, this work implemented the conditional phase shift with the pulse sequence $R^+(\pi/2, 0)R^+(\sqrt{2}\pi, \pi/2)R^+(\pi/2, \pi)$ yielding a fidelity of up to 0.926(6).

4.2. Entangled states with trapped ions

One important application of quantum computers in basic research is the generation of interesting quantum states as for instance the first deterministic generation of entangled particles with ${}^9\text{Be}^+$ ions (Turchette et al., 1998). In addition, new applications of entangled states especially for metrology appear constantly (Blatt and Wineland, 2008). Entangled states play an important role in discussions on the foundations of quantum mechanics. Especially since Bell formulated inequalities which could distinguish between so-called local realistic theories and quantum theories (Bell, 1965, 1971; Clauser et al., 1969), physicists were keen to produce these states and to check the predictions of quantum mechanics. Since then, there have been numerous experiments demonstrating a violation of a Bell inequality. Almost all of these experiments were carried out with photons (for a summary see e.g. Clauser and Shimony (1978), Weihs et al. (1998) and Tittel et al. (1998)). Photons naturally explore the non-locality of entanglement and thus violations over distances of many kilometers were established. However, current detection efficiencies of photons are not high enough to close the so-called ‘detection loophole’, i.e. one must assume that the detected particles represent a fair sample of all particles emitted by the source (Clauser et al., 1969). Therefore, there is a large interest in testing Bell-inequalities with trapped ions where the detection fidelities approach unity. Such an experiment was conducted with ${}^9\text{Be}^+$ ions by Rowe et al. (2001) and closed the detection loophole. However, the ions were not detected outside their respective light cone, i.e. the detection time was longer than the time it takes light to travel between the ions. Thus there could still exist a combined detection-locality loophole. This loophole could be excluded for instance by creating entanglement between ions or atoms separated by several kilometers.

Another interesting aspect of the ion trap experiments is that the entangled states are produced deterministically. That means that in contrast to the photon experiments, the entangled states are created on demand. More importantly, the entangled states are not destroyed during their creation such that they can be used for further experiments.

Current research is directed towards entangled states with more than two particles. Already for three qubits, two classes of entanglement appear: GHZ states (Greenberger et al., 1989) and W states (Dür et al., 2000; Zeilinger et al., 1992). These two classes of entanglement cannot be transformed into each other by local operations and classical communication, i.e. with single-qubit operations and measurements of the individual qubits (Dür et al., 2000). Both classes are not only maximally entangled but also violate Bell-type inequalities.

GHZ states are states of the form

$$|\text{GHZ}\rangle_N = (|00\cdots 0\rangle + |11\cdots 1\rangle)/\sqrt{2}. \quad (22)$$

GHZ states with many qubits can be interpreted as Schrödinger-cat states. For this, e.g. the first qubit is treated as a separate degree freedom and all other qubits as a single quantum system, i.e. the cat system. Then the state of the first qubit indicates the state of the second “macroscopic” system. Another use of GHZ states is by encoding quantum information in a superposition of the form $\alpha|000\rangle + \beta|111\rangle$. If a single qubit flips, the original state can still be recovered with so-called quantum error correction protocols (Shor, 1995; Steane, 1996).

W states are states of the form

$$|W\rangle_N = (|0\cdots001\rangle + |0\cdots010\rangle + |0\cdots0100\rangle + \cdots + |10\cdots0\rangle)/\sqrt{N}. \quad (23)$$

They are remarkably stable against various decoherence sources: they are intrinsically stable against collective dephasing mechanisms (Roos et al., 2004b) and even loss of qubits does not completely destroy the entanglement present in them.

A four ion GHZ state was first produced by Sackett et al. (2000) using a Mølmer–Sørensen type gate (see Section 2.6.3). The produced GHZ-state was analyzed by applying $R^C(\pi/2, \varphi)$ -pulses to all ions simultaneously and measuring the number of fluorescing ions with a photo multiplier. Here, we will illustrate this procedure used by Sackett et al. (2000) for the two particle Bell state $(|00\rangle + |11\rangle)/\sqrt{2}$:

$$\begin{aligned} & |00\rangle + |11\rangle \xrightarrow{R_2^C(\pi/2, \varphi), R_1^C(\pi/2, \varphi)} \\ & \quad (|0\rangle + ie^{i\varphi}|1\rangle)(|0\rangle + ie^{i\varphi}|1\rangle) + (|1\rangle + ie^{-i\varphi}|0\rangle)(|1\rangle + ie^{-i\varphi}|0\rangle) \\ & = (1 - e^{-2i\varphi})|00\rangle + ie^{i\varphi}(1 + e^{-2i\varphi})|01\rangle + ie^{i\varphi}(1 + e^{-2i\varphi})|10\rangle + (1 - e^{-2i\varphi})|11\rangle, \end{aligned} \quad (24)$$

where we used Eq. (10) in the first step and omitted the normalization factors. To find an estimate for the fidelity of the original Bell state, it is useful to introduce the parity operator P which is defined as $P = P_{00} - P_{01} - P_{10} + P_{11}$. Here P_{xy} are the probabilities to find the ions in state $|xy\rangle$. Plotting the expectation value of the parity, we see that it oscillates twice as fast as the phase φ of the analyzing pulses. This behavior can also be interpreted as a consequence of the doubled energy difference between the $|00\rangle$ and the $|11\rangle$ state as compared with the single ion case.

To find the fidelity of the Bell state, two sets of experiments can be carried out: first a Bell state is created and the populations P_{00} and P_{11} are recorded. In a second set of experiments, the maximum ($\max P$) and minimum ($\min P$) of parity oscillations as described in Eq. (24) are determined. The overlap F of the experimentally produced state with a state of the form $(|00\rangle + e^{i\varphi}|11\rangle)/\sqrt{2}$ is given then by $F = (P_{00} + P_{11})/2 + (\max P - \min P)/4$ (Sackett et al., 2000). No individual addressing of the ions is required in the analysis procedure. In addition, the parity can be inferred from the global fluorescence of the ion string. Thus, this analysis method is relatively simple and efficient. Furthermore, it can be generalized to GHZ states with an arbitrary number of ions and is thus very useful to gain information on the generated GHZ states, without individual qubit addressing and read-out.

This analysis technique was also used to verify the creation of a three particle GHZ-states with fidelities of up to 0.89 (Leibfried et al., 2004). The quality of the GHZ state was high enough, that from the resulting generalized Ramsey fringes (c.f. Eq. (24)) the phase could be estimated 1.45 times more accurately than using three uncorrelated particles. Estimating the phase of superpositions is quite important in frequency measurements. The high fidelity of the GHZ states was made possible by using the geometric phase gate (Section 2.6.4). Encouraged by this, the NIST group applied this gate also to create four-, five- and six-particle entangled GHZ-states, with lower bounds for the fidelities of 0.76 (1), 0.60 (2) and 0.509 (4), respectively (Leibfried et al., 2005). As for GHZ states, a fidelity above 0.5 implies automatically the presence of genuine N -partite entanglement, the latter experiments demonstrated up to six partite GHZ-like entanglement.

While the NIST group uses predominantly global addressing and state read-out, the Innsbruck group entangled ions mainly with laser pulses addressed to individual ions. For instance, a Bell can be created in the following way (please note that the right-most ion is the first one) (Roos et al., 2004a):

$$\begin{aligned} & |SS, 0\rangle \xrightarrow{R_1^+(\pi/2, \varphi+\pi/2)} (|SS, 0\rangle + e^{i\varphi}|SD, 1\rangle)/\sqrt{2} \\ & \xrightarrow{R_2^C(\pi, 0)} (|DS, 0\rangle + e^{i\varphi}|DD, 1\rangle)/\sqrt{2} \\ & \xrightarrow{R_2^+(\pi, 0)} (|DS, 0\rangle + e^{i\varphi}|SD, 0\rangle)/\sqrt{2}. \end{aligned} \quad (25)$$

The success of the Bell-state generation is usually verified using a procedure called state tomography (see Section 4.4). The laser phase offset φ of the first pulse determines phase of the Bell state. In addition, an additional $R_2^C(\pi, 0)$ -pulse on the second ion transfers the $(|DS, 0\rangle + e^{i\varphi}|SD, 0\rangle)/\sqrt{2}$ state to $(|SS, 0\rangle + e^{i\varphi}|DD, 0\rangle)/\sqrt{2}$. Thus, using this toolbox all four Bell-states can be created in the same set-up.

Furthermore, the Innsbruck group used the flexibility of the entangling method to create three particle GHZ and W states (Roos et al., 2004b). The idea to create a GHZ state (Cirac and Zoller, 1995), is to apply a controlled-NOT gate while the motional degree is still in a superposition of $|0\rangle$ and $|1\rangle$ (see Eq. (25)). For this CNOT-operation, the motion is the control bit and the new ion is the target bit (the second line in Fig. 24) (Rauschenbeutel et al., 2000; Raimond et al., 2001). Inserting more and more CNOT's, this GHZ-state generation method is straightforwardly generalized to more particles.

In order to create a three-ion W state $|W_3\rangle = (|DDS + |DSD\rangle + |SDD\rangle)/\sqrt{3}$, Eq. (25) can be generalized differently: the length of the first blue sideband pulse is adjusted such that the state $(|SSS, 0\rangle + \sqrt{2}|SSD, 1\rangle)/\sqrt{3}$ is created and ions

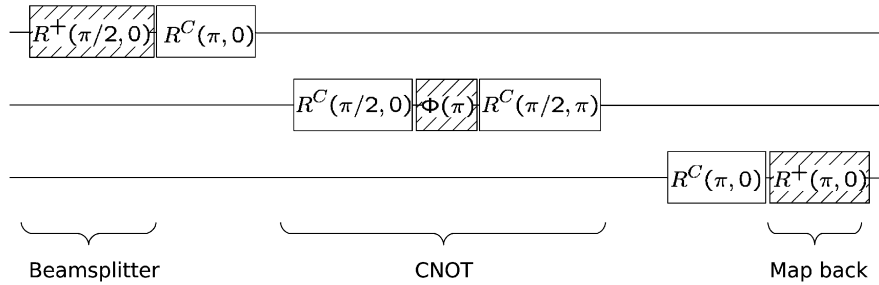


Fig. 24. Pulse sequence to generate a GHZ state. The controlled-NOT operation is implemented with a composite phase gate $\Phi(\pi)$ (see Section 2.7.3) sandwiched in between two R^C -pulses on the center ion. Hatched areas indicate sideband pulses.

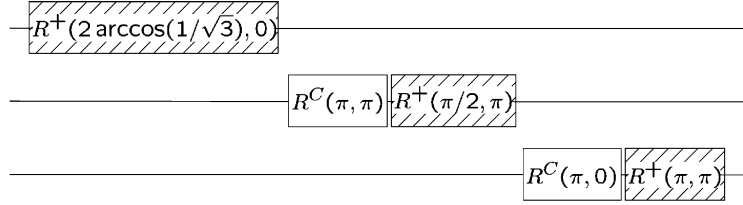


Fig. 25. Pulse sequence to create the W state $(|DDS\rangle + |DSD\rangle + |SDD\rangle)/\sqrt{3}$ from the $|SSS\rangle$ state. Hatched areas indicate sideband pulses.

#2 and #3 are flipped to obtain $(|DDS, 0\rangle + \sqrt{2}|DDD, 1\rangle)/\sqrt{3}$. Then the phonon is shared between the remaining ions #2 and #3 to create $(|DDS, 0\rangle + |DSD, 0\rangle + |SDD, 0\rangle)/\sqrt{3}$. Fig. 25 shows the corresponding pulse sequence (See also Fig. 26.). It can also be directly generalized to N ions by adjusting the pulse area of the first beam splitter to $\arccos(1/\sqrt{N})$ and then sharing the phonon excitation among the other ions equally (Häffner et al., 2005a). Interestingly, the required blue sideband pulse area grows only logarithmically with the ion number and thus the generation time grows sublinear with the number of ions. Therefore, this scheme opens the possibility to generate large entangled states (Fig. 27). In experiments, W states ranging from four up to eight ions have been created (Häffner et al., 2005a). Using a technique called state tomography (see Section 4.4), the experimentally obtained states have been fully characterized (Fig. 27). Analyzing the measured density matrix showed that the generated states indeed carried genuine N -particle entanglement.

We add that an even faster scheme to produce W states was proposed which does not require individual addressing in the entangling procedure (Retzker et al., 2007; Solano, 2005). The idea here is that first a $|DD \cdots D, 1\rangle$ state is created. Then a $R^+(\pi, 0)$ pulse addressed to all ions is supposed to generate the desired W state by mapping the phonon to the electronic state of one of the ions, i.e. creating a symmetric superposition with exactly one electronic state flipped. Retzker et al. (2007) further generalized this procedure to W states with more than one excitation (Dicke states).

Entangled states have also been produced with trapped $^{111}\text{Cd}^+$ and $^{40}\text{Ca}^+$ ions by the Ann–Arbor (Haljan et al., 2005b) and the Oxford groups (Home et al., 2006), respectively. For the two qubit levels, the Ann–Arbor group used the $|F = 0, m_F = 0\rangle$ and $|F = 1, m_F = 0\rangle$ state of the ground state of $^{111}\text{Cd}^+$, taking advantage of its insensitivity to the Zeeman effect in first order. The geometric phase gate (Section 2.6.4) does not work efficiently on magnetic field insensitive transitions (Langer, 2006). Instead, the Ann–Arbor group used a Mølmer–Sørensen gate (Section 2.6.3) to entangle the two ions (Haljan et al., 2005a,b). Furthermore, a tomographic state characterization was applied to evaluate the produced states and the degree of entanglement thoroughly (see Section 4.4). To achieve the required individual addressing capability, a combination of ion selective AC-Stark shifts and microwave fields was used (c.f. Section 2.5.1).

The Oxford group created Bell states with two trapped $^{40}\text{Ca}^+$ ions (Home et al., 2006). They encoded the quantum information in the Zeeman manifold of the $S_{1/2}$ -ground state, thus effectively using the direction of the valence electron's spin. Adopting the geometric phase gate (Section 2.6.4) for $^{40}\text{Ca}^+$, they created the Bell state $(|\uparrow\uparrow\rangle - |\downarrow\downarrow\rangle)/\sqrt{2}$.

In Innsbruck, a Mølmer–Sørensen gate was used to prepare a pair of $^{40}\text{Ca}^+$ ions in the entangled state $\psi = (|SS\rangle + i|DD\rangle)/\sqrt{2}$, where $|S\rangle \equiv |S_{1/2}, m = 1/2\rangle$ and $|D\rangle \equiv |D_{5/2}, m = 3/2\rangle$. Using a gate time $\tau = 50 \mu\text{s}$ with the laser light being smoothly switched on and off within $2.5 \mu\text{s}$, a Bell state fidelity of 0.993(1) was achieved (Benhelm et al., 2008b) when the ions were cooled to the ground state of the motional mode mediating the coupling. Moreover, uneven multiples $k = 1, 3, 5, \dots, 21$ of the gate were used to create entangled states. For $k = 21$, the state fidelity was still 0.8. Finally, the gate yielded Bell states with a fidelity of 0.96 even with the ion string cooled only to the Doppler limit ($\langle n_{\text{bus}} \rangle = 17$).

4.3. Decoherence free subspaces

Laser frequency and magnetic field fluctuations are usually the dominant decoherence mechanisms in ion traps. Both mechanisms lead to fluctuations of the phase between the laser and the atomic polarization and thus to dephasing of each qubit, however, to a good approximation by the same amount for all qubits. If one encodes a single qubit in two ions in such a way that the two phase evolutions cancel each other, the original qubit is protected from this global dephasing

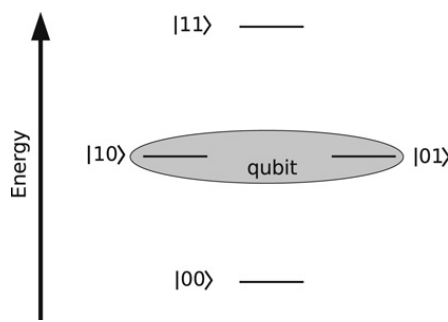


Fig. 26. Energy level diagram for two ions with ground state $|0\rangle$ and excited state $|1\rangle$. A collective-dephasing free qubit is formed by the degenerate logical basis $\{|10\rangle, |01\rangle\}$.

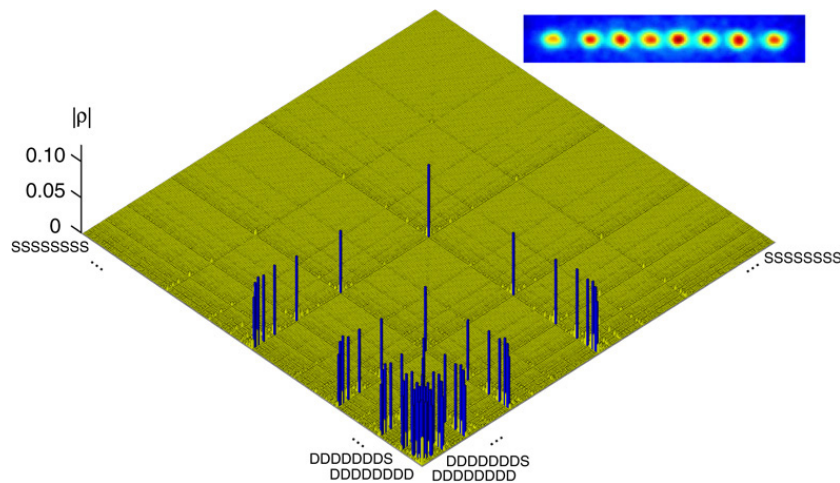


Fig. 27. Absolute values of the density matrix of an eight-ion W state (from Häffner et al. (2005a)). In addition, in the upper right corner the CCD-image of an eight-ion string is displayed. For the state tomography, the experiment was repeated 100 times for each of the 6561 measurement settings. The total measurement time amounted to more than 10 h. The fidelity of the W state was determined to 0.722(1).

and the quantum information is encoded into a decoherence free subspace (DFS). In particular, superpositions of the form $\alpha|01\rangle + \beta|10\rangle$ are transformed by the global single-qubit phase-change $|1\rangle \rightarrow e^{i\phi}|1\rangle$ in the following way:

$$\alpha|01\rangle + \beta|10\rangle \rightarrow \alpha e^{i\phi}|01\rangle + \beta e^{i\phi}|10\rangle. \quad (26)$$

The global phase factor $e^{i\phi}$ cannot be observed, such that the state remains immune against collective dephasing.

This property was demonstrated by Kielinski et al. (2001) using an engineered dephasing mechanism. The qubits were encoded in the hyperfine-states of ${}^9\text{Be}^+$. As a controlled dephasing mechanism, Kielinski et al. (2001) chose an unfocused off-resonant laser beam with “random” intensity. The laser beam leads for each experimental realization to a different AC-Stark effect, however, common to both ions.

In an environment with natural dephasing, Roos et al. (2004a) observed also much increased lifetimes of qubits encoded in a DFS as compared with single ion qubits. In these experiments, the coherence of a state formed by two ${}^{40}\text{Ca}^+$ ions $|\Psi_{\text{qubit}}\rangle = (|DS\rangle + e^{i\varphi}|SD\rangle)/\sqrt{2}$ was retained for 1 s, the dominant decoherence mechanism being spontaneous decay of the $D_{5/2}$ level. For comparison, laser frequency noise and magnetic field fluctuations led to a single ion coherence time of 1 ms.

Furthermore, both the Innsbruck (Häffner et al., 2005b) and the NIST (Langer et al., 2005) groups encoded quantum information in the ground states of two-ion strings with ${}^{40}\text{Ca}^+$ and ${}^9\text{Be}^+$, respectively. Coherence times of 34 s and 7 s, respectively, were measured. In both cases, fluctuations of the magnetic field gradient were believed to be the reason for the decoherence in the DFS. For these experiments, extreme care must be taken to switch off the laser light properly. Not only residual light scattering rates on the order of 0.1 photon/s destroy the coherence, but also fluctuating differential AC-Stark shifts on the order of 1 Hz destroy the phase coherence of the entangled states. Finally, we note that these experiments also demonstrated extremely long lived entanglement of up to 20 s between two parties separated by 5 μm .

Apart from robustly encoding quantum information, decoherence-free subspaces have also found an application in quantum metrology. In Roos et al. (2006), a Bell state was encoded in a combination of Zeeman sublevels of the $D_{5/2}$ level of two ${}^{40}\text{Ca}^+$ ions. The state was decoherence-free with respect to fluctuations of the magnetic field but sensitive to energy level shifts caused by static electric field gradients. In this way, the quadrupole moment of the metastable state could be determined with high precision by monitoring the Bell state’s phase evolution over a duration orders of magnitude longer than the single-qubit coherence time.

4.4. State tomography

Quantum state tomography (Paris and Rehacek, 2004) is a measurement technique that provides access to all the information stored in density matrices describing pure and mixed quantum states. It requires the quantum state of interest to be available in many copies. While the basic measurement principle dates back fifty years (Fano, 1957), experimental implementations of quantum state tomography started only in the 1990's (Smithey et al., 1993; Dunn et al., 1995; Leibfried et al., 1996). Tomographic measurements of systems composed of qubits have been implemented in experiments with nuclear magnetic resonance, photons, trapped ions and superconductors (Chuang et al., 1998a; White et al., 1999; Roos et al., 2004a; Steffen et al., 2006).

Noting that the density matrix of a single qubit can be represented by

$$\rho = \frac{1}{2} \left(I + \sum_{\alpha} \langle \sigma_{\alpha} \rangle \sigma_{\alpha} \right), \quad (27)$$

we see that the density matrix of a single qubit can be inferred by measuring the expectation values $\langle \sigma_{\alpha} \rangle$, ($\alpha = x, y, z$), of the Pauli spin matrices. The measurement of σ_z is accomplished by projecting the qubit onto its energy eigenstate basis. For the measurement of $\sigma_{x,y}$, an additional $\pi/2$ -pulse of suitable phase precedes the projective measurement. The tomographic procedure can be easily extended to systems of several qubits by measuring the joint spin expectation values $\sigma_{\alpha_1}^{(n_1)} \otimes \sigma_{\alpha_2}^{(n_2)} \otimes \cdots \otimes \sigma_{\alpha_k}^{(n_k)}$ where σ_{α_j} denotes a spin component of qubit n_j ($\sigma_{\alpha_j} \in \{I, \sigma_x, \sigma_y, \sigma_z\}$). This way, the determination of the density matrix of an N -qubit system requires the measurement of 4^N expectation values. As some of the operators commute, a total of 3^N measurement bases is necessary. While in principle the number of measurements could be reduced by projecting onto mutually unbiased bases (Wootters and Fields, 1989), this procedure is of no practical importance in current ion trap experiments as it would demand high-fidelity entangling gate operations for mapping the required bases to product state bases.

A slight complication arises, since in every experimental implementation of quantum state tomography, expectation values are never exactly determined but only estimated based on a finite number of measurements. The naïve replacement of the expectation values $\langle \sigma_{\alpha} \rangle$ in Eq. (27) can give rise to unphysical density matrices with negative eigenvalues. This problem is avoided by employing a maximum likelihood estimation of the density matrix (Hradil, 1997; James et al., 2001) that makes use of the estimated expectation values for searching in the set of meaningful density matrices the 'most likely one'. The maximum likelihood algorithm identifies the sought-for density matrix with the one that maximizes the probability of observing the experimentally recorded set of measurement results. Even though maximum likelihood estimation has been criticized (Blume-Kohout, 2006) for being less accurate than Bayesian estimation techniques (Paris and Rehacek, 2004), it has the practical merit of being easily implemented in experiments.

Starting with Roos et al. (2004a), almost all Innsbruck experiments made heavy use of quantum state tomography. Even an eight particle W state has been fully characterized (Häffner et al., 2005a). Fig. 27 shows the experimentally obtained density matrix of an eight-ion W state. A particular merit of quantum state tomography is that all physically available information on the quantum register is extracted. Thus, all aspects of the generated states can be thoroughly analyzed without taking new data.

An alternative to the above described method, was demonstrated by the Oxford group (Home et al., 2006). They used a refined, albeit partial tomographic procedure: instead of choosing three measurement settings for each qubit (either one of the pulses $R^C(0, 0)$, $R^C(\pi/2, 0)$, or $R^C(\pi/2, \pi/2)$ preceding the qubit detection), they choose to apply before the detection the pulses $R^C(\theta_i, \varphi)$ with θ_i either 0, 0.66π , or 0.54π and evenly distributed phases $\varphi \in [0, 2\pi]$. In this way, the reconstruction is less biased and thus more robust against systematic errors or equivalently against decoherence.

4.5. Selective read-out of a quantum register

For some quantum algorithms like teleportation and most error-correction protocols a part of the quantum register has to be read out while leaving the rest of the register intact. Both the Innsbruck and the NIST group succeeded in this task. Barrett et al. (2004) employed segmented traps to separate the ions to be read out from the ions which should remain coherent. Now, one set of ions can be illuminated safely with detection light while the other ions are left dark.

The Innsbruck group chose a different route to selectively read out the quantum register (Roos et al., 2004b; Riebe et al., 2004). Qubits were protected from being measured by transferring their quantum information to superpositions of levels which are not affected by the detection, that is, a light scattering process on the $S_{1/2} \rightarrow P_{1/2}$ -transition in Ca^+ . In the experiments, a π pulse on the $S_{1/2} \rightarrow D_{5/2}$ ($m_j = -5/2$)-transition transfers the quantum information into the $\{D' \equiv D_{5/2} (m_j = -5/2), D \equiv D_{5/2} (m_j = -1/2)\}$ manifold. Fig. 28 shows two ions which are protected from the detection light at 397 nm and the third ion with the original encoding which is measured. After the selective readout, a second set of π -pulses on the D' to S transition transfers the quantum information back to the original computational subspace $\{D, S\}$.

It is interesting to apply the selective read-out to an entangled qubit register and to demonstrate the collapse and even partial collapse of a wave function. For this Roos et al. (2004b) first prepared a three-ion GHZ- and a W-state and then detected one of the ions while the quantum information of the other ions was still protected in the D -level. Fig. 29

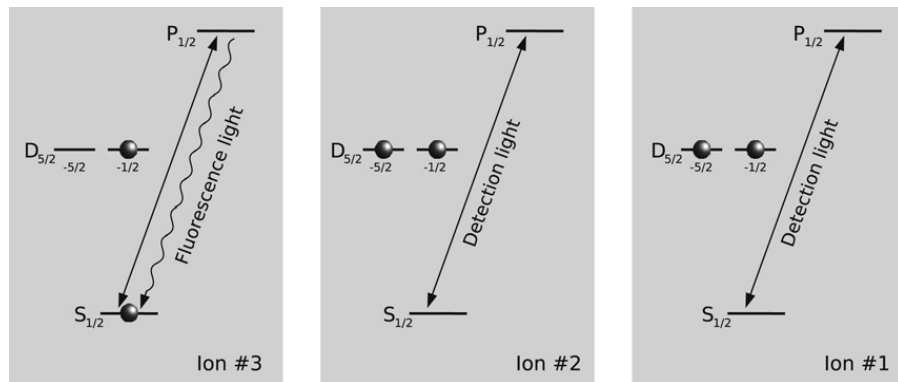


Fig. 28. Partial level scheme of the three Ca-ions (from Roos et al. (2004b)). Only ion #3 is read out. Ion #1 and #2's quantum information is protected in the Zeeman manifold of the $D_{5/2}$ -level, namely the $m_j = -1/2$ and $m_j = -5/2$ levels.

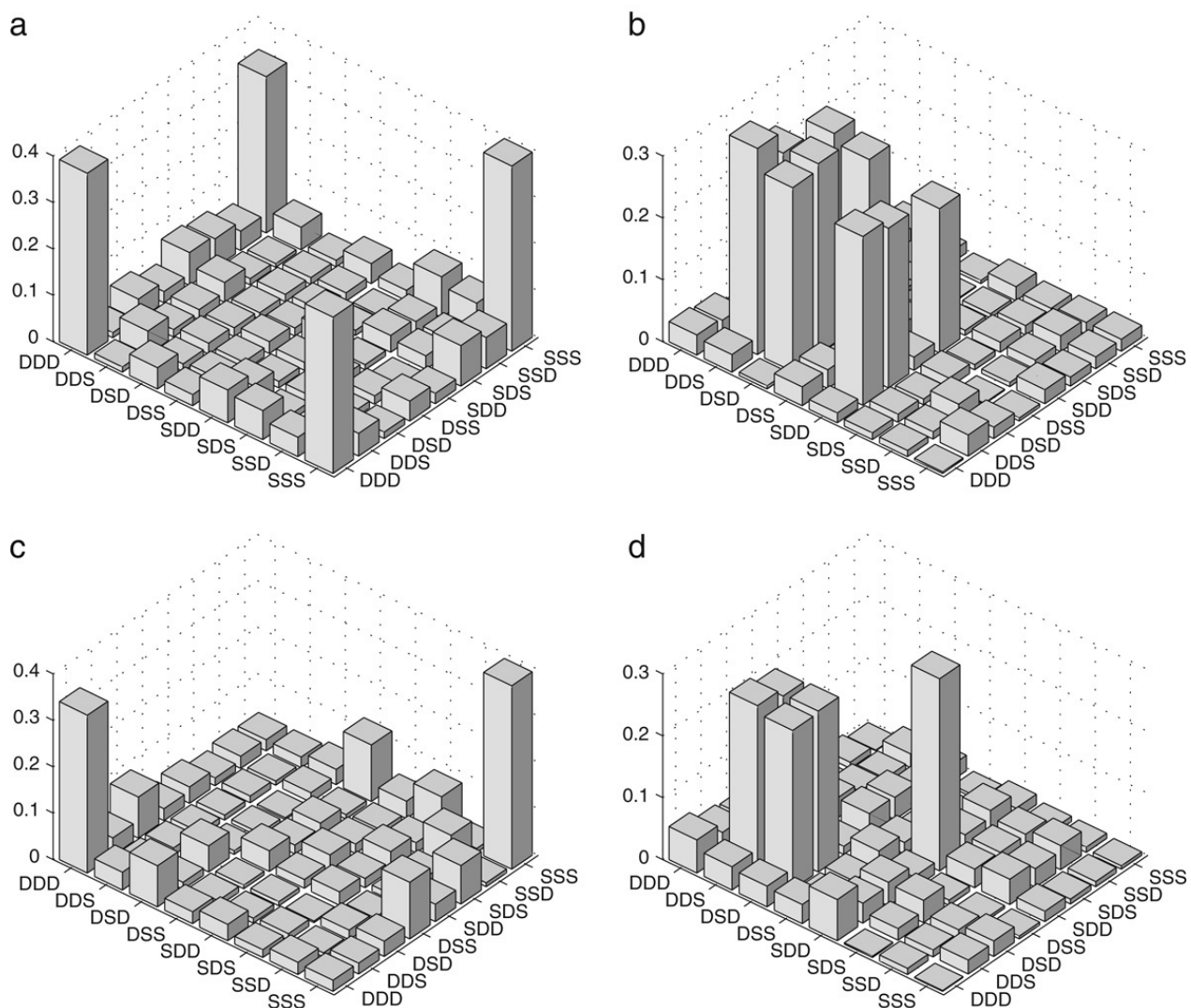


Fig. 29. Absolute values of density matrices after measuring ion #3 (from Roos et al. (2004b)). (a) shows the density matrix of a GHZ-state before measuring and (c) after ion #3 is measured. The same for a W-state ((b) before and (d) after the measurement of ion #3).

shows the results of these measurements. The quantum nature of the GHZ-state was completely destroyed by measuring a single constituent, i.e. it was projected into a mixture of $|SSS\rangle$ and $|DDD\rangle$ (Fig. 29a and c). By contrast, for the W-state, the quantum register remained partially entangled as coherences between ion #1 and #2 persisted after measuring ion #3 (Fig. 29b and d).

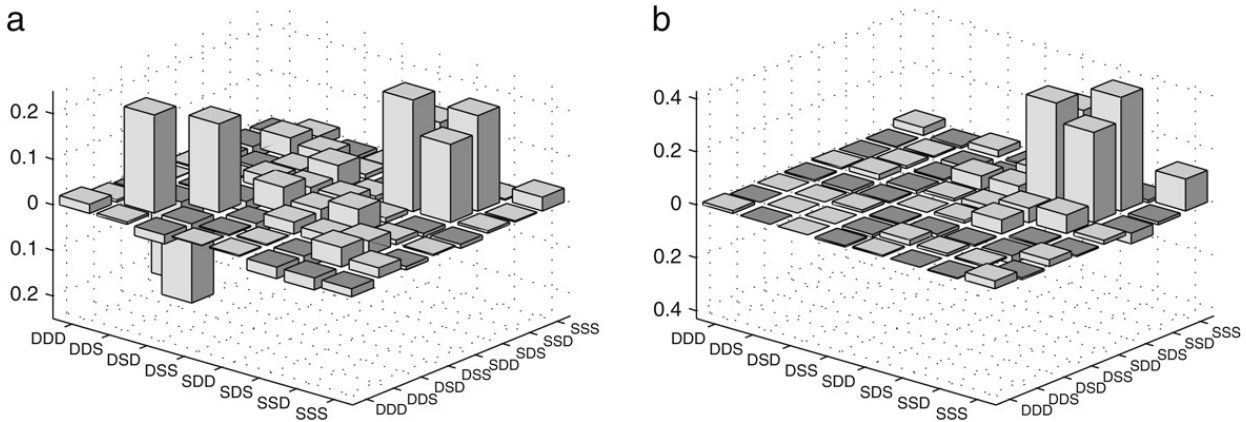


Fig. 30. Density matrices during the individual steps of the deterministic generation of a Bell state from a GHZ-state (from Roos et al. (2004b)). (a) Real part of the density matrix elements of the system after ion #1 of the GHZ-state $(|DSD\rangle + |SDS\rangle)/\sqrt{2}$ has been measured in a rotated basis. (b) Transformation of the GHZ-state $(|DSD\rangle + |SDS\rangle)/\sqrt{2}$ into the bipartite entangled state $|S\rangle(|DS\rangle + |SD\rangle)/\sqrt{2}$ by conditional local operations. Note the different vertical scaling of (a) and (b).

4.6. Conditional single-qubit operations

One can take the partial read-out of a quantum register one step further and perform operations conditioned on the read-out result. As will be discussed in Section 5.2, both the NIST and the Innsbruck group demonstrated this procedure within their respective teleportation experiments (Barrett et al., 2004; Riebe et al., 2004). Furthermore, the Innsbruck group employed conditional operations to deterministically transfer a three-particle GHZ-state with local operations into a two-particle Bell state (Roos et al., 2004b). This procedure can also be regarded as an implementation of a three-spin quantum eraser as proposed by Garisto and Hardy (1999).

In the experiment by Roos et al. (2004b), first the GHZ-state $(|DSD\rangle + |SDS\rangle)/\sqrt{2}$ was created. Application of $R_3(\pi/2, 3\pi/2)$ yielded the GHZ state $|D\rangle(|SD\rangle - |DS\rangle) + |S\rangle(|SD\rangle + |DS\rangle)/2$. Measuring ion #3, projected ions #1 and #2 either onto $(|SD\rangle - |DS\rangle)/\sqrt{2}$ or onto $(|SD\rangle + |DS\rangle)/\sqrt{2}$ with ion #3 indicating in which of the two states the first two ions were (see Fig. 30a). This mixture of the two Bell states can then be transferred to a pure Bell state by inducing a phase shift of π on ion #2 (pulse sequence $R_2^C(\pi, \pi/2)R_2^C(\pi, 0)$) if, and only if, ion #3 was measured to be in the D -state. In addition, the state of ion #3 was reset to $|S\rangle$. Fig. 30 shows the intermediate result before applying the conditional rotation as well as the resulting Bell state. The bipartite entangled state $|S\rangle(|SD\rangle + |DS\rangle)/\sqrt{2}$ was produced with fidelity of 0.75.

4.7. Process tomography

Process tomography is a method to characterize a quantum mechanical evolution (Chuang and Nielsen, 1997; Poyatos et al., 1997). Measurements are made to determine how an arbitrary input state, characterized by the density matrix ρ_{in} , is transformed by the quantum process. The output density matrix ρ_{out} of the process can be expressed as

$$\rho_{out} = \sum_{i,j=0}^{2^N-1} \chi_{ij} \hat{A}_i \rho_{in} \hat{A}_j. \quad (28)$$

Here χ_{ij} is the so-called process matrix, N is the number of qubits and the operators \hat{A}_i form a basis of the space of the $2^N \times 2^N$ matrices. All relevant information on the quantum process is contained in the process matrix χ_{ij} . In the standard procedure, the 4^N separable states – $\{|0\rangle_i, |1\rangle_i, (|0\rangle_i + |1\rangle_i)/\sqrt{2}, (|0\rangle_i + i|1\rangle_i)/\sqrt{2}\}$ for a single qubit – are prepared and then the output of the process is characterized each time with a full state tomography (3^N measurement settings). Inverting Eq. (28) yields the process matrix χ_{ij} .

Such a process tomography has been carried out for characterizing quantum gates in NMR (Childs et al., 2001) and in linear-optics quantum computing (O'Brien et al., 2004; Kiesel et al., 2005). For ion traps, a one-qubit process (the teleportation of a qubit (Riebe et al., 2007)) and two-qubit processes (a CNOT and its square (Riebe et al., 2006)) have been characterized.

Knowing the process matrix χ_{ij} for all basic operations of a quantum computer is a very good basis for estimating the computer's performance. However, there are a few caveats: the number of necessary measurements to determine the process matrix χ_{ij} scales quite dramatically and thus it becomes quickly impractical to characterize processes with numerous qubits. Already for a four-qubit process, 20 736 measuring settings would be required summing up to about 24 h measurement time with the current parameters of the Innsbruck experiment (100 experiments/setting, 25 repetitions/s). In addition, it is not clear that the subsequent application of two processes corresponds to the product of the process matrices.

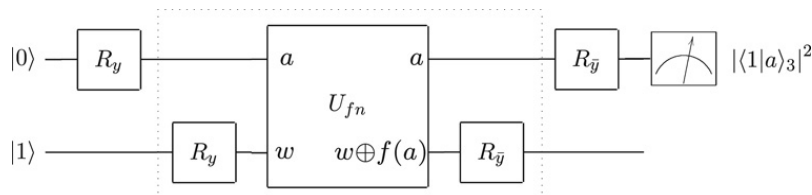


Fig. 31. General scheme of the Deutsch–Josza algorithm (from Gulde et al. (2003)). The upper line represents the qubit holding the input variable a which – if prepared in a logical eigenstate – does not change its value when U_{f_n} is called. The lower line holds the work qubit w . To this number, the value of the function f_n is added modulo 2. The Hadamard rotations R_{y_w} (and $R_{\bar{y}_w}$) transfer the quantum bits into superpositions so that the inherent parallelism of quantum mechanics can be used.

This assumption usually holds only if the relevant environment is time invariant, i.e. the process interacts only with a bath without memory. For example, for the Cirac–Zoller gate, the phonon mode might keep the memory about the failure of an earlier gate operation and thus induce a failure of the next gate. Furthermore, the realization of the process can depend on whether it is executed at the beginning or the end of an algorithm. In particular, experiments are often triggered to the phase of the power line to reduce dephasing due to magnetic field fluctuations caused by 50 Hz or 60 Hz noise and their multiples. Executing a certain gate operation a few milliseconds earlier or later within the experimental sequence leads easily to a change of the qubit resonance frequency of 100 Hz and the realization of the process becomes time dependent.

Process tomography, as presented above, requires at least $4^N 3^N$ measurement settings and is thus quite costly. Above, we have restricted ourselves to the separable operators \hat{A}_j . Using entangled auxiliary qubits and/or measuring in non-separable bases, the number of settings could be reduced, however, scales still exponentially in the qubit number N (Mohseni and Lidar, 2006). Furthermore, most likely the total number of measurement runs has to be on the same order of magnitude as in the standard method to obtain a similar accuracy. Therefore, we conclude that a full quantum process tomography of a large quantum systems will be not practical.

Finally, we note that there exist other approaches to estimate the fidelity of quantum processes. For instance, Knill et al. (2008) employ long sequences of randomly chosen gates. The main idea is that while the result of each gate sequence is known in an ideal implementation, noise leads to deviations from the expected results. Measuring the deviations, the average fidelity of the gate operations can be inferred. Choosing random sequences guarantees that the gate operation is investigated with various input states and in various combinations.

5. Algorithms with trapped ions

5.1. Deutsch–Josza algorithm

The Deutsch–Josza (DJ) algorithm detects the parity of an unknown function (Deutsch, 1989; Nielsen and Chuang, 2000). Concentrating on a single bit, there exist four different functions which map one (qu)bit with value $a = \{0, 1\}$ onto another one. These functions can be divided into constant (even) ($f_1(a) = 0$ and $f_2(a) = 1$) and balanced (odd) functions ($f_3(a) = a$ and $f_4(a) = \text{NOT } a$). With a classical machine, it is necessary to call f_n at least twice to decide whether f_n is odd or even, i.e. one needs to calculate $f_n(0)$ and $f_n(1)$. However, formulating the procedure quantum mechanically, the question whether f_n is constant or balanced can be decided by calling it only once.

In order to formulate the problem quantum mechanically, the functions f_n have to be generalized to take qubits as inputs. Within the framework of quantum mechanics all operations are unitary and therefore another qubit (the work or auxiliary qubit) is added to allow for non-invertible functions f_1 and f_2 . Rephrasing the task, qubit $|a\rangle$ holds the input variable x while qubit $|w\rangle$ (the work qubit) will receive the result of the evaluation $f_n(a)$ plus the initial value w of qubit $|w\rangle$ to guarantee invertibility (see Fig. 31). Thus, we define the unitary U_{f_n} representing the implementation of the function acting on $|w\rangle|a\rangle$ with values w and a , respectively:

$$U_{f_n}|w\rangle|a\rangle = |f_n(a) \oplus w\rangle|a\rangle. \quad (29)$$

Here, \oplus denotes an addition modulo 2.

The DJ-algorithm consists of the following steps (c.f. Fig. 31):

- (1) Initialize the system in the state $|0_a\rangle|1_w\rangle$.
- (2) Transfer the input qubit $|a\rangle$ into $(|0\rangle + |1\rangle)/\sqrt{2}$ and the work-qubit $|w\rangle$ into $(|0\rangle - |1\rangle)/\sqrt{2}$ with Hadamard operations R_y .
- (3) Call the (unknown) function with these superimposed values by implementing U_{f_n} .
- (4) Close the interferometer by applying an inverse Hadamard operation ($R_{\bar{y}}$) on $|a\rangle$.
- (5) Read out the result in $|a\rangle$.

The ion trap experiment used only a single $^{40}\text{Ca}^+$ -ion (Gulde et al., 2003). The internal state acted as the qubit $|a\rangle$ to hold the input variable for the function with the logical assignment $|0\rangle \equiv |S\rangle$, while the axial vibrational degree of freedom was used as the work qubit $|w\rangle$ (logical assignment $|0\rangle \equiv |1\rangle_{\text{ax}}$ and $|1\rangle \equiv |0\rangle_{\text{ax}}$). Thus, ground state cooling to $|S, 0\rangle$ initialized

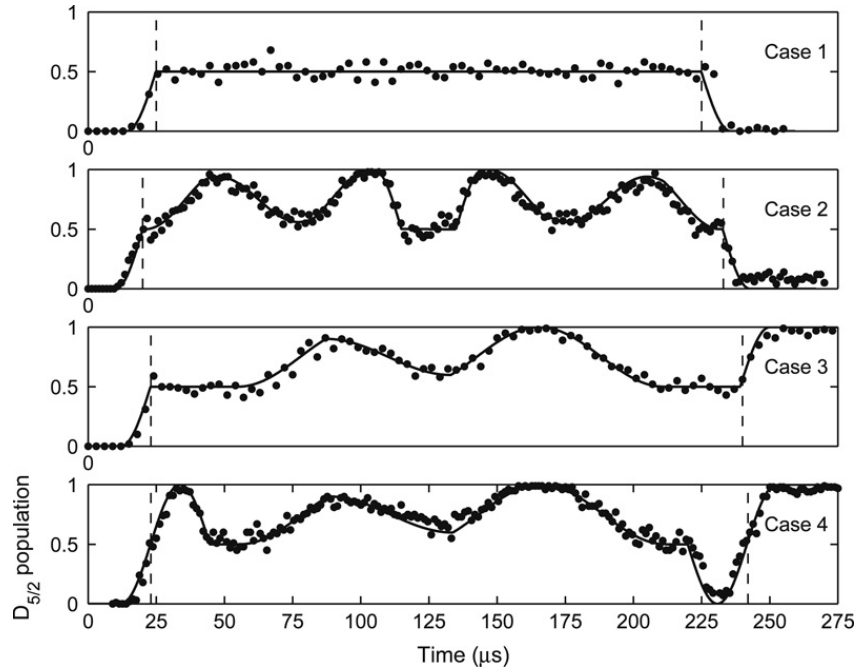


Fig. 32. Traces for the implementation of the DJ-algorithm (from Gulde et al. (2003)). The solid line is not a fit but a calculation based solely on the independently measured Rabi frequencies. The vertical dashed lines enfold the pulse sequences in Table 1.

Table 1

Laser pulses for the implementation of the algorithm inside the dashed box in Fig. 31 ($R_{\bar{y}_w} U_{f_n} R_{y_w}$) on a single ion. φ_{swap} is given by $\arccos(\cot^2(\pi/\sqrt{2}))$. For the whole DJ-algorithm an $R^C(\pi/2, 0)$ -pulse just before and an $R^C(\pi/2, \pi)$ -pulse after implementing $R_{\bar{y}_w} U_{f_n} R_{y_w}$ is applied.

$f_n(x)$	Logic ($R_{\bar{y}_w} U_{f_n} R_{y_w}$)	Laser pulses
$f_1 = 0$	$R_{\bar{y}_w} R_{y_w}$	–
$f_2 = 1$	$R_{\bar{y}_w} \text{SWAP}^{-1}$ NOT _a SWAP R_{y_w}	$R^+(\frac{\pi}{\sqrt{2}}, 0) R^+(\frac{2\pi}{\sqrt{2}}, \varphi_{\text{swap}}) R^+(\frac{\pi}{\sqrt{2}}, 0)$ $R^C(\frac{\pi}{2}, 0) R^C(\pi, \frac{\pi}{2}) R^C(\frac{\pi}{2}, \pi)$ $R^+(\frac{\pi}{\sqrt{2}}, \pi) R^+(\frac{2\pi}{\sqrt{2}}, \pi + \varphi_{\text{swap}}) R^+(\frac{\pi}{\sqrt{2}}, \pi)$
$f_3 = x$	$R_{\bar{y}_w} \text{CNOT} R_{y_w}$	$R^+(\frac{\pi}{\sqrt{2}}, 0) R^+(\pi, \frac{\pi}{2}) R^+(\frac{\pi}{\sqrt{2}}, 0) R^+(\pi, \frac{\pi}{2})$ $R^C(\pi, 0)$
$f_4 = \text{NOT } x$	$R_{\bar{y}_w} \text{0-CNOT} R_{y_w}$	$R^+(\frac{\pi}{\sqrt{2}}, 0) R^+(\pi, \frac{\pi}{2}) R^+(\frac{\pi}{\sqrt{2}}, 0) R^+(\pi, \frac{\pi}{2})$ $R^C(\pi, 0)$

the system in $|0_a\rangle|1_w\rangle$, as required. A peculiarity of encoding a qubit within the ion's motional state is that one has to take care that the system does not leave the computational subspace $\{|S, 0\rangle, |D, 0\rangle, |S, 1\rangle, |D, 1\rangle\}$. In the experiment, this was achieved with the composite pulse techniques described in Section 2.7.3 (Childs and Chuang, 2000). Furthermore, single-qubit operations on the motional degree of freedom had to be carried out. For this, the quantum information in the motional degree of freedom was swapped to the electronic degree of freedom such that ordinary carrier pulses could be used. Finally, the quantum information was swapped back to the motional degree of freedom. The Hadamard rotations R_{y_w} and $R_{\bar{y}_w}$ were absorbed into the definitions of the functions such that only for f_2 this swapping of the quantum information had to be employed.

To decide on the class of the implemented function, only qubit $|a\rangle$ had to be measured. Finding $|a\rangle$ in $|0\rangle$ indicated that the function was even, finding $|1\rangle$ showed that the function was odd (see points at the end of the traces in Fig. 32). For the functions f_1, f_3 and f_4 the fidelity to identify the functions class with a single measurement exceeded 0.97, for f_2 it was still above 0.9.

In order to follow the evolution of $|\langle 1|a\rangle|^2$, the pulse sequence was truncated at a certain time t and the qubit a was measured (see Fig. 32). Repeating this sequence for various times, it is possible to follow the algorithm through its evolution. This procedure helps to debug algorithms and makes sure that the desired algorithm is implemented.

5.2. Teleportation

In quantum teleportation, the state of a qubit is transferred from one physical system to another one. This can be achieved with the following protocol (Bennett et al., 1993): first two parties share an entangled qubit pair. The quantum information

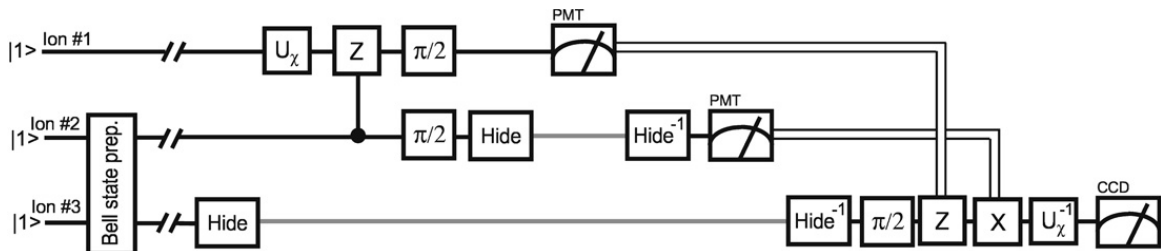


Fig. 33. The teleportation algorithm's quantum circuit as implemented in the Innsbruck experiment (from Riebe et al. (2004)). Double lines represent flow of classical information, whereas single lines represent flow of quantum information. The gray lines indicate when a qubit is protected from detection light via so-called hiding-pulses. First, ions #2 and #3 are entangled, creating the quantum link between the source region (ions #1 and #2) and the target ion (ion #3). Then, after some waiting time, the state to be teleported (on ion #1) is prepared via the unitary operation U_χ . A controlled phase gate together with detection via a photomultiplier tube (PMT) implements the Bell state measurement.

contained in an additional qubit (the source qubit) can be transferred from one party to the other party by performing a Bell-state measurement on the source qubit and one of the entangled qubits. To conclude the transfer, the result of this Bell-state measurement is communicated via a classical channel to the receiver party and the receiver performs one of four rotations depending on the result of the Bell-state measurement. Thus, it is possible to transfer the information content of a qubit by communicating two classical bits (the result of the Bell measurement) and using entanglement. Therefore, teleportation demonstrates a way to break down quantum information into a purely classical part and a quantum part.

Another feature of teleportation is that it is not merely a simple transmission of a quantum state: it does not need a quantum channel to be open at the time the transfer is carried out. Instead, it uses the non-local properties of quantum mechanics, established by a quantum channel prior to the generation of the state to be teleported. Once that link has been established, an unknown state can be transferred deterministically at any later time using classical communication only. Especially this feature was highlighted by the two ion trap teleportation experiments (Barrett et al., 2004; Riebe et al., 2004) by entangling the auxiliary and the target qubits before writing the quantum information into the source qubit. Thus these experiments demonstrate that unknown quantum information can be transferred on demand without using an active quantum channel.

The teleportation circuit displayed in Fig. 33 is formally equivalent to the one proposed by Bennett et al. (1993), but adapted to the Innsbruck ion-trap quantum processor. The Innsbruck group reached fidelities of about 0.75 (Riebe et al., 2004) and 0.83 (Riebe et al., 2007), while the NIST group measured a fidelity of 0.78 (Barrett et al., 2004). Teleportation based on a completely classical resource instead of a quantum entangled resource yields a maximal possible fidelity of 0.667 (Massar and Popescu, 1995). We note that to rule out hidden variable theories, a fidelity in excess of 0.87 is required (Gisin, 1996).

To emphasize the role of the shared entangled pair as a resource, in the Innsbruck experiments, a delay between the creation of the Bell state and the state preparation of the input qubit was introduced. For waiting times of up to 20 ms (exceeding the time required for the teleportation by more than a factor of 10) no significant decrease in the fidelity was observed. For longer waiting times, the measured heating of the ion crystal of less than 1 phonon/100 ms is expected to reduce the fidelity significantly, because the Cirac-Zoller gate requires the center-of-mass mode of the ion string to be in the ground state.

The implementation of the NIST group (Barrett et al., 2004) demonstrates how segmented traps facilitate ion trap quantum computation. The authors use a segmented linear trap (Rowe et al., 2002), where the two DC-electrodes rails are each split into eight segments. Fig. 34 shows the ion positions in each step during the teleportation procedure. By changing the potentials on the electrodes (top), the ion strings can be moved, split and merged. The teleportation algorithm was implemented in the following way (see Fig. 34): first the leftmost and rightmost ions (auxiliary and target, respectively) were prepared in the Bell state $|\downarrow\downarrow\rangle_{13} - i|\uparrow\uparrow\rangle_{13}$ using the geometric phase gate discussed in Section 2.6.4 (Leibfried et al., 2003b). As the bus mode, the stretch mode was used. The center ion does not couple to the stretch mode and thus an effective two-qubit gate between the outer ions is implemented. For the experiments, it proved useful to transfer this Bell state into a singlet state ($|\Psi\rangle = |\uparrow\downarrow\rangle_{13} - |\downarrow\uparrow\rangle_{13}$) as the singlet state remains invariant under global rotations allowing for an effective single-qubit addressing of the source ion #2. This was achieved by changing the relative position of the ions by varying the trap strength such that the subsequent laser pulses had the desired phases at the new ion positions (Rowe et al., 2001). To implement the teleportation, the Bell state measurement has to be carried out on the source ion #1 and the auxiliary ion #2. For this, the target ion #3 was first separated from the string in trap #6 and ions #1 and #2 were transferred back into trap #5. Most importantly, the stretch mode of the two ions was still close to the ground state and the required rotation into the Bell basis could be directly implemented with the geometric phase gate (Section 2.6.4) without the need of a sympathetic cooling step (c.f. Section 6). Then, ion #1 and #2 were measured by transporting first the auxiliary ion into trap #5, measuring there its fluorescence (see Section 2.4) and pumping it into state $|\downarrow\rangle$. Next, ion #2 was also transported to trap #5 and the total fluorescence was detected, revealing the state of the source ion. In a last step, ion #3 was transferred into trap #5 and conditioned on the result of the Bell measurement, the corresponding single-qubit operation was applied.

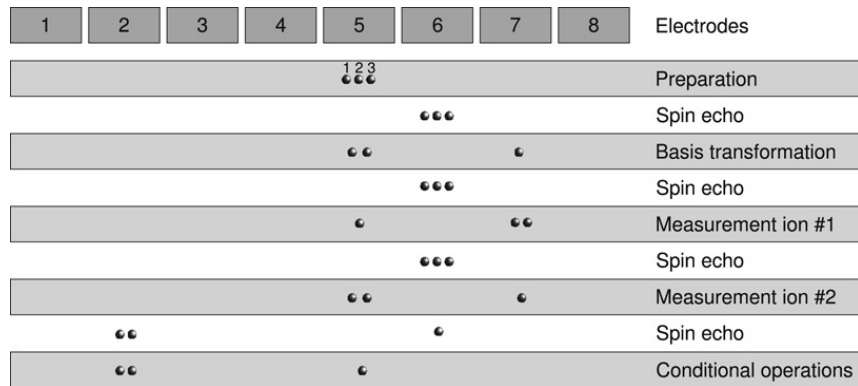


Fig. 34. Position of the ions within the segmented trap during the execution of the NIST groups teleportation implementation (after Barrett et al. (2004)).

5.3. Quantum error correction

Classical computers use error correction schemes intensively. It is to be expected that quantum computers will employ error correction schemes as well. However, due to the continuous nature of quantum information, it might seem difficult to apply the ideas of classical error correction to quantum computers. However, Shor (1995) and Steane (1996) both found algorithms which correct errors by moving the errors from the quantum register to ancilla systems. In these procedures, a logical qubit is encoded in a number of qubits such that the two-dimensional Hilbert space of a single qubit is embedded in a higher-dimensional space. Errors will then rotate the state vector out of the allowed subspace. Generalized measurements can project the system back to the allowed subspace and in case of small errors the original state is recovered. Quantum error codes were implemented in NMR for the first time (Cory et al., 1998; Knill et al., 2001a).

Using trapped ions, Chiaverini et al. (2004) implemented a rudimentary quantum error correction protocol. In these experiments, the authors encoded the (arbitrary) state of a source qubit in a superposition of two distinct three-qubit states (the primary qubit + two ancilla qubits), introduced controlled errors (spin flips only) on all three of them, before they decoded the state with the inverse operation used to encode the primary qubit. Small errors occurring on the encoded state rotated the state such that after decoding, the error could be corrected for. Read-out of the ancilla qubits provided the error syndrome, based on which the primary ion was returned in its original state. Using the language of quantum error correction, the stabilizer code {ZZX, ZXZ} (for an introduction to stabilizer codes see for instance Refs. Gottesman (1997) and Nielsen and Chuang (2000)) was employed in these experiments. This encoding procedure was conveniently implemented by an entangling operation similarly to the ones discussed in Section 2.6.4 and used in Section 4.2. However, in this particular instance, the three ions were placed in the standing wave such that they experienced the phases $\{\varphi, \varphi + 2/3\pi, \varphi + 4/3\pi\}$ in the lattice. In this symmetric configuration, the ions felt no force if they were all in the same state. In all other logical basis states the total averaged force had the same absolute value and thus the same phase was acquired. Most notably, the heart of the algorithm (encoding and decoding) was executed only with global qubit operations, i.e. without individual addressing. Only for the preparation of the primary qubit, was individual addressing necessary and for detecting the error syndrome, selective state read-out was used.

The NIST-group studied the performance of the error correction for the three different input states $\{| \downarrow \rangle, \sqrt{0.10} | \uparrow \rangle - i\sqrt{0.90} | \downarrow \rangle, \sqrt{0.22} | \uparrow \rangle - i\sqrt{0.78} | \downarrow \rangle\}$ for artificial error angles θ_e applied to all qubits simultaneously while the qubit was protected by the encoding. Technical imperfections led to a fidelity of about 0.8 even if no error was applied. Therefore the NIST group compared results where the error syndrome was used to results where the correction pulses were not used to correct the primary qubit. For the measurement eigenstate $| \downarrow \rangle$ and error angles $\theta_e < \pi/2$, the fidelity stayed close to 0.8, whereas in the uncorrected case, the fidelity dropped to 0.5. For the two other superposition states, a clear improvement over the uncorrected implementation was also found.

One of the biggest challenges in quantum information processing will be to improve the fidelity of an error correction algorithm such that it is below a fault-tolerant threshold. Furthermore, the qubit should never be left unprotected. This implies that the error correction has to be applied directly on the encoded qubit. Finally, it will be necessary to apply the error correction repeatedly and to extend the algorithm to correct for spin flips as well as for phase flips.

5.4. Semiclassical quantum Fourier-transform

The quantum Fourier transform is the final step in Shor's algorithm to factor large integers. It is designed to find the periodicity of a quantum state (Shor, 1994; Coppersmith, 1994; Ekert and Jozsa, 1996; Nielsen and Chuang, 2000). Nielsen and Chuang (2000) show that the quantum Fourier transformation transforms an N -qubit register in binary notation according to ($k_i \in \{0, 1\}$)

$$\begin{aligned} |k_N k_{N-1} \cdots k_2 k_1\rangle &\longrightarrow [(|0\rangle + e^{2\pi i[0.k_1]}|1\rangle) \otimes (|0\rangle + e^{2\pi i[0.k_2 k_1]}|1\rangle) \otimes \cdots \\ &\quad \otimes (|0\rangle + e^{2\pi i[0.k_{N-1} \cdots k_2 k_1]}|1\rangle) \otimes (|0\rangle + e^{2\pi i[0.k_{N-1} \cdots k_2 k_1]}|1\rangle)]/\sqrt{2^N}. \end{aligned} \quad (30)$$

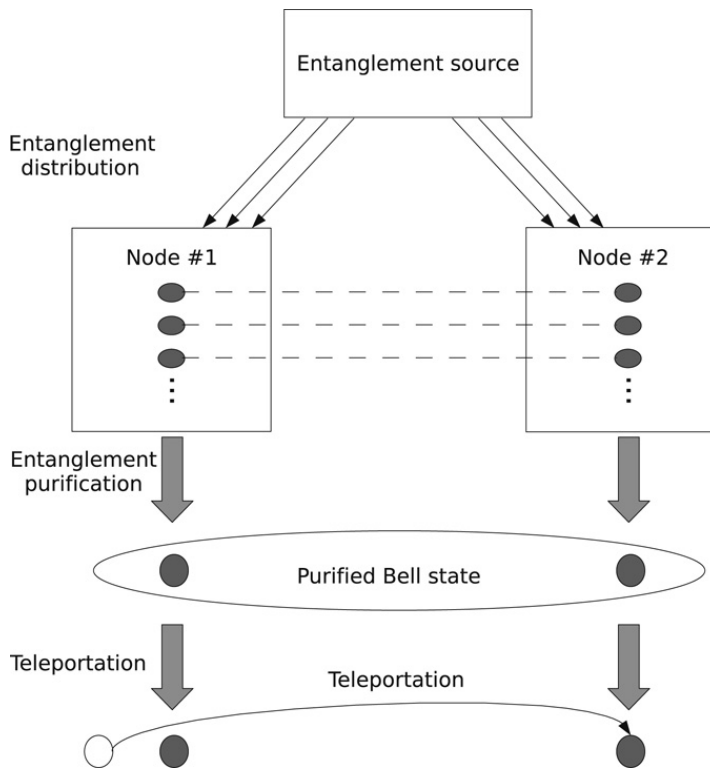


Fig. 35. Schematics of a high-fidelity transfer of quantum information over a noisy quantum channel. First, a number of entangled states of moderate fidelity (>0.5) is shared by both parties (quantum nodes). Next, local operations and measurements are used to create a single Bell state with high fidelity. Finally, this qubit pair is used to teleport quantum information from one node to the other.

Here $[0.k_N k_{N-1} \dots k_2 k_1]$ stands for $k_N/2 + k_{N-1}/4 + \dots + k_2/2^{N-1} + k_1/2^N$. Each qubit is rotated by $R^C(\pi/2, -\pi/2)$ and has acquired a phase shift conditional on other qubits. If the quantum Fourier-transform is the last step in a quantum algorithm, one can take advantage of this structure and perform the semiclassical quantum Fourier-transform (Griffiths and Niu, 1996). Starting with the first qubit $k_{i=1}$, first an $R_i^C(\pi/2, -\pi/2)$ pulse is applied to qubit k_i . Then qubit k_i is measured and conditioned on the result $\exp(i\pi\sigma_z/2^{(j-i+1)})$ rotations are carried out on qubits k_j for all $j > i$. Note that a z rotation directly preceding a measurement does not change the measurement result, such that the last z rotation before a measurement can be omitted. This procedure is then repeated for the next qubit i with i increased by one.

Chiaverini et al. (2005b) implemented this procedure and tested it on a variety of separable and entangled three-qubit states. The implementation used a segmented trap, such that the state of one ion could be measured without destroying the quantum state of the others. In this way, one after the other ion was measured and appropriate single-qubit operations were carried out conditioned on the measurement result. Four states $(|001\rangle + |010\rangle + \dots + |111\rangle, |001\rangle + |011\rangle + |101\rangle + |111\rangle, |011\rangle + |111\rangle, |111\rangle)$ representing all the possible periods one, two, four and eight, respectively, of three bits were successfully tested. In addition, the entangled state $a_{001}|001\rangle + a_{011}|011\rangle + a_{100}|100\rangle + a_{110}|110\rangle$ ($|a_i| = |a_j|$) with approximate period three was investigated. This state has the particular property that the result depends on the relative phases of the coefficients a_i which was confirmed in the experiments, too.

5.5. Entanglement purification

High fidelity entanglement can be obtained from multiple entangled states of lower fidelity by a procedure called entanglement purification. In the context of fault-tolerant quantum computing, entanglement purification can alleviate thus the stringent requirements for quantum communication (Bennett et al., 1996; Gottesman and Chuang, 1999): first many entangled states of a relatively moderate fidelity are created and shared between the two communicating parties. Next, each party carries out local high fidelity quantum operations and measurements before it communicates the measurement results to the other party (see Fig. 35). Based on this, the parties can decide when the entanglement purification was successful and which states to keep for further use. This shared entanglement can be employed to perform a high fidelity state transfer between the two nodes via quantum teleportation (see Section 5.2). In this way, two quantum nodes can be linked with high fidelity even if the direct transfer of quantum information between them limits the fidelity of Bell pairs to just above 0.5. Together with quantum teleportation, this Bell state can be used for a high fidelity state transfer (see Section 5.2).

Reichle et al. (2006b) demonstrated the entanglement purification procedure by purifying a two-atom Bell state out of two pairs of Bell states. First, the NIST-group used the geometric phase gate (see Section 2.6.4) to entangle four ions pairwise in a single step. To achieve this, the ions were placed such that ions #1 and #2 as well as ions #3 and #4 were spaced each

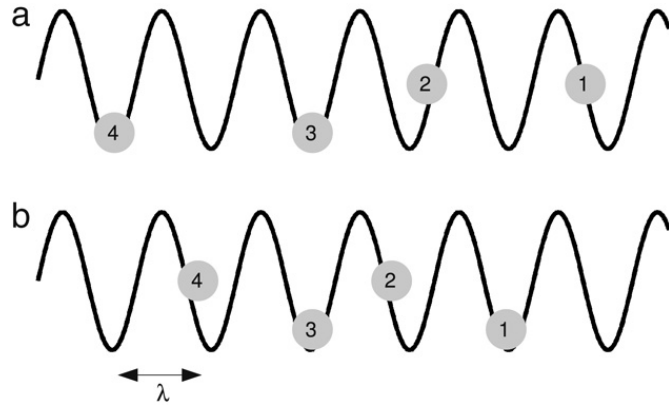


Fig. 36. Location of the ions inside the standing wave pattern for a given point in time during the phase gate operations used by the NIST group for entanglement purification. Panel (a) shows the situation for entangling ion #1 and #2 on one side and for entangling ion #3 and #4 on the other side. The situation to carry out the two phase gates between ion #1 and #3 and between ion #2 and #4 is illustrated in panel (b).

by multiples of the standing wave ($\Delta x = n\lambda$), while between ions #2 and #3 was a distance of $(n \pm 1/4)\lambda$ (see Fig. 36). In this way, the interaction between the two pairs vanished while within each pair the ions were entangled (ion #1 and #2 on one side and #3 and #4 on the other side). To implement the purifying procedure, a controlled-NOT operation has to be implemented on each quantum node, ion #1 and #3 on one side and ion #2 and #4 on the other side. For this, the axial confinement was changed such that there was a distance of $n\lambda$ between ions #1 and #3 as well as between ions #2 and #4, while the distance was $(n \pm 1/4)\lambda$ between ions belonging to different nodes. Thus another geometric phase gate executed two (local) phase-gate operations simultaneously. Measuring ion #1 and #2 (originally entangled with each other) in opposite states signaled success of the purification and the entanglement of the other entangled pair increased, while measuring them in the same state signaled failure of the protocol. In order to verify the entanglement between ions #3 and #4, the NIST group split these ions off from the other two ions prior to the measurement, such that the measurement did not destroy their coherence. In this way, a Bell state with a fidelity of 0.629 ± 0.0015 was obtained starting from two states of the form $\alpha|\uparrow\uparrow\rangle + \beta|\downarrow\downarrow\rangle$ with a Bell-state fidelity of 0.614 ± 0.0015 .

5.6. Quantum simulations

Quantum simulations appear to be very appealing and especially feasible applications of quantum computers. The idea was first put forward by Feynman (1982) and can be actually thought of as the birth of the field of quantum information processing. Later Lloyd verified this suggestion (Lloyd, 1996) and together with Braunstein showed how a quantum system with continuous variables can be simulated efficiently (Lloyd and Braunstein, 1999). Quantum simulations appear so attractive because they require only the interactions which are present in the system to be simulated. In addition, often only moderate manipulation fidelities are necessary to obtain meaningful results.

Leibfried et al. (2002) show that the quantum dynamics of a spin-1/2 particle in an arbitrary potential can be efficiently simulated with a single trapped ion. In the same publication, the NIST-group simulates the action of an optical Mach-Zehnder interferometer and thus a first quantum simulation with a single ion. In this work, a beam splitter is implemented in the following way: the electronic state of the ion represents the number of photons in one of the incoming modes,² while the motional state of the ion describes the state of one of the output modes. An $R^+(\pi/2, 0)$ pulse on the blue sideband can transfer photons from one mode to the other and thus implements the beam splitter. Thus, a sequence of two $R^+(\pi/2)$ -pulses on the blue sideband, resembles the action of two beam splitters of a Mach-Zender interferometer. Furthermore, using second and third order sideband pulses (detuning $\Delta = n\omega_t$, $n = \{2, 3\}$) a non-linear interferometer can be implemented where one photon in one mode can generate two and more photons in the other mode. This process is equivalent to parametric down conversion – a quite important process in quantum information science with photons (Tittel and Weihs, 2001).

In the experiments, first a single ${}^9\text{Be}^+$ -ion was cooled to the motional ground state. Next, a $\pi/2$ -sideband pulse of order $n = 1, 2, 3$ was applied on the axial motional sideband to create the state $(|\downarrow, 0\rangle + |\uparrow, n+1\rangle)/\sqrt{2}$. Then a change in trap frequency induced a phase shift between the two eigenstates. Finally, the phase shift was analyzed with another $\pi/2$ -sideband pulse of order n . The phase shift acquired between the two $\pi/2$ pulses is proportional to the energy separation. Thus, the fringes are more sensitive to the trap frequency change for larger n . This demonstrates the enhanced sensitivity of a non-linear interferometer as compared with a linear one.

Quantum simulations with trapped ions have also been investigated in the context of quantum phase transitions. Porras and Cirac (2004) propose that each ion in the crystal represents a spin. Irradiating the string, for example, with off-resonant

² Since only one photon is assumed at the input this description is complete.

laser radiation produces in each ion a differential level shift which can be interpreted as a magnetic field acting on the spins. Interaction between the spins, i.e. an effective spin–spin interaction, can be simulated by coupling the ions to a collective vibrational mode. Thus, a wide class of Hamiltonians can be investigated efficiently. In particular, it should be possible to observe quantum phase transitions in ion traps.

A first step in this direction has already been taken by the Max Planck group in Garching by simulating the phase transition of a tiny quantum magnet consisting of two $^{25}\text{Mg}^+$ ions from a paramagnetic to a ferromagnetic order (Schaetz et al., 2004; Friedenauer et al., 2008). The spin–spin interaction was realized by the same laser-ion coupling used in geometric phase gates (see Section 2.6.4) while the action of a magnetic field in the x direction was simulated by driving local spin-flips between the hyperfine states of the ions with an RF field of frequency ω_{qubit} . The ground state of an ion with a magnetic field in x direction is given by $|\rightarrow\rangle = (|\uparrow\rangle + e^{i\omega_{\text{qubit}}t}|\downarrow\rangle)/\sqrt{2}$. Tuning the ratio of the two simultaneously applied Hamiltonians adiabatically, the ground state $|\rightarrow\rangle$ of the parametric phase was transferred to the ground state $|\langle\uparrow\uparrow+\downarrow\downarrow\rangle/\sqrt{2}\rangle$ of the ferromagnetic phase with a fidelity of 0.88.

6. Shuttling and sympathetic cooling of ions

Shuttling ions between various traps might relieve the requirements for scalable ion trap quantum computing considerably (Wineland et al., 1998; Kielpinski et al., 2002). In accelerator experiments, shuttling of ions between different traps and re-cooling has been long established to slow down fast ions efficiently (Herfurth et al., 2001). Also single ions have been transported reliably between Penning traps (Häffner et al., 2000). However, for ion trap quantum computing, the requirements are more stringent: in particular, ion strings have to be separated, moved through junctions, recombined and the quantum information must be preserved during all these operations.

In this context, Rowe et al. (2002) demonstrated the reliable transport of single $^9\text{Be}^+$ -ions over 1.2 mm within tens of microseconds in a segmented ion trap. Moreover, they showed that the coherence of the hyperfine qubit was not affected by the transport. For this they first transfer the ion in a superposition with a $\pi/2$ -pulse, transported the ion and tested for the coherence. A contrast of $95.8\% \pm 0.8\%$ limited by magnetic field fluctuations was measured. In a second set of experiments, the NIST-group used a spin echo sequence to reduce the influence of magnetic field fluctuations. Here, the ion (put again in a superposition of physical eigenstates with $\pi/2$ pulses) was transported back and forth. A spin-echo π pulse was applied in the remote trap. The contrast of this measurement, as well as of a control experiment without transport was almost 97%, limited by imperfections of the Raman pulses and off-resonant scattering from the P-level. These results demonstrated that the transport did not affect the coherence of the quantum state.

Furthermore, Rowe et al. (2002) investigated motional heating for various transport speeds. For this, the voltages on the trap electrodes were changed such that the trap minimum moved with time along a \sin^2 function. This ensures that not only the velocity but also the acceleration varies smoothly with time. They found that the ions can be transported between the two traps within 54 μs with hardly any observable motional heating (axial trap frequency 2.9 MHz, heating $\lesssim 0.01$ quanta/transport). Only for shorter transporting times heating of the ion motion was observed in agreement with a classical simulation.

In addition, Rowe et al. (2002) demonstrate splitting of ion strings. However, their electrode structure was not optimized for this task as the size of the separation electrodes was too large. Therefore, only success rates of 95% were achieved as well as relatively long separation times of about 10 ms were required. Furthermore, the ions heated excessively by 140 ± 70 quanta due to the fact that during the separation the ion oscillation frequency was quite small. Later the NIST group demonstrated that these problems can be overcome (Barrett et al., 2004) (c.f. Section 5.2). Separation times of a few 100 μs as well as small motional heating have been achieved in these experiments. In particular, after splitting one ion from a three ion crystal, the stretch mode of the remaining two-ion crystal was still in the ground state, while the center-of-mass mode had acquired one motional quantum. A theoretical study of the splitting process and the required electrode structures can be found in Ref. Home and Steane (2006).

Another requirement for the proposal by Kielpinski et al. (2002) is the transport through junctions. First experiments were carried out by Pearson et al. (2006) and Hensinger et al. (2006). In the former experiment, charged nano-particles were transported through a four-way crossing of a planar segmented trap. In the latter, Cd^+ ions were moved through a T-junction. Recently, the linear transport of ions was studied within the framework of quantum mechanics (Reichle et al., 2006a), while the non-adiabatic transport was investigated theoretically by Schulz et al. (2006) and experimentally by Huber et al. (2008). Finally, Hucul et al. (2008) analyzed the transport through various junction geometries (including T junctions) quantum mechanically.

After transport, the ion strings might have to be re-cooled such that the subsequent operations can be carried out with high fidelity. In order to achieve this while maintaining coherence, a viable way seems to use the strong Coulomb coupling and to cool only a part of or even only one ion of an ion string. Such sympathetic cooling was demonstrated in various experiments (Drullinger et al., 1980; Larson et al., 1986; Rohde et al., 2001; Hornekaer et al., 2001). Furthermore, it has been established in various contexts ranging from precision measurements (Roth et al., 2005) to electron cooling in accelerators (Meshkov, 1997).

Within the context of quantum information, Rohde et al. (2001) cooled a two ion string to the motional ground state as required for many two-qubit proposals. However, in these experiments two ions of the same species were used. As,

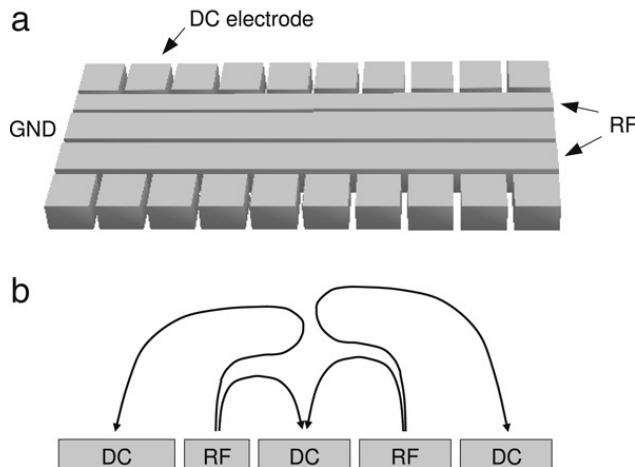


Fig. 37. Electrode configuration of a planar trap. (a) shows the a three-dimensional view of the asymmetric electrode arrangement, while (b) shows a side view with some of the electric field lines.

typically, one of the qubit levels takes part in the cooling process, it is important to shield other nearby ions from the radiation to maintain the coherence of the qubits during the cooling process. This is very difficult if only one ion species is employed. Blinov et al. (2002) cool a $^{112}\text{Cd}^+$ ion via Doppler cooling of $^{114}\text{Cd}^+$. Isotope shift would help to preserve the coherence, however, it might be better to use a completely different ion species as done in the early experiments by the NIST group. Barrett et al. (2003) cooled Be^+ with Mg^+ to the motional ground state (vice versa only to the Doppler limit) and in separate measurements showed that even on time scales of 30 ms a qubit encoded in the hyperfine manifold of $^9\text{Be}^+$ is not affected by the strong cooling light for Mg^+ . Finally, Schmidt et al. (2005) took the idea one step further and cooled and detected the internal state of Al^+ via Be^+ .

While all prerequisites for quantum computing by shuttling ion strings have now been demonstrated in separate experiments, a combination of shuttling ions, splitting and re-cooling the ion strings in the same experiment and at the same time preserving the quantum information has yet to be accomplished.

7. New trap developments

Parallel with the efforts to shuttle and split ion strings, in particular the NIST group has put quite some effort into developing new traps manufactured by microfabrication techniques to build a medium sized quantum computer. Microfabrication techniques allow for complicated and precise electrode structures. Trap sizes (measured as the distance between two RF electrodes) range from about 200 μm down to a few tens of μm . While in the beginning mainly three-dimensional designs were built using two substrates, recently a new, planar trap design was invented by Chiaverini et al. (2005a). In such traps, the electrodes are arranged all in a plane such that a single substrate suffices to mount the electrodes. Typically there are five (four) electrode groups in such a linear surface trap (see Fig. 37): on the center electrode, ground or a small DC potential is applied. The two neighboring electrodes receive an RF potential which provides the radial confinement. The outer electrodes are often structured and various DC potentials provide the axial confinement. The ions are trapped in the center of the field lines in Fig. 37b where the RF field vanishes. The asymmetry of the RF electrodes tilts the principle axes of the quadrupole field such that a laser beam traveling parallel with the trap surface has a projection along both radial motional degrees of freedom and all modes can be cooled satisfactorily. Two trap designs were successfully used by the NIST group, one based on gold on a quartz substrate (Seidelin et al., 2006) and the other one based solely on silicon (Britton et al., 2006). Ions have been trapped as close as 40 μm to the surface with still reasonable heating rates of a few phonons/ms (Seidelin et al., 2006; Epstein et al., 2007). The MIT group developed a trap based on printed circuit board fabrication techniques (Pearson et al., 2006). They also built traps using silver on a quartz substrate (Labaziewicz et al., 2008a). For trap sizes between 75 μm and 150 μm (ion-substrate distance), heating rates between 2 and 20 phonons/s were measured at 4 K (see Section 3.2).

8. Future challenges and prospects for ion trap quantum computing

In order to achieve universal quantum computing, the algorithms have to be implemented in a fault-tolerant way. It is commonly accepted that this requires quantum error correction. Therefore, currently one of the most important goals is to implement quantum error correction repeatedly with high fidelity to prolong coherence times and to correct for errors induced by the gate operations. The largest obstacle to perform a successful quantum error correction protocol seems to be the limited fidelity of the operations. The current state of the art for the control in ion trap quantum computing can be summarized as follows:

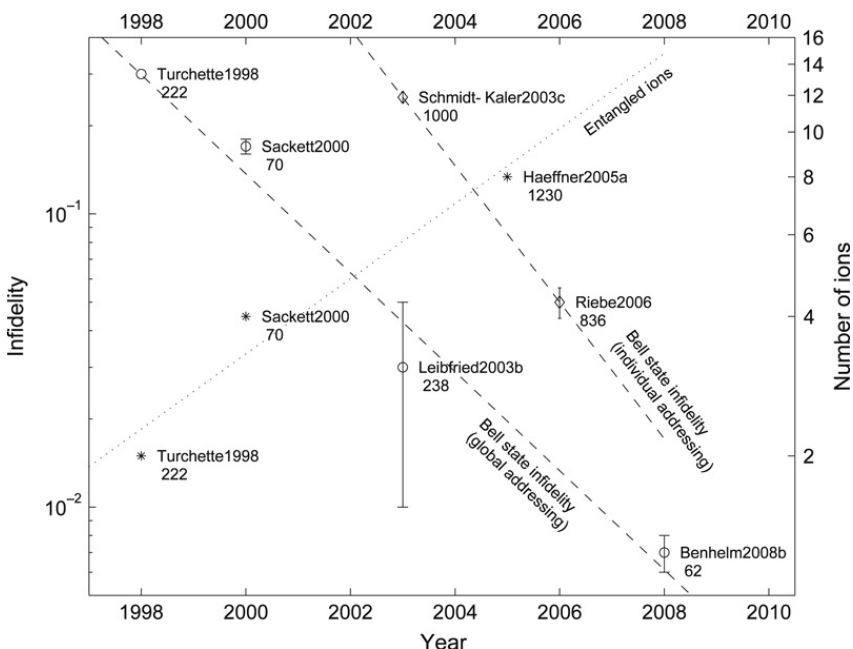


Fig. 38. Progress in reducing the error rate of two-qubit gates (taken from Ref. Benhelm (2008)) and in increasing the number of entangled ions. Open circles represent experiments using two-qubit gate operations with global addressing while diamonds show results based on individual addressing. The performance is measured in terms of the infidelity of produced Bell states. Stars mark the largest number of entangled ions obtained at that time. Numbers below the reference indicate the number of trap cycles required for the operation. Dashed and dotted lines indicate the trends.

- The qubit coherence times are one or two orders of magnitude longer than the basic (gate) operations. In specific cases, coherence times longer by more than five orders of magnitude the gate time are available (see Section 3.1.2). In most current experiments, motional decoherence is not a problem. In addition, it can be further suppressed with cooling of the trap electrodes (see Section 3.2).
- Initialization accuracies are on the order of 0.999 as discussed in Section 2.4. Most likely, they can be improved further if necessary.
- Single qubit operation can be carried out with fidelities exceeding 0.995 (Knill et al., 2008). If required, further improvements are possible with more stable laser fields at the ion positions.
- Implementations of two-qubit gate operations achieve fidelities of about 0.9–0.99. Depending on the gate type, various sources limit the fidelity. Errors are caused by off-resonant scattering, imperfect addressing of individual qubits, insufficient cooling, laser frequency and intensity noise.
- The read-out of a single qubit can be performed with a fidelity of 0.999. Further improvements seem possible (see Section 2.4).
- Ion strings can be shuttled, split and merged (see Section 6) with high fidelity and small decoherence.

Currently, two-qubit gate operations seem to be the main limiting factor and receive therefore most attention both from experimenters and theoreticians. Fig. 38 shows the progress of the fidelity achieved in the last decade. Most notably Benhelm et al. (2008b) demonstrate two-qubit gate fidelities high enough to allow in principle fault tolerant quantum computation according to the scheme proposed by Knill (2005). In addition, one must always keep in mind that all these requirements have to be met at the same time. Furthermore, some emphasis should be given to parallel processing quantum information (Steane, 2004). However, initialization of the necessary ancillas, read-out, coherence times and the particular layout and the attainable degree of parallelization are important.

Both analytical and numerical results indicate that operational fidelities on the order of 0.9999/operation seem to be sufficient to achieve fault tolerance (the so-called fault-tolerant threshold), provided certain other criteria can be met, too (Steane, 2004): specific errors, error propagation, the allowed overhead, specific requirements, the amount of possible parallelization, amongst others have to be considered to get a full grasp on the situation at hand. Thus the concept of thresholds is oversimplifying the situation. For instance, Knill (2005) published numerical results which indicate that even error rates on the order of 10^{-2} are permitted, however with a huge overhead of 10^6 physical qubits for one logical qubit. It seems reasonable that every operation in a quantum computer should be treated with the same meticulous attention and be implemented as perfect as possible to achieve fault tolerance while keeping the overhead as small as possible.

Interestingly, state transfer between interconnected ion trap quantum computers at the fault-tolerant level is not necessary as discussed in Section 5.5 (Gottesman and Chuang, 1999; Reichle et al., 2006b): quantum information can be teleported deterministically between two locations using a purified entangled Bell-state. Entanglement between distant ions can, for example, be generated by splitting an entangled two-ion string and transporting one of the ions or by interfering fluorescence light from two ions on a beam splitter as demonstrated already by Maunz et al. (2007), Moehring et al. (2007) and Matsukevich et al. (2008).

Another important issue is the speed of the operations. Having in mind universal quantum computing to outperform classical computers, e.g. in factoring large integers, billions of operations have to be carried out. Thus, the current typical time scales for the basic operations of a few hundreds of μs seem simply too slow for factoring large numbers even if the operations are carried out to a large extent in parallel. There exist proposals for gate operations which are faster than the trapping frequencies (García-Ripoll et al., 2003, 2005; Zhu et al., 2006), however, there are other bottlenecks such as read-out and ion string separation which might slow down the processor speed.

From this perspective, it seems attractive to work on hybrid devices where e.g. quantum information is stored in trapped ions (incl. error correction) and most of the processing is implemented e.g. with Josephson junctions (Makhlin et al., 2001; Steffen et al., 2006; Plantenberg et al., 2007) which operate at speeds roughly three orders of magnitude faster than current ion trapping approaches. Before this can happen, however, tremendous difficulties have to be solved in transferring quantum information between the two systems within the short coherence times of the Josephson junction qubits. Currently, there exist a few proposals to couple ion-trap and Josephson junction qubits (Tian et al., 2004, 2005; Sørensen et al., 2004), but so far almost no experimental results were achievable. Furthermore, within the field of Josephson junction quantum information processing, there are some open challenges before advantage can be taken of the speed of this system. The biggest of these seems to be that coherence times of only a few μs have been achieved so far.

The original proposal of Cirac and Zoller (1995) is scalable in the sense that it does not require exponentially many resources with an increasing number of qubits. Indeed, Fig. 38 shows that in the last decade larger and larger ion strings have been entangled. However, it seems impractical to construct a device for a large number of qubits by trapping all ions in the same trap because it gets more and more difficult to obtain the required strong radial confinements to work with linear ion strings at reasonably high axial trapping frequencies. Furthermore, the mode structure of the ion crystal gets more complicated with more ions as well as the speed of the sideband operations is reduced with the larger mass of the crystal. Up to date, there is a couple of routes known which potentially ease these technological challenges. Almost all of them are based on distributing the ions across different traps and to interconnect these traps via photons (Cirac et al., 1997), superconducting strip lines (Tian et al., 2004; Heinzen and Wineland, 1990) or even via auxiliary ions (Cirac and Zoller, 2000).

The currently most advanced procedure, however, is to merge and shuttle small ion strings in segmented traps (Wineland et al., 1998; Kielpinski et al., 2002). Those ideas have been studied in detail and seem to offer a practicable and viable way to scale ion trap quantum computers. Currently, large efforts are under way in realizing this architecture (c.f. Section 6). Major challenges are the fabrication of such complex small ion traps combining high flexibility of ion movement (junctions), low motional heating rates and high trap frequencies. It is also strongly desirable to integrate the control electronics and optics on such ion trap devices.

In summary, the basic requirements for a general purpose quantum computing device with trapped ions have been demonstrated and no fundamental road block is in sight. However, building such a device is extremely challenging. Especially, the stringent requirements for fault tolerance and for scalability to many thousands of qubits pose huge difficulties. However, reaching a good control over a reasonable number of qubits seems feasible in the next decade and might be of quite some interest: already with about forty qubits, physical systems can be simulated which are intractable with current computing technology. It remains to be seen whether and how the dream of universal quantum computing can be implemented with trapped ions.

Acknowledgments

We thank Ferdinand Schmidt-Kaler, Wolfgang Hänsel, Stephan Gulde, Mark Riebe, Gavin Lancaster, Jürgen Eschner, Christoph Becher, Michael Chwalla, Jan Benhelm, Umakant Rapol, Timo Körber, Thomas Monz, Philipp Schindler, Kihwan Kim and Piet Schmidt for their ideas, work on the ion trap apparatus and moral support. Furthermore, we thank Dietrich Leibfried for carefully reading the manuscript. H.H. was partially funded by the Marie-Curie program of the European Union. We gratefully acknowledge also support by the Austrian Science Fund (FWF), the Army Research Office, by the Institut für Quanteninformation Ges.mbH and by the European Commission within the QUEST, CONQUEST, QGATES and SCALA networks.

References

- Acton, M., Brickman, K.-A., Haljan, P., Lee, P., Deslauriers, L., Monroe, C., 2006. Near-perfect simultaneous measurement of a qubit register. *Quant. Inf. Comp.* 6, 465.
- Aolita, L., Kim, K., Benhelm, J., Roos, C.F., Häffner, H., 2007. High-fidelity ion-trap quantum computing with hyperfine clock states. *Phys. Rev. A* 76 (4), 040303.
- Army Research Office (USA), 2005. ARDA quantum computation roadmap. http://qist.lanl.gov/qcomp_map.shtml.
- Barenco, A., Bennett, C.H., Cleve, R., DiVincenzo, D.P., Margolus, N., Shor, P., Sleator, T., Smolin, J.A., Weinfurter, H., 1995. Elementary gates for quantum computation. *Phys. Rev. A* 52 (5), 3457–3467.
- Barrett, M.D., Chiaverini, J., Schaetz, T., Britton, J., Itano, W.M., Jost, J.D., Knill, E., Langer, C., Leibfried, D., Ozeri, R., Wineland, D.J., 2004. Deterministic quantum teleportation of atomic qubits. *Nature* 429, 737–739.
- Barrett, M.D., DeMarco, B., Schaetz, T., Leibfried, D., Britton, J., Chiaverini, J., Itano, W.M., Jelenković, B., Jost, J.D., Langer, C., Rosenband, T., Wineland, D.J., 2003. Sympathetic cooling of $^9\text{Be}^+$ and $^{24}\text{Mg}^+$ for quantum logic. *Phys. Rev. A* 68, 042302.
- Barton, P.A., Donald, C.J.S., Lucas, D.M., Stevens, D.A., Steane, A.M., Stacey, D.N., 2000. Measurement of the lifetime of the $3d\ ^2D_{5/2}$ state in $^{40}\text{Ca}^+$. *Phys. Rev. A* 62, 032503.

- Bell, J., 1965. On the Einstein–Podolsky–Rosen paradox. *Physics* 1, 195.
- Bell, J., 1971. Foundations of Quantum Mechanics. Academic, New York, pp. 171–181.
- Benhelm, J., 2008. Precision spectroscopy and quantum information processing with trapped calcium ions. Ph.D. Thesis, Universität Innsbruck.
- Benhelm, J., Kirchmair, G., Rapol, U., Körber, T., Roos, C.F., Blatt, R., 2007. Measurement of the hyperfine structure of the $S_{1/2}$ – $D_{5/2}$ transition in $^{43}\text{Ca}^+$. *Phys. Rev. A* 75, 032506.
- Benhelm, J., Kirchmair, G., Roos, C.F., Blatt, R., 2008a. Experimental quantum-information processing with $^{43}\text{Ca}^+$ ions. *Phys. Rev. A* 77, 062306.
- Benhelm, J., Kirchmair, G., Roos, C.F., Blatt, R., 2008b. Towards fault-tolerant quantum computing with trapped ions. *Nat. Phys.* 4, 463.
- Bennett, C.H., Brassard, G., Crépeau, C., Jozsa, R., Peres, A., Wootters, W., 1993. Teleporting an unknown quantum state via dual classical and Einstein–Podolsky–Rosen channels. *Phys. Rev. Lett.* 70, 1895–1899.
- Bennett, C.H., Brassard, G., Popescu, S., Schumacher, B., Smolin, J., Wootters, W.K., 1996. Purification of noisy entanglement and faithful teleportation via noisy channels. *Phys. Rev. Lett.* 76 (5), 722–725.
- Bergquist, J.C., Hulet, R.G., Itano, W.M., Wineland, D.J., 1986. Observation of quantum jumps in a single atom. *Phys. Rev. Lett.* 57 (14), 1699–1702.
- Blatt, R., Wineland, D., 2008. Entangled states of trapped atomic ions. *Nature* 453, 1008–1015.
- Blinov, B., Deslauriers, L., Lee, P., Madsen, M., Miller, R., Monroe, C., 2002. Sympathetic cooling of trapped Cd isotopes. *Phys. Rev. A* 65, 040304.
- Blinov, B.B., Moehrung, D.L., Duan, L.-M., Monroe, C., 2004. Observation of entanglement between a single trapped atom and a single photon. *Nature* 428 (6979), 153–157.
- Blume-Kohout, R., 2006. Optimal, reliable estimation of quantum states. [arXiv:quant-ph/0611080](https://arxiv.org/abs/quant-ph/0611080).
- Bollinger, J.J., Heinzen, D.J., Itano, W.M., Gilbert, S.L., Wineland, D.J., 1991. A 303 MHz frequency standard based on trapped Be^+ ions. *IEEE Trans. Instr. Meas.* 40, 126.
- Brickman, K.-A., 2007. Implementation of grover's quantum search algorithm with two trapped ions. Ph.D. Thesis, University of Michigan.
- Brickman, K.-A., Haljan, P.C., Lee, P.J., Acton, M., Deslauriers, L., Monroe, C., 2005. Implementation of Grover's quantum search algorithm in a scalable system. *Phys. Rev. A* 72, 050306–1.
- Britton, J., Leibfried, D., Beall, J., Blakestad, R.B., Bollinger, J.J., Chiaverini, J., Epstein, R.J., Jost, J.D., Kielpinski, D., Langer, C., Ozeri, R., Reichle, R., Seidelin, S., Shiga, N., Wesenberg, J.H., Wineland, D.J., 2006. A microfabricated surface-electrode ion trap in silicon. [arXiv:quant-ph/0605170](https://arxiv.org/abs/quant-ph/0605170).
- Brossel, J., Kastler, A., Winter, J., 1952. Optical method of creating an inequality of population between Zeeman sub-levels of atomic ground states. *J. Phys. Rad.* 13, 668.
- Brune, M., Nussenzveig, P., Schmidt-Kaler, F., Bernardot, F., Maali, A., Raimond, J.M., Haroche, S., 1994. From Lamb shift to light shifts: Vacuum and subphoton cavity fields measured by atomic phase sensitive detection. *Phys. Rev. Lett.* 72 (21), 3339–3342.
- Chiaverini, J., Blakestad, R.B., Britton, J., Jost, J.D., Langer, C., Leibfried, D., Ozeri, R., Wineland, D., 2005a. Surface-electrode architecture for ion-trap quantum information processing. *Quant. Inf. Comp.* 5, 419.
- Chiaverini, J., Britton, J., Leibfried, D., Knill, E., Barrett, M.D., Blakestad, R.B., Itano, W.M., Jost, J.D., Langer, C., Ozeri, R., Schaetz, T., Wineland, D.J., 2005b. Implementation of the semiclassical quantum Fourier transform in a scalable system. *Science* 308, 997–1000.
- Chiaverini, J., Leibfried, D., Schaetz, T., Barrett, M.D., Blakestad, R.B., Britton, J., Itano, W.M., Jost, J.D., Knill, E., Langer, C., Ozeri, R., Wineland, D.J., 2004. Realization of quantum error correction. *Nature* 432, 602–605.
- Chiaverini, J., W.E., Lybarger, J., 2008. Laserless trapped-ion quantum simulations without spontaneous scattering using microtrap arrays. *Phys. Rev. A* 77, 022324.
- Childs, A.M., Chuang, I.L., 2000. Universal quantum computation with two-level trapped ions. *Phys. Rev. A* 63, 012306.
- Childs, A.M., Chuang, I.L., Leung, D.W., 2001. Realization of quantum process tomography in NMR. *Phys. Rev. A* 64, 012314.
- Chuang, I.L., Gershenfeld, N., Kubinec, M., 1998a. Experimental implementation of fast quantum searching. *Phys. Rev. Lett.* 80 (15), 3408–3411.
- Chuang, I.L., Nielsen, M.A., 1997. Prescription for experimental determination of the dynamics of a quantum black box. *J. Modern Opt.* 44, 2455.
- Chuang, I.L., Vandersypen, L.M.K., Zhou, X., Leung, D.W., Lloyd, S., 1998b. Experimental realization of a quantum algorithm. *Nature* 393, 143.
- Cirac, J.I., Zoller, P., Kimble, J., Mabuchi, H., 1997. Quantum state transfer and entanglement distribution among distant nodes in a quantum network. *Phys. Rev. Lett.* 78, 3221.
- Cirac, J.I., Zoller, P., 1995. Quantum computations with cold trapped ions. *Phys. Rev. Lett.* 74 (20), 4091–4094.
- Cirac, J.I., Zoller, P., 2000. A scalable quantum computer with ions in an array of microtraps. *Nature* 404, 579–581.
- Clauser, J., Shimony, A., 1978. Bell's theorem: Experimental tests and implications. *Rep. Progr. Phys.* 41, 1883.
- Clauser, J.F., Horne, M.A., Shimony, A., Holt, R.A., 1969. Proposed experiment to test local hidden-variable theories. *Phys. Rev. Lett.* 23, 880.
- Coppersmith, D., 1994. An approximate Fourier transform useful in quantum factoring. *Tech. Rep. IBM Research Report RC19642*.
- Cory, D.G., Price, M.D., Maas, W., Knill, E., Laflamme, R., Zurek, W.H., Havel, T.F., Somaroo, S.S., 1998. Experimental quantum error correction. *Phys. Rev. Lett.* 81, 2152.
- Dehmelt, H.G., 1975. Proposed $10^{14}\delta\nu < \nu$ laser fluorescence spectroscopy on Tl^+ mono-ion oscillator II (spontaneous quantum jumps). *Bull. Am. Phys. Soc.* 20, 60.
- DeMarco, B., Ben-Kish, A., Leibfried, D., Meyer, V., Rowe, M., Jelenković, B.M., Itano, W.M., Britton, J., Langer, C., Rosenband, T., Wineland, D.J., 2002. Experimental demonstration of a controlled-NOT wave-packet gate. *Phys. Rev. Lett.* 89 (26), 267901.
- Deslauriers, L., Olmschenk, S., Stick, D., Hensinger, W.K., Sterk, J., Monroe, C., 2006. Scaling and suppression of anomalous heating in ion traps. *Phys. Rev. Lett.* 97, 103007.
- Deutsch, D., 1989. Quantum computational networks. In: *Proc. R. Soc. London A*, 425, p. 73.
- Diedrich, F., Bergquist, J.C., Itano, W.M., Wineland, D.J., 1989. Laser cooling to the zero-point energy of motion. *Phys. Rev. Lett.* 62, 403–406.
- Diedrich, F., Peik, E., Chen, J.M., Quint, W., Walther, H., 1987. Observation of a phase transition of stored laser-cooled ions. *Phys. Rev. Lett.* 59 (26), 2931–2934.
- DiVincenzo, D.P., 2001. Dogma and heresy in quantum computing. *Quant. Inf. Comp.* 1, 1.
- Donley, E.A., Heavner, T.P., Levi, F., Tataw, M.O., Jefferts, S.R., 2005. Double-pass acousto-optic modulator system. *Rev. Sci. Inst.* 76, 063112.
- Drees, J., Paul, W., 1964. Beschleunigung von Elektronen in einem Plasmabetatron. *Z. Phys.* 180, 340.
- Drullinger, R., Wineland, D., Bergquist, J., 1980. High-resolution optical spectra of laser cooled ions. *Appl. Phys.* 22, 365.
- Duan, L.-M., Kimble, H.J., 2004. Scalable photonic quantum computation through cavity-assisted interactions. *Phys. Rev. Lett.* 92 (12), 127902.
- Dunn, T.J., Walmsley, I.A., Mukamel, S., 1995. Experimental-determination of the quantum-mechanical state of a molecular vibrational-mode using fluorescence tomography. *Phys. Rev. Lett.* 74 (6), 884–887.
- Dür, W., Vidal, G., Cirac, J.I., 2000. Three qubits can be entangled in two inequivalent ways. *Phys. Rev. A* 62, 062314.
- Dyck, R.S.V., D.L., Farnham, J., Zafonte, S.L., Schwinberg, P.B., 1999. Ultrastable superconducting magnet system for a Penning trap mass spectrometer. *Rev. Sci. Inst.* 70, 1665.
- Ekert, A., Jozsa, R., 1996. Shor's quantum algorithm for factorising numbers. *Rev. Modern Phys.* 68, 733.
- Epstein, R.J., Seidelin, S., Leibfried, D., Wesenberg, J.H., Bollinger, J.J., Amini, J.M., Blakestad, R.B., Britton, J., Home, J.P., Itano, W.M., Jost, J.D., Knill, E., Langer, C., Ozeri, R., Shiga, N., Wineland, D.J., 2007. Simplified motional heating rate measurements of trapped ions. *Phys. Rev. A* 76, 033411.
- Eschner, J., Morigi, G., Schmidt-Kaler, F., Blatt, R., 2003. Laser cooling of trapped ions. *J. Opt. Soc. Amer. B* 20, 1003.
- Fano, U., 1957. Description of states in quantum mechanics by density matrix and operator techniques. *Rev. Modern Phys.* 29 (1), 74–93.
- Feynman, R., 1982. Simulating physics with computers. *Int. J. Theoret. Phys.* 21, 467.
- Freeman, R., 1997. Spin Choreography. Spektrum, Oxford.
- Friedenauer, H., Schmitz, H., Glueckert, J., Porras, D., Schaetz, T., 2008. Simulating a quantum magnet with trapped ions. *Nature Physics Advance Online Publication (AOP)* on 27 July 2008.
- García-Ripoll, J.J., Zoller, P., Cirac, J.I., 2003. Speed optimized two-qubit gates with laser coherent control techniques for ion trap quantum computing. *Phys. Rev. Lett.* 91 (15), 157901.

- García-Ripoll, J.J., Zoller, P., Cirac, J.I., 2005. Coherent control of trapped ions using off-resonant lasers. *Phys. Rev. A* 71, 062309.
- Garisto, R., Hardy, L., 1999. Entanglement of projection and a new class of quantum erasers. *Phys. Rev. A* 60, 827.
- Gershenfeld, N.A., Chuang, I.L., 1997. Bulk spin-resonance quantum computation. *Science* 275 (5298), 350–356.
- Gisin, N., 1996. Nonlocality criteria for quantum teleportation. *Phys. Lett. A* 210, 157.
- Gottesman, D., 1997. Stabilizer codes and quantum error correction. [arXiv:quant-ph/9705052v1](https://arxiv.org/abs/quant-ph/9705052v1).
- Gottesman, D., Chuang, I.L., 1999. Quantum teleportation is a universal computational primitive. *Nature* 402, 390.
- Greenberger, D.M., Horne, M.A., Zeilinger, A., 1989. Going beyond Bell's Theorem. In: *Bell's Theorem, Quantum Theory and Conceptions of the Universe*. Kluwer Academic, Dordrecht, pp. 69–72.
- Griffiths, R.B., Niu, C.-S., 1996. Semiclassical Fourier transform for quantum computation. *Phys. Rev. Lett.* 76 (17), 3228–3231.
- Gulde, S., 2003. Experimental realization of quantum gates and the deutsch-josza algorithm with trapped $^{40}\text{Ca}^+$ -ions. Ph.D. Thesis, Universität Innsbruck.
- Gulde, S., Häffner, H., Riebe, M., Lancaster, G., Becher, C., Eschner, J., Schmidt-Kaler, F., Chuang, I.L., Blatt, R., 2003. Quantum information processing with trapped Ca^+ ions. *Proc. R. Soc. Lond. A* 361, 1363–1374.
- Häffner, H., Beier, T., Djekic, S., Hermanspahn, N., Kluge, H.-J., Quint, W., Stahl, S., Verdú, J., Valenzuela, T., Werth, G., 2003a. Double Penning trap technique for precise g factor determinations in highly charged ions. *Eur. Phys. J. D* 22, 163.
- Häffner, H., Beier, T., Hermanspahn, N., Kluge, H.-J., Quint, W., Stahl, S., Verdú, J., Werth, G., 2000. High-accuracy measurement of the magnetic moment anomaly of the electron bound in hydrogenlike carbon. *Phys. Rev. Lett.* 85 (25), 5308–5311.
- Häffner, H., Gulde, S., Riebe, M., Lancaster, G., Becher, C., Eschner, J., Schmidt-Kaler, F., Blatt, R., 2003b. Precision measurement and compensation of optical Stark shifts for an ion-trap quantum processor. *Phys. Rev. Lett.* 90, 143602.
- Häffner, H., Hänsel, W., Roos, C.F., Benhelm, J., Chek-al-Kar, D., Chwalla, M., Körber, T., Rapol, U.D., Riebe, M., Schmidt, P.O., Becher, C., Gühne, O., Dür, W., Blatt, R., 2005a. Scalable multiparticle entanglement of trapped ions. *Nature* 438 (7068), 643–646.
- Häffner, H., Schmidt-Kaler, F., Hänsel, W., Roos, C.F., Körber, T., Chwalla, M., Riebe, M., Benhelm, J., Rapol, U.D., Becher, C., Blatt, R., 2005b. Robust entanglement. *Appl. Phys. B* 81, 151.
- Hahn, E.L., 1950. Spin echoes. *Phys. Rev.* 80, 580.
- Haljan, P.C., Brickman, K.-A., Deslauriers, L., Lee, P.J., Monroe, C., 2005a. Spin-dependent forces on trapped ions for phase-stable quantum gates and entangled states of spin and motion. *Phys. Rev. Lett.* 94 (15), 153602.
- Haljan, P.C., Lee, P.J., Brickman, K.-A., Acton, M., Deslauriers, L., Monroe, C., 2005b. Entanglement of trapped-ion clock states. *Phys. Rev. A* 72, 062316.
- Hall, J.L., Notcutt, M., Ye, J., 2006. Improving laser coherence. In: Hinds, E., Ferguson, A., Riis, E. (Eds.), *Proceedings, International Conference on Laser Spectroscopy XVII*. World Scientific, Singapore, p. 3.
- Hänsel, W., 2003. Private communication, Innsbruck.
- Happer, W., 1972. Optical pumping. *Rev. Modern Phys.* 44, 169–249.
- Hawkins, W.B., Dicke, R.H., 1953. The polarization of sodium atoms. *Phys. Rev.* 91, 1008.
- Heinzen, D., Wineland, D., 1990. Quantum-limited cooling and detection of radio-frequency oscillations by laser-cooled ions. *Phys. Rev. A* 42, 2977.
- Hensinger, W.K., Olmschenk, S., Stick, D., Hucul, D., Yeo, M., Acton, M., Deslauriers, L., Monroe, C., 2006. T-junction ion trap array for two-dimensional ion shuttling storage, and manipulation. *Appl. Phys. Lett.* 88, 034101.
- Herfurth, F., Dilling, J., Kellerbauer, A., Bollen, G., Henry, S., Kluge, H.-J., Lamour, E., Lunney, D., Moore, R.B., Scheidenberger, C., Schwarz, S., Sikler, G., Szerypo, J., 2001. A linear radiofrequency ion trap for accumulation, bunching, and emittance improvement of radioactive ion beams. *Nucl. Instrum. Methods Phys. Res., Sect. A* 469, 254–275.
- Home, J.P., McDonnell, M.J., Lucas, D.M., Imreh, G., Keitch, B.C., Szwer, D.J., Thomas, N.R., Webster, S.C., Stacey, D.N., Steane, A.M., 2006. Deterministic entanglement and tomography of ion spin qubits. *New J. Phys.* 8, 188.
- Home, J.P., Steane, A.M., 2006. Electrode configurations for fast separation of trapped ions. *Quant. Inf. Comp.* 6, 289.
- Hornekaer, L., Kjaergaard, N., Thommesen, A.M., Drewsen, M., 2001. Structural properties of two-component Coulomb crystals in linear Paul traps. *Phys. Rev. Lett.* 86 (10), 1994–1997.
- Hradil, Z., 1997. Quantum-state estimation. *Phys. Rev. A* 55 (3), R1561–R1564.
- Huber, G., Deuschle, T., Schnitzler, W., Reichle, R., Singer, K., Schmidt-Kaler, F., 2008. Transport of ions in a segmented linear Paul trap in printed-circuit-board technology. *New J. Phys.* 10, 013004.
- Hucul, D., Yeo, M., Hensinger, W., Rabchuk, J., Olmschenk, S., Monroe, C., 2008. On the transport of atomic ions in linear and multidimensional ion trap arrays. *Quant. Inf. Comp.* 8, 501–578.
- Hume, D.B., Rosenband, T., Wineland, D.J., 2007. High-fidelity adaptive qubit detection through repetitive quantum nondemolition measurements. *Phys. Rev. Lett.* 99 (12), 120502.
- James, D.F.V., 1998. Quantum dynamics of cold trapped ions with application to quantum computation. *Appl. Phys. B* 66, 181.
- James, D.F.V., Kwiat, P.G., Munro, W.J., White, A.G., 2001. Measurement of qubits. *Phys. Rev. A* 64 (5), 052312.
- Jonathan, D., Plenio, M.B., Knight, P.L., 2000. Fast quantum gates for cold trapped ions. *Phys. Rev. A* 62, 042307.
- Jones, J., Mosca, M., 1998. Implementation of a quantum algorithm on a nuclear magnetic resonance quantum computer. *J. Chem. Phys.* 109, 1648.
- Jones, J.A., 2000. NMR quantum computation: A critical evaluation. *Fortschr. Phys.* 48, 909.
- Kaplan, A., Fredslund Andersen, M., Davidson, N., 2002. Suppression of inhomogeneous broadening in rf spectroscopy of optically trapped atoms. *Phys. Rev. A* 66, 045401.
- Kastler, A., 1950. Quelques suggestions concernant la production optique et la détection optique d'une inégalité de population des niveaux de quantification spatiale des atomes. *J. Phys. Rad.* 11, 255.
- Khaneja, N., Reiss, T., Kehlet, C., Schulthe-Herbrüggen, T., Glaser, S.J., 2005. Optimal control of coupled spin dynamics: Design of NMR pulse sequences by gradient ascent algorithms. *J. Magn. Reson.* 172, 296.
- Kielpinski, D., 2001. Entanglement and decoherence in a trapped-ion quantum register. Ph.D. Thesis, Department of Physics, University of Colorado, Boulder.
- Kielpinski, D., Meyer, V., Rowe, M.A., Sackett, C.A., Itano, W.M., Monroe, C., Wineland, D.J., 2001. A decoherence-free quantum memory using trapped ions. *Science* 291 (5506), 1013–1015.
- Kielpinski, D., Monroe, C., Wineland, D.J., 2002. Architecture for a large-scale ion-trap quantum computer. *Nature* 417 (6890), 709–711.
- Kiesel, N., Schmid, C., Weber, U., Ursin, R., Weinfurter, H., 2005. Linear optics controlled-phase gate made simple. *Phys. Rev. Lett.* 95, 210505.
- King, B., 1999. Quantum state engineering and information processing with trapped ions. Ph.D. Thesis, Department of Physics, University of Colorado, Boulder.
- Kjærgaard, N., Hornekær, L., Thommesen, A., Videsen, Z., Drewsen, M., 2000. Isotope selective loading of an ion trap using resonance-enhanced two-photon ionization. *Appl. Phys. B* 71, 207.
- Knill, E., 2005. Quantum computing with realistically noisy devices. *Nature* 434 (7029), 39–44.
- Knill, E., Laflamme, R., Martinez, R., Negrevergne, C., 2001a. Benchmarking quantum computers: The five-qubit error correcting code. *Phys. Rev. Lett.* 86 (25), 5811–5814.
- Knill, E., Laflamme, R., Milburn, G.J., 2001b. A scheme for efficient quantum computation with linear optics. *Nature* 409 (6816), 46–52.
- Knill, E., Leibfried, D., Reichle, R., Britton, J., Blakestad, R.B., Jost, J.D., Langer, C., Ozeri, R., Seidelin, S., Wineland, D.J., 2008. Randomized benchmarking of quantum gates. *Phys. Rev. A* 77, 012307.
- Kreuter, A., Becher, C., Lancaster, G.P.T., Mundt, A.B., Russo, C., Häffner, H., Roos, C., Eschner, J., Schmidt-Kaler, F., Blatt, R., 2004. Spontaneous emission lifetime of a single trapped Ca^+ ion in a high finesse cavity. *Phys. Rev. Lett.* 92 (20), 203002.
- Kreuter, A., Becher, C., Lancaster, G.P.T., Mundt, A.B., Russo, C., Häffner, H., Roos, C., Hänsel, W., Schmidt-Kaler, F., Blatt, R., Safranova, M.S., 2005. Experimental and theoretical study of the 3d ^2D -level lifetimes of $^{40}\text{Ca}^+$. *Phys. Rev. A* 71 (3), 032504.

- Labaziewicz, J., Ge, Y., Antohi, P., Leibrandt, D., Brown, K., Chuang, I., 2008a. Suppression of heating rates in cryogenic surface-electrode ion traps. *Phys. Rev. Lett.* 100, 013001.
- Labaziewicz, J., Ge, Y., Leibrandt, D., Wang, S.X., Shewmon, R., Chuang, I.L., 2008b. Temperature dependence of electric field noise above gold surfaces. *arXiv: 0804.2665v1*.
- Langer, C., Ozeri, R., Jost, J.D., Chiaverini, J., Demarco, B., Ben-Kish, A., Blakestad, R.B., Britton, J., Hume, D.B., Itano, W.M., Leibfried, D., Reichle, R., Rosenband, T., Schaetz, T., Schmidt, P.O., Wineland, D.J., 2005. Long-lived qubit memory using atomic ions. *Phys. Rev. Lett.* 95, 060502.
- Langer, C.E., 2006. High fidelity quantum information processing with trapped ions. Ph.D. Thesis, Department of Physics, University of Colorado, Boulder.
- Lanyon, B.P., Weinhold, T.J., Langford, N.K., O'Brien, J.L., Resch, K.J., Gilchrist, A., White, A.G., 2008. Manipulating biphotonic qutrits. *Phys. Rev. Lett.* 100 (6), 060504.
- Larson, D.J., Bergquist, J.C., Bollinger, J.J., Itano, W.M., Wineland, D.J., 1986. Sympathetic cooling of trapped ions: A laser-cooled two-species nonneutral ion plasma. *Phys. Rev. Lett.* 57 (1), 70–73.
- Lee, P.J., 2006. Quantum information processing with two trapped cadmium ions. Ph.D. Thesis, University of Michigan.
- Lee, P.J., Brickman, K.A., Deslauriers, L., Haljan, P.C., Duan, L., Monroe, C., 2005. Phase control of trapped ion quantum gates. *J. Opt. B* 7, 371.
- Leibfried, D., Barrett, M.D., Schaetz, T., Britton, J., Chiaverini, J., Itano, W.M., Jost, J.D., Langer, C., Wineland, D.J., 2004. Toward Heisenberg-limited spectroscopy with multiparticle entangled states. *Science* 304 (5676), 1476–1478.
- Leibfried, D., Blatt, R., Monroe, C., Wineland, D., 2003a. Quantum dynamics of single trapped ions. *Rev. Modern Phys.* 75, 281.
- Leibfried, D., DeMarco, B., Meyer, V., Lucas, D., Barrett, M., Britton, J., Itano, W.M., Jelenković, B., Langer, C., Rosenband, T., Wineland, D.J., 2003b. Experimental demonstration of a robust, high-fidelity geometric two ion-qubit phase gate. *Nature* 422, 412–415.
- Leibfried, D., DeMarco, B., Meyer, V., Rowe, M., Ben-Kish, A., Britton, J., Itano, W.M., Jelenković, B., Langer, C., Rosenband, T., Wineland, D.J., 2002. Trapped-ion quantum simulator: Experimental application to nonlinear interferometers. *Phys. Rev. Lett.* 89 (24), 247901.
- Leibfried, D., Knill, E., Ospelkaus, C., Wineland, D.J., 2007. Transport quantum logic gates for trapped ions. *Phys. Rev. A* 76, 032324.
- Leibfried, D., Knill, E., Seidelin, S., Britton, J., Blakestad, R.B., Chiaverini, J., Hume, D.B., Itano, W.M., Jost, J.D., Langer, C., Ozeri, R., Reichle, R., Wineland, D.J., 2005. Creation of a six-atom ‘Schrödinger cat’ state. *Nature* 438, 639–642.
- Leibfried, D., Meekhof, D.M., King, B.E., Monroe, C., Itano, W.M., Wineland, D.J., 1996. Experimental determination of the motional quantum state of a trapped atom. *Phys. Rev. Lett.* 77 (21), 4281–4285.
- Letchumanan, V., Wilson, M.A., Gill, P., Sinclair, A.G., 2005. Lifetime measurement of the metastable $4d^2D_{5/2}$ state in $^{88}\text{Sr}^+$ using a single trapped ion. *Phys. Rev. A* 72, 012509.
- Levitt, M., 1986. Composite pulses. *Prog. NMR Spectrosc.* 18, 61.
- Levitt, M., Freeman, R., 1979. NMR population inversion using a composite pulse. *J. Magn. Reson.* 33, 473.
- Linden, N., Popescu, S., 2001. Good dynamics versus bad kinematics: Is entanglement needed for quantum computation? *Phys. Rev. Lett.* 87, 047901.
- Lloyd, S., 1996. Universal quantum simulators. *Science* 273 (5278), 1073–1078.
- Lloyd, S., Braunstein, S.L., 1999. Quantum computation over continuous variables. *Phys. Rev. Lett.* 82, 1784.
- Loss, D., DiVincenzo, D.P., 1998. Quantum computation with quantum dots. *Phys. Rev. A* 57, 120.
- Lucas, D.M., Keitch, B.C., Home, J.P., Imreh, G., McDonnell, M.J., Stacey, D.N., Szwer, D.J., Steane, A.M., 2007. A long-lived memory qubit on a low-decoherence quantum bus. *arXiv: 0710.4421v1*.
- Majer, J., Chow, J.M., Gambetta, J.M., Koch, J., Johnson, B.R., Schreier, J.A., Frunzio, L., Schuster, D.I., Houck, A.A., Wallraff, A., Blais, A., Devoret, M.H., Girvin, S.M., Schoelkopf, R.J., 2007. Coupling superconducting qubits via a cavity bus. *Nature* 449 (7161), 443–447.
- Makhlin, Y., Schön, G., Shnirman, A., 2001. Quantum-state engineering with Josephson-junction devices. *Rev. Modern Phys.* 73, 357.
- Marzoli, I., Cirac, J.I., Blatt, R., Zoller, P., 1994. Laser cooling of trapped three-level ions: Designing two-level systems for sideband cooling. *Phys. Rev. A* 49 (4), 2771–2779.
- Massar, S., Popescu, S., 1995. Optimal extraction of information from finite quantum ensembles. *Phys. Rev. Lett.* 74, 1259.
- Matsukevich, D., Maunz, P., Moehrung, D.L., Olmschenk, S., Monroe, C., 2008. Bell inequality violation with two remote atomic qubits. *Phys. Rev. Lett.* 100, 150404.
- Maunz, P., Moehrung, D.L., Olmschenk, S., Younge, K.C., Matsukevich, D.N., Monroe, C., 2007. Quantum interference of photon pairs from two remote trapped atomic ions. *Nature Phys.* 3, 538.
- Meshkov, I., 1997. Electron cooling—Recent developments and trends. *Nucl. Instrum. Methods Phys. Res., Sect. A* 391, 1.
- Milburn, G.J., Schneider, S., James, D.F., 2000. Ion trap quantum computing with warm ions. *Fortschr. Phys.* 48, 801.
- Mintert, F., Wunderlich, C., 2001. Ion-trap quantum logic using long-wavelength radiation. *Phys. Rev. Lett.* 87 (25), 257904.
- Moehrung, D.L., Maunz, P., Olmschenk, S., Younge, K.C., Matsukevich, D.N., Duan, L.-M., Monroe, C., 2007. Entanglement of single-atom quantum bits at a distance. *Nature* 449 (7158), 68–71.
- Mohseni, M., Lidar, D.A., 2006. Direct characterization of quantum dynamics. *Phys. Rev. Lett.* 97 (17), 170501.
- Mølmer, K., Sørensen, A., 1999. Multiparticle entanglement of hot trapped ions. *Phys. Rev. Lett.* 82, 1835.
- Monroe, C., Itano, W.M., Kielpinski, D., King, B.E., Leibfried, D., Myatt, C.J., Turchette, Q.A., Wineland, D.J., Wood, C.S., 1999. Quantum logic with a few trapped ions. *AIP Conference Proceedings* CP457, 378.
- Monroe, C., Leibfried, D., King, B., Meekhof, D., Itano, W., Wineland, D., 1997. Simplified quantum logic with trapped ions. *Phys. Rev. A* 55, R2489.
- Monroe, C., Meekhof, D.M., King, B.E., Itano, W.M., Wineland, D.J., 1995a. Demonstration of a fundamental quantum logic gate. *Phys. Rev. Lett.* 75 (25), 4714–4717.
- Monroe, C., Meekhof, D.M., King, B.E., Jefferts, S.R., Itano, W.M., Wineland, D.J., Gould, P.L., 1995b. Resolved-sideband Raman cooling of a bound atom to the 3D zero-point energy. *Phys. Rev. Lett.* 75 (22), 4011–4014.
- Morigi, G., Eschner, J., Keitel, C., 2000. Ground state laser cooling using electromagnetically induced transparency. *Phys. Rev. Lett.* 85 (21), 4458–4461.
- Myerson, A.H., Szwer, D.J., Webster, S.C., Allcock, D.T.C., Curtis, M.J., Imreh, G., Sherman, J.A., Stacey, D.N., Steane, A.M., Lucas, D.M., 2008. High-fidelity readout of trapped-ion qubits. *Phys. Rev. Lett.* 100, 200502.
- Nagourney, W., Sandberg, J., Dehmelt, H., 1986. Shelved optical electron amplifier: Observation of quantum jumps. *Phys. Rev. Lett.* 56 (26), 2797–2799.
- Nebendahl, V., Häffner, H., Roos, C.F., 2008. Optimal control of entangling operations for trapped ion quantum computing. *arXiv:0809.1414v3* [quant-ph].
- Neuhauser, W., Hohenstatt, M., Toschek, P., Dehmelt, H., 1978. Optical-sideband cooling of visible atom cloud confined in parabolic well. *Phys. Rev. Lett.* 41, 233.
- Nielsen, M.A., Chuang, I.L., 2000. *Quantum Computation and Quantum Information*. Cambridge Univ. Press, Cambridge.
- Notcutt, M., Ma, L.-S., Ye, J., Hall, J.L., 2005. Simple and compact 1-Hz laser system via an improved mounting configuration of a reference cavity. *Opt. Lett.* 30, 1815–1817.
- O'Brien, J.L., Pryde, G.J., Gilchrist, A., James, D.F.V., Langford, N., Ralph, T., White, A.G., 2004. Quantum process tomography of a controlled-NOT gate. *Phys. Rev. Lett.* 93, 080502.
- Ospelkaus, C., Langer, C.E., Amini, J.M., Brown, K.R., Leibfried, D., Wineland, D.J., 2008. Trapped-ion quantum logic gates based on oscillating magnetic fields. *arXiv:0805.2165*.
- Ozeri, R., Itano, W.M., Blakestad, R.B., Britton, J., Chiaverini, J., Jost, J.D., Langer, C., Leibfried, D., Reichle, R., Seidelin, S., Wesenberg, J.H., Wineland, D.J., 2007. Errors in trapped-ion quantum gates due to spontaneous photon scattering. *Phys. Rev. A* 75, 042329.
- Ozeri, R., Langer, C., Jost, J.D., DeMarco, B., Ben-Kish, A., Blakestad, R.B., Britton, J., Chiaverini, J., Itano, W.M., Hume, D.B., Leibfried, D., Rosenband, T., Schmidt, P.O., Wineland, D.J., 2005. Hyperfine coherence in the presence of spontaneous photon scattering. *Phys. Rev. Lett.* 95 (3), 030403.
- Paris, M., Rehacek, J. (Eds.), 2004. *Quantum State Estimation*. In: *Lecture Notes in Physics*, Springer.
- Pearson, C.E., Leibrandt, D.R., Bakr, W.S., Mallard, W.J., Brown, K.R., Chuang, I.L., 2006. Experimental investigation of planar ion traps. *Phys. Rev. A* 73, 032307.
- Peik, E., Abel, J., Becker, T., von Zanthier, J., Walther, H., 1999. Sideband cooling of ions in radio-frequency traps. *Phys. Rev. A* 60, 439.

- Petta, J.R., Johnson, A.C., Taylor, J.M., Laird, E.A., Yacoby, A., Lukin, M.D., Marcus, C.M., Hanson, M.P., Gossard, A.C., 2005. Coherent manipulation of coupled electron spins in semiconductor quantum dots. *Science* 309 (5744), 2180–2184.
- Plantenberg, J.H., de Groot, P.C., Harmans, C.J.P.M., Mooij, J.E., 2007. Demonstration of controlled-NOT quantum gates on a pair of superconducting quantum bits. *Nature* 447 (7146), 836–839.
- Porras, D., Cirac, J.I., 2004. Bose-Einstein condensation and strong-correlation behavior of phonons in ion traps. *Phys. Rev. Lett.* 93, 263602.
- Poyatos, J.F., Cirac, J.I., Zoller, P., 1997. Complete characterization of a quantum process: The two-bit quantum gate. *Phys. Rev. Lett.* 78, 390.
- Raimond, J.M., Brune, M., Haroche, S., 2001. Manipulating quantum entanglement with atoms and photons in a cavity. *Rev. Modern Phys.* 73, 565.
- Raizen, M.C., Bergquist, J.C., Gilligan, J.M., Itano, W.M., Wineland, D.J., 1992a. Linear trap for high-accuracy spectroscopy of stored ions. *J. Modern Opt.* 39, 233.
- Raizen, M.G., Gilligan, J.M., Bergquist, J.C., Itano, W.M., Wineland, D.J., 1992b. Ionic crystals in a linear Paul trap. *Phys. Rev. A* 45 (9), 6493–6501.
- Rauschenbeutel, A., Nogues, G., Osnaghi, S., Bertet, P., Brune, M., Raimond, J.M., Haroche, S., 2000. Step-by-step engineered multiparticle entanglement. *Science* 288 (5473), 2024–2028.
- Reichle, R., Leibfried, D., Blakestad, R., Britton, J., Jost, J., Knill, E., Langer, C., Ozeri, R., Seidelin, S., Wineland, D., 2006a. Transport dynamics of single ions in segmented microstructured paul trap arrays. *Fortschr. Phys.* 54, 666.
- Reichle, R., Leibfried, D., Knill, E., Britton, J., Blakestad, R.B., Jost, J.D., Langer, C., Ozeri, R., Seidelin, S., Wineland, D.J., 2006b. Experimental purification of two-atom entanglement. *Nature* 443 (7113), 838–841.
- Retzker, A., Solano, E., Reznik, B., 2007. Tavis-cummings model and collective multiqubit entanglement in trapped ions. *Phys. Rev. A* 75, 022312.
- Riebe, M., Chwalla, M., Benhelm, J., Häffner, H., Hänsel, W., Roos, C.F., Blatt, R., 2007. Teleportation with atoms: Quantum process tomography. *New J. Phys.* 9, 211.
- Riebe, M., Häffner, H., Roos, C.F., Hänsel, W., Benhelm, J., Lancaster, G.P.T., Körber, T.W., Becher, C., Schmidt-Kaler, F., James, D.F.V., Blatt, R., 2004. Deterministic quantum teleportation with atoms. *Nature* 429 (6993), 734–737.
- Riebe, M., Kim, K., Schindler, P., Monz, T., Schmidt, P.O., Körber, T.K., Hänsel, W., Häffner, H., Roos, C.F., Blatt, R., 2006. Process tomography of ion trap quantum gates. *Phys. Rev. Lett.* 97, 220407.
- Rohde, H., Gulde, S.T., Roos, C.F., Barton, P.A., Leibfried, D., Eschner, J., Schmidt-Kaler, F., Blatt, R., 2001. Sympathetic ground state cooling and coherent manipulation with two-ion-crystal. *J. Opt. B* 3, S34.
- Roos, C., 2000. Controlling the quantum state of trapped ions. Ph.D. Thesis, Universität Innsbruck.
- Roos, C., Zeiger, T., Rohde, H., Nägerl, H., Eschner, J., Leibfried, D., Schmidt-Kaler, F., Blatt, R., 1999. Quantum state engineering on an optical transition and decoherence in a Paul trap. *Phys. Rev. Lett.* 83, 4713.
- Roos, C.F., 2008. Ion trap quantum gates with amplitude-modulated laser beams. *New J. Phys.* 10, 013002.
- Roos, C.F., Chwalla, M., Kim, K., Riebe, M., Blatt, R., 2006. Designer atoms' for quantum metrology. *Nature* 443 (7109), 316–319.
- Roos, C.F., Lancaster, G.P.T., Riebe, M., Häffner, H., Hänsel, W., Gulde, S., Becher, C., Eschner, J., Schmidt-Kaler, F., Blatt, R., 2004a. Bell states of atoms with ultralong lifetimes and their tomographic state analysis. *Phys. Rev. Lett.* 92 (22), 220402.
- Roos, C.F., Leibfried, D., Mundt, A., Schmidt-Kaler, F., Eschner, J., Blatt, R., 2000. Experimental demonstration of ground state laser cooling with electromagnetically induced transparency. *Phys. Rev. Lett.* 85, 5547–5550.
- Roos, C.F., Riebe, M., Häffner, H., Hänsel, W., Benhelm, J., Lancaster, G.P.T., Becher, C., Schmidt-Kaler, F., Blatt, R., 2004b. Control and measurement of three-qubit entangled states. *Science* 304 (5676), 1478–1480.
- Roth, B., Frohlich, U., Schiller, S., 2005. Sympathetic cooling of $^4\text{He}^+$ ions in a radio-frequency trap. *Phys. Rev. Lett.* 94 (5), 053001.
- Rowe, M.A., Ben-Kish, A., DeMarco, B., Leibfried, D., Meyer, V., Beall, J., Britton, J., Hughes, J., Itano, W.M., Jelenković, B., Langer, C., Rosenband, T., Wineland, D.J., 2002. Transport of quantum states and separation of ions in a dual RF ion trap. *Quant. Inf. Comp.* 2, 257–271.
- Rowe, M.A., Kielpinski, D., Meyer, V., Sackett, C.A., Itano, W.M., Monroe, C., Wineland, D.J., 2001. Experimental violation of a Bell's inequality with efficient detection. *Nature* 409 (6822), 791–794.
- Sackett, C.A., Kielpinski, D., King, B.E., Langer, C., Meyer, V., Myatt, C.J., Rowe, M., Turchette, Q.A., Itano, W.M., Wineland, D.J., Monroe, C., 2000. Experimental entanglement of four particles. *Nature* 404, 256–259.
- Šašura, M., Bužek, V., 2002. Tutorial review: Cold trapped ions as quantum information processors. *J. Modern Opt.* 49, 1593.
- Sauter, T., Neuhauser, W., Blatt, R., Toschek, P.E., 1986. Observation of quantum jumps. *Phys. Rev. Lett.* 57 (14), 1696–1698.
- Schaetz, T., Barrett, M.D., Leibfried, D., Britton, J., Chiaverini, J., Itano, W.M., Jost, J.D., Knill, E., Langer, C., Wineland, D.J., 2005. Enhanced quantum state detection efficiency through quantum information processing. *Phys. Rev. Lett.* 94 (1), 010501.
- Schaetz, T., Leibfried, D., Chiaverini, J., Barrett, M., Britton, J., DeMarco, B., Itano, W., Jost, J., Langer, C., Wineland, D., 2004. Towards a scalable quantum computer/simulator based on trapped ions. *Appl. Phys. B* 79, 923.
- Schmidt, P.O., Rosenband, T., Langer, C., Itano, W.M., Bergquist, J.C., Wineland, D.J., 2005. Spectroscopy using quantum logic. *Science* 309 (5735), 749–752.
- Schmidt-Kaler, F., Gulde, S., Riebe, M., Deusche, T., Kreuter, A., Lancaster, G., Becher, C., Eschner, J., Häffner, H., Blatt, R., 2003a. The coherence of qubits based on single Ca^+ ions. *J. Phys. B: At. Mol. Opt. Phys.* 36, 623.
- Schmidt-Kaler, F., Häffner, H., Gulde, S., Riebe, M., Lancaster, G., Eschner, J., Becher, C., Blatt, R., 2004. Quantized ac-Stark shifts and their use for multiparticle entanglement and quantum gates. *Europhys. Lett.* 65, 587.
- Schmidt-Kaler, F., Häffner, H., Gulde, S., Riebe, M., Lancaster, G.P.T., Becher, C., Hänsel, W., Eschner, J., Roos, C.F., Blatt, R., 2003b. How to realize a universal quantum gate with trapped ions. *Appl. Phys. B* 77, 789.
- Schmidt-Kaler, F., Häffner, H., Riebe, M., Gulde, S., Lancaster, G.P.T., Deusche, T., Becher, C., Roos, C.F., Eschner, J., Blatt, R., 2003c. Realization of the Cirac-Zoller controlled-NOT quantum gate. *Nature* 422 (6930), 408–411.
- Schrader, D., Dotsenko, I., Khudaverdyan, M., Miroshnychenko, Y., Rauschenbeutel, A., Meschede, D., 2004. Neutral atom quantum register. *Phys. Rev. Lett.* 92, 150501.
- Schulz, S., Poschinger, U., Singer, K., Schmidt-Kaler, F., 2006. Optimization of segmented linear Paul traps and transport of stored particles. *Fortschr. Phys.* 54, 648.
- Seidelin, S., Chiaverini, J., Reichle, R., Bollinger, J.J., Leibfried, D., Britton, J., Wesenberg, J.H., Blakestad, R.B., Epstein, R.J., Hume, D.B., Itano, W.M., Jost, J.D., Langer, C., Ozeri, R., Shiga, N., Wineland, D.J., 2006. Microfabricated surface-electrode ion trap for scalable quantum information processing. *Phys. Rev. Lett.* 96 (25), 253003.
- Sengstock, K., Sterr, U., Rieger, V., Bettermann, D., Müller, J., Ertmer, W., 1994. Optical ramsey spectroscopy on laser trapped and thermal Mg-atoms. *Appl. Phys. B* 59, 99.
- Shockley, W., 1938. Currents to conductors induced by a moving point charge. *J. Appl. Phys.* 9, 635.
- Shor, P.W., 1994. Algorithms for quantum computation: Discrete logarithms and factoring. In: Proceedings of the 35th Annual Symposium on Foundations of Computer Science, Santa Fe, NM, Nov. 20–22. IEEE Computer Society Press, pp. 124–134.
- Shor, P.W., 1995. Scheme for reducing decoherence in quantum computer memory. *Phys. Rev. A* 52 (4), R2493–R2496.
- Smithey, D.T., Beck, M., Raymer, M.G., Faridani, A., 1993. Measurement of the Wigner distribution and the density-matrix of a light mode using optical homodyne tomography—Application to squeezed states and the vacuum. *Phys. Rev. Lett.* 70 (9), 1244–1247.
- Solano, E., 2005. Private communication, Munich.
- Solano, E., de Matos Filho, R.L., Zagury, N., 1999. Deterministic Bell states and measurement of the motional state of two trapped ions. *Phys. Rev. A* 59, R2539–R2543.
- Sørensen, A., Mølmer, K., 1999. Quantum computation with ions in thermal motion. *Phys. Rev. Lett.* 82, 1971.
- Sørensen, A., Mølmer, K., 2000. Entanglement and quantum computation with ions in thermal motion. *Phys. Rev. A* 62, 022311.
- Sørensen, A.S., van der Wal, C.H., Childress, L.I., Lukin, M.D., 2004. Capacitive coupling of atomic systems to mesoscopic conductors. *Phys. Rev. Lett.* 92 (6), 063601.

- Staanum, P., Drewsen, M., 2002. Trapped-ion quantum logic utilizing position-dependent ac-Stark shifts. *Phys. Rev. A* 66, 040202.
- Staanum, P., Drewsen, M., Mølmer, K., 2004. Geometric quantum gate for trapped ions based on optical dipole forces induced by gaussian laser beams. *Phys. Rev. A* 70, 052327.
- Steane, A., 1997. The ion trap quantum information processor. *Appl. Phys. B* 64, 623.
- Steane, A., Roos, C.F., Stevens, D., Mundt, A., Leibfried, D., Schmidt-Kaler, F., Blatt, R., 2000. Speed of ion-trap quantum-information processors. *Phys. Rev. A* 62, 042305.
- Steane, A.M., 1996. Error correcting codes in quantum theory. *Phys. Rev. Lett.* 77 (5), 793–797.
- Steane, A.M., 2004. How to build a 300 bit, 1 giga-operation quantum computer. [arXiv:quant-ph/0412165](https://arxiv.org/abs/quant-ph/0412165).
- Steffen, M., Ansmann, M., Bialczak, R.C., Katz, N., Lucero, E., McDermott, R., Neeley, M., Weig, E.M., Cleland, A.N., Martinis, J.M., 2006. Measurement of the entanglement of two superconducting qubits via state tomography. *Science* 313 (5792), 1423–1425.
- Stenholm, S., 1986. Semiclassical theory of laser cooling. *Rev. Modern Phys.* 58, 699.
- Thompson, R.C., 1990. Precision measurement aspects of ion traps. *Meas. Sci. Technol.* 1, 93.
- Tian, L., Blatt, R., Zoller, P., 2005. Scalable ion trap quantum computing without moving ions. *Eur. Phys. J. D* 32, 201.
- Tian, L., Rabl, P., Blatt, R., Zoller, P., 2004. Interfacing quantum-optical and solid-state qubits. *Phys. Rev. Lett.* 92 (24), 247902.
- Timoney, N., Elman, V., Glaser, S., Weiss, C., Johanning, M., Neuhauser, W., Wunderlich, C., 2008. Error-resistant single-qubit gates with trapped ions. *Phys. Rev. A* 77, 052334.
- Tittel, W., Brendel, J., Zbinden, H., Gisin, N., 1998. Violation of Bell inequalities by photons more than 10 km apart. *Phys. Rev. Lett.* 81 (17), 3563–3566.
- Tittel, W., Weihs, G., 2001. Photonic entanglement for fundamental tests and quantum communication. *Quant. Inf. Comp.* 1, 3.
- Turchette, Q., Wood, C., King, B., Myatt, C., Leibfried, D., Itano, W., Monroe, C., Wineland, D., 1998. Deterministic entanglement of two ions. *Phys. Rev. Lett.* 81, 3631.
- Turchette, Q.A., Kielpinski, B.E., King, D., Leibfried, D.M., Meekhof, C.J., Myatt, M.A., Rowe, C.A., Sackett, C.S., Wood, W.M., Itano, C., Monroe, D.J., Wineland, D.J., 2000. Heating of trapped ions from the quantum ground state. *Phys. Rev. A* 61, 063418.
- Vandersypen, L.M., Steffen, M., Breyta, G., Yannoni, C.S., Sherwood, M.H., Chuang, I.L., 2001. Experimental realization of Shor's quantum factoring algorithm using nuclear magnetic resonance. *Nature* 414 (6866), 883–887.
- Wallraff, A., Schuster, D.I., Blais, A., Frunzio, L., Huang, R.-S., Majer, J., Kumar, S., Girvin, S.M., Schoelkopf, R.J., 2004. Strong coupling of a single photon to a superconducting qubit using circuit quantum electrodynamics. *Nature* 431 (7005), 162–167.
- Walther, P., Resch, K.J., Rudolph, T., Schenck, E., Weinfurter, H., Vedral, V., Aspelmeyer, M., Zeilinger, A., 2005. Experimental one-way quantum computing. *Nature* 434 (7030), 169–176.
- Warren, W.S., 1997. The usefulness of NMR quantum computing. *Science* 277, 1688.
- Weber, E.W., 1977. Optical pumping of ions. *Phys. Rev.* 32, 123.
- Weihs, G., Jennewein, T., Simon, C., Weinfurter, H., Zeilinger, A., 1998. Violation of Bell's inequality under strict Einstein locality conditions. *Phys. Rev. Lett.* 81 (23), 5039–5043.
- Wesenberg, J.H., Epstein, R.J., Leibfried, D., Blakestad, R.B., Britton, J., Home, J.P., Itano, W.M., Jost, J.D., Knill, E., Langer, C., Ozeri, R., Seidelin, S., Wineland, D.J., 2007. Fluorescence during Doppler cooling of a single trapped atom. *Phys. Rev. A* 76, 053416.
- White, A.G., James, D.F.V., Eberhard, P.H., Kwiat, P.G., 1999. Nonmaximally entangled states: Production, characterization, and utilization. *Phys. Rev. Lett.* 83 (16), 3103–3107.
- Wineland, D., Bergquist, J., Itano, W., Drullinger, R., 1980. Double-resonance and optical-pumping experiments on electromagnetically confined, laser-cooled ions. *Opt. Lett.* 5, 254.
- Wineland, D.J., Barrett, M., Britton, J., Chiaverini, J., DeMarco, B., Itano, W.M., Jelenković, B., Langer, C., Leibfried, D., Meyer, V., Rosenband, T., Schätz, T., 2003. Quantum information processing with trapped ions. *Proc. R. Soc. Lond. A* 361 (1808), 1349–1361.
- Wineland, D.J., Bergquist, J.C., Itano, W.M., Bollinger, J.J., Manney, C.H., 1987. Atomic ion Coulomb clusters in an ion trap. *Phys. Rev. Lett.* 59 (26), 2935–2938.
- Wineland, D.J., Dehmelt, H.G., 1975. Principles of the stored ion calorimeter. *J. App. Phys.* 46, 919.
- Wineland, D.J., Itano, W.M., 1979. Laser cooling of atoms. *Phys. Rev. A* 21, 1521.
- Wineland, D.J., Monroe, C., Itano, W.M., Leibfried, D., King, B., Meekhof, D.M., 1998. Experimental issues in coherent quantum-state manipulation of trapped atomic ions. *J. Res. Natl. Inst. Stand. Technol.* 103, 259.
- Wootters, W.K., Fields, B.D., 1989. Optimal state determination by mutually unbiased measurements. *Ann. Phys.* 191 (2), 363–381.
- Young, B., Cruz, F., Itano, W., Bergquist, J., 1999a. Visible lasers with subhertz linewidths. *Phys. Rev. Lett.* 82, 3799.
- Young, B.C., Rafac, R.J., Beall, J.A., Cruz, F.C., Itano, W.M., Wineland, D.J., Bergquist, J.C., 1999b. Hg^+ optical frequency standard: Recent progress. In: Blatt, R., Eschner, J., Leibfried, D., Schmidt-Kaler, F. (Eds.), *Laser Spectroscopy, Proceedings of the XIV International Conference*. World Scientific, Singapore, p. 61.
- Zeilinger, A., Horne, M., Greenberger, D., 1992. Higher-order quantum entanglement. *NASA Conf. Publ.* 3135, 73.
- Zhu, S.-L., Monroe, C., Duan, L.-M., 2006. Arbitrary-speed quantum gates within large ion crystals through minimum control of laser beams. *Europhys. Lett.* 73, 485.